NASA Technical Memorandum 81721

Ion Beam Applications Research—a 1981 Summary of Lewis Research Center Programs

Bruce A. Banks
Lewis Research Center
Cleveland, Ohio

Prepared for the
Fifteenth International Electrical Propulsion Conference
cosponsored by the American Institute of Aeronautics and Astronautics,
the Japan Society for Aeronautical and Space Sciences,
and Deutsche Gesselschaft fur Luft- und Raumfahrt
Las Vegas, Nevada, April 21-23, 1981

NASA

TABLE OF CONTENTS

ION BEAM APPLICATIONS RESEARCH - A 1981 SUMMARY OF LEWIS RESEARCH CENTER PROGRAMS

Bruce A. Banks
NASA Lewis Research Center
Cleveland, Ohio

ABSTRACT

In 1975 the NASA's Lewis Research Center initiated a technology specific spinoff program to more broadly utilize benefits resulting from ion thruster technology. An Ion Beam Applications Research (IBAR) program was organized to enable the development of new or improved materials, products, and processes through the nonpropulsive application of ion thruster technology. Focused efforts to identify, evaluate, develop and transfer applications to the user community were conducted. A summary of the NASA Lewis Research Center's in-house, grant, and contract projects involving IBAR is given. Specific application efforts utilizing ion beam sputter etching, deposition, and texturing are discussed as well as ion source and component technology applications.

INTRODUCTION

Research and development of electron-bombardment ion thrusters has been in progress since approximately 1959. As a direct result of these efforts a wealth of technology now exits relating to specialized fabrication techniques and the effects of ion bombardment of materials. In 1975 the Lewis Research Center initiated a program aimed at more broadly utilizing ion thruster technology. Specifically, a small focused effort was organized whose objectives were to enable the development of new or improved materials, products, and processes through the nonpropulsive application of ion thruster technology. The activities of this group involved the identification, evaluation, development, and transfer to the user community of these nonpropulsive applications. The purpose of this paper is to make available to a wide spectrum of potential users a summary of the NASA Lewis Research Center's in-house, grant, and contract projects involving nonpropulsive applications of ion thruster technology. An attempt has been made to describe the application research projects in a manner predominantly suitable to each specific user audience. Although many applications exist which involve utilization of technology associated with the ion source or its components, most of the applications research efforts have been associated with utilization of the exhaust ion beam and its interaction with materials. As a result, the entire assortment of research activities associated with nonpropulsive applications has collectively been called the Ion Beam Applications Research (IBAR) Program.

This paper describes ion thruster technology relating to the ion source, its components and fabrication processes, and the interaction of the exhaust ion beam with materials. Three sputtering processes which involve ion beam interaction with materials are described. These processes are: ion beam sputter etching, deposition, and texturing. Application research projects utilizing ion thruster technology for industrial and biomedical applications are summarized. These efforts include applications being investigated under NASA supported contracts, grants, and Lewis Research Center in-house projects.

ION THRUSTER TECHNOLOGY

Ion thrusters have been of interest for space propulsion because of their capability for producing much higher propellant exhaust velocities than possible with chemical propulsion.[1] The benefits of the higher exhaust velocities has contributed toward the serious consideration of these devices for station keeping and orbit transfer of geocentric spacecraft, and in solar system exploration.

Figure 1 shows a schematic drawing of an operating electron-bombardment ion thruster system. As can be seen the electron-bombardment ion thruster is a low pressure gaseous discharge device, and thus can operate only in a vacuum environment. The propellant, shown as mercury in Fig. 1, can be any liquid or gas capable of being easily vaporized and ionized. Other propellants such as cesium, hydrogen, argon, and xenon have been frequently used. The propellant is vaporized and fed into a discharge chamber where it is ionized by electron bombardment. An axially diverging magnetic field is used to increase the path length, and thereby the ionization efficiency, of electrons leaving the cathode toward the anode. Thrust is produced as a result of electrostatic acceleration of ions under the influence of the high electric field between the screen and accelerator grids. The exhaust ions have energies equal to the voltage of the screen supply, typically between 200 and 2000 eV. Electrons must be added to the exhaust ion beam to maintain charge neutralization of the ion beam and to prevent an accumulation of electrons on the spacecraft. Figure 2 is a photograph of a 30 cm diameter ion thruster which is the type currently proposed for earth orbit transfer and solar system exploration.

Over the past two decades significant progress has been achieved in increasing the performance, durability, and reliability of ion thrusters for both auxiliary and prime space propulsion.[2-5] In addition to laboratory research and development two space tests have been performed with mercury ion thrusters. Space Electric Rocket Test I (SERT I), shown in Fig. 3, was launched July 20, 1964 and demonstrated, during a brief ballistic space trajectory, that thruster operation and neutralization were possible.[6] SERT II was launched on Feb. 3, 1970 into a circular polar orbit and demonstrated the long term space operation on an ion thruster (Fig. 4, ref. 7).

During the course of research and development relating to the electron-bombardment ion thruster, a great volume of more broadly useful information in many specific technical areas evolved which includes:

1. Electrical isolation of low pressure gases
2. Hollow cathodes
3. Electron emitting surfaces
4. Ionization and acceleration of gases
5. Surfaces for the retardation of peeling of sputtered deposits
6. Maintenance of high voltage isolation in a high temperature vacuum or plasma environment

7. Photochemical fabrication of large area ion optics
8. Fabrication processes for the production of high span to gap ion optics
9. Long life ion source and components
10. Controlled porosity of refractory materials
11. Sputter yields for materials at very low voltages
12. Efficient production and practical control of low pressure plasmas
13. Broad beam ion sources

Many of these technology areas have and will continue to find applicability in the nonpropulsive sector. At present there is at least four companies within the United States that fabricate and supply broad beam ion sources as a direct result of ion thruster technology spinoff.[8] At least six companies currently provide ion beam sputtering services for research and industrial users.

SPUTTERING PROCESSES

Although many applications of ion thruster technology utilize components and/or processes occurring within the ion source, a broader range of applications relate to utilization of the exhaust ion beam. Ion beam interaction with materials placed downstream of the ion source has been a subject of interest or concern since their earliest days of ion thruster testing in vacuum facilities. Only in the past decade has any concerted effort been applied to constructively use ion beams for sputtering.

Most of the applications discussed in this report involve sputter etching, sputter deposition and/or sputter texturing. These phenomena will be discussed separately in the following sections.

SPUTTER ETCHING

Sputter etching is the removal of material from a surface by energetic ion or neutral particle bombardment. The bombarding particles interact with the surface through collision processes so as to cause the ejection of surface atoms, molecules, or molecular fragments. Figure 5 depicts an ion source used for sputter etching a target that is partially protected by a sputter mask. The sputter mask material also is sputter etched and is typically chosen of a material more sputter resistant than the target. Depending upon the specific sputter etching application, the mask may be a polymer applied as a photo resist, a metal or a metal-oxide. Documentation of the sputter yield of many materials has been performed by Wehner and others.[9-14] Table I from Ref. 15 lists the sputter yield of various elements and compounds for 500 eV argon ion bombardment at normal incidence. The sputter yield in terms of atoms ejected per incident ion is sometimes more usefully appreciated in terms of sputter etch rate in angstroms per minute. Figure 6, from Ref. 16, lists a range of values of observed ion beam sputter etch rates in Å/min for various materials bombarded by a normally incident 500 eV argon ion beam at a current density of 1 mA/cm^2. The Fig. 6 values are measurements made separately from Table I and are not necessarily completely consistent with it. Other materials not shown in Fig. 6 that have extremely high ion beam sputter etch rates are polytetrafluoroethylene (PTFE Teflon®), fluorinated ethylene propylene (FEP Teflon®), chlorotrifluoroethylene (CTFE Teflon®), perfluoroalkoxyn (PFA Teflon®), and polyoxymethylene (Delvin®).[17,18] Reference 17 projects ion beam etch rates of approximately 6.2x10^4 Å/min for PTFE Teflon® being bombarded by 500 eV argon ions at a current density of 1 mA/cm^2.

The sputter etch rate of materials is dependent to varying degrees upon the following parameters:

- bombarding species
- target material
- energy of the bombarding species
- current density of the incident ion beam
- angle of incidence with respect to the target surface
- background environmental gas pressure and composition
- target temperature (which may also be influenced by the ion beam power density)
- target purity and composition of impurities
- target crystallographic structure and orientation of crystaline planes

Many of the above parameters that have a significant influence upon the sputter etch rate can be utilized advantageously when sputtering is being performed as a fabrication process or as a diagonistic technique.

Ion beams used to sputter etch materials offer some advantages over other sputtering techniques such as D.C. or R.F. sputtering. The directed nature of the ion beam and the separation of the source of energetic ions from the sputter target allows sputter etching with nonnormal incidence and to do so at a lower or more independently controlled pressure and temperature environment than by other processes. High rate sputter etching can be more readily accomplished by D.C. and R.F. discharge sputtering techniques provided that target temperature is not of concern or can be controlled.

SPUTTER DEPOSITION

Sputter deposition is the accumulation of material that occurs if the sputter etched material is allowed to deposit on another surface. Deposition utilizing electric discharge processes has been observed and reported as early as 1775 by Joseph Priestley in his "Experiments on the Effects of Giving a Metallic Tinge to the Surface of Glass".[19] W. R. Grove in 1852 reported experiments in which a partial vacuum electrical discharge was employed to produce deposited films.[20]

Ion beam sputter deposition is simply the deposition of the sputter efflux from the ion beam sputter etched target material. Ion beam sputter deposition differs from other D.C. and R.F. discharge sputter deposition techniques in that the deposition substrate can be placed in a lower pressure and thermally isolated environment. Figure 7 depicts sputter deposition with an ion source. The sputter deposition rate is, of course, dependent upon the sputter etch rate of the target, the angular distribution of sputter efflux as well as geometric factors. For normal ion beam incidence sputter ejected atoms typically leave the target surface in approximately a cosine distribution about the surface normal if the surface is polycrystalline. However, single crystal targets give rise to a much more structured ejection pattern.

Ejection energies of sputtered ejected atoms are considerably below those of the ion beam and are

typically reported to be in the 1-20 eV range.[15] These ejection energies are still considerably above those experienced by thermal ejection processes such as thermal evaporation.

Depending upon the composition of the target, the sputter depositing species may be atoms, molecules, or molecular scission fragments. Thus the chemical properties of the deposits may differ from those of the targets especially if the targets are compounds or alloys. Often, for example, metal oxide targets will require the introduction of additional environmental oxygen to produce a metal oxide deposit. Sputter deposited fluoropolymers from fluoropolymer targets are highly crosslinked as a result of the sputter efflux being predominantly composed of low molecular weight free radicals.[17] Sputter deposition from a nonmagnetic stainless steel target will result in a magnetic deposit because the deposition builds up as an atomic mixture rather than an alloy.

Sputter deposits on room temperature substrates generally are amorphous or have extremely small crystallite sites.

Successful sputter deposition of adherent films usually requires that the substrate surface is clean prior to sputter deposition. This can be accomplished by ion beam sputtering of the substrate surface immediately prior to deposition to remove surface oxides, organic contaminants, and adsorbed gases.

SPUTTER TEXTURING

Sputter texturing is the microroughening of the bombarded surface of a sputter target that occurs if there are spatial variations in the sputter yield of the target surface. There are a variety of ways in which spatial variations in the sputter yield of target surfaces can occur. The target may be composed of two or more materials or forms of materials that are present in a spatially segregated heterogeneous mixture throughout the target. Such targets develop a natural texture when sputtered. If the target is a homogeneous and pure material, sputter texturing can be produced by seeding the surface with atoms of a different material and allowing these atoms to nucleate into segregated microscopic sites of sputter resistance.

Natural Texturing

Sputter targets composed of materials that present a spatially varying sputter yield surface to incident ions will cause natural texturing. A chemically pure material may be composed of randomly oriented crystallites with each having a different sputter yield which is dependent upon their orientation. Sputtering such surfaces results in a patchy textured surface showing enhanced visibility of these crystallites.[21]

Some materials such as fluoropolymers are composed of segregated amorphous and crystalline regions. The amorphous regions sputter etch faster than the crystalline regions which causes left standing surface structures to appear as a result of preferential sputter removal of the amorphous material. Figure 8 depicts natural texturing by ion beam sputtering. Figure 9 is a scanning electron photomicrograph of a natural textured polytetrafluoroethylene (PTFE Teflon®) surface. Depending upon the sputtering conditions and duration, the surface cones can be made to be submicron to hundreds of microns high. The heights of the surface cone structures are approximately 10-20 percent of the total depth of sputter etching.[18]

Heterogeneous materials with microscopic sites of compositional segregation will produce a natural textured surface if there is adequate differences in the sputter yields of the various sites.[22-24] Figures 10(a) and (b) are scanning electron photomicrographs of an untreated and sputter textured surfaces of a sample of coal. As can be seen by the difference between the two photomicrographs, natural texturing develops well defined pillars and cones which are probably due to sites of compositional segregation.

Homogeneous materials may also develop a natural texture if the target is sufficiently hot to provide surface atom migration to result in sites of nucleation of segregated elements. Nucleation sites of more sputter resistant elements covering in a patch like manner less sputter resistant bulk material would then become the tops and/or sides of left standing surface structures. Figure 11 is a scanning electron photomicrograph of natural textured MP35N (a multiphase alloy of 35% Ni, 35% Co, 20% Cr, and 10% Mo). At low temperatures this alloy does not develop any significant natural texture, however exposure to a high power density ion beams raises the target temperature sufficiently to promote surface atom migration and segregated nucleation which in turn promotes the development of a natural texture.

Pure materials may also develop a microrough natural texture if there are small voids distributed throughout the bulk that are exposed by the ion beam. Variations in sputter yield with angle of incidence and the presence of voids can result in a pitted surface as shown in Fig. 12 for natural textured Al_2O_3.

Seed Texturing

Sputter target surfaces can be supplied via sputter or vapor deposition with atoms of a lower sputter yield to foster the development of nucleation sites of higher sputter resistance and result in left standing surface microstructures. This sputter texturing seeding technique, referred to as seed texturing is extremely useful for texturing nonrefractory metals. Seed texturing has been observed for numerous combinations of target and seed materials.[25-28] Figure 13 depicts a seed texturing technique utilizing ion beam sputtering. The simultaneous sputter etching of the target to be textured and the seed target provides a continually replenished supply of seed atoms on the target surface to be textured. Figure 14 from Hudson[26] is a periodic chart of the elements indicating those elements which can be textured using tantalum as the seed material. Robinson[29] has made analytical models of the dynamics of seed texturing. Both Robinson[29] and Wehner[30] report that a sufficiently high sputter target surface temperature must be present to enable surface diffusion and clustering of the seed material, otherwise texturing will not take place. Wehner[30] finds that the seed material sputter yield does not always have to be lower than the target material in order that texturing occur. He presented experimental evidence[30] indicating that the seed material must simply have a higher

melting temperature than the target material to be textured.

Figure 15 shows scanning electron photomicrographs of some of the types of surface morphologies created by seed texturing using tantalum as a seed material. Types of morphologies typically generated include: pointed cones, faceted cones, blunt grass like stalks, and various forms of rill like structures. The type of structure depends upon both the seed and target material along with the seed texturing conditions, geometries, and environmental gas species.

APPLICATION RESEARCH PROJECTS

Beginning in 1975 efforts were initiated at the NASA Lewis Research Center to investigate potential nonpropulsive applications of ion thruster technology.[27-28] A wide spread industrial technology transfer had already spontaneously occurred for many high resolution microelectronics applications of ion beam technology. However, there were many generically different types of potential industrial and biomedical applications that might emerge if sufficient applications research and evaluation efforts were carried out to demonstrate to the user industry the merits of these specific technology applications. Rather than assisting in the already-recognized high resolution microelectronics applications area, the efforts of this program were focused at broadening the scope of technology application through the identification of new areas of applications.

Several university and industrial contractual efforts have been supported by the Lewis Research Center to identify new potential applications.[31-34] Potential application concepts were then prioritized in a team manner in accordance with the following formula:

$$\text{Priority} = \frac{1}{n^6}\left(\sum_{i=1}^{n} T_i\right)\left(\sum_{i=1}^{n} E_i\right)\left(\sum_{i=1}^{n} P_i\right)\left(\sum_{i=1}^{n} I_i\right)^3$$

where the largest priority number represents the concept assessed with the highest expectation and:

- n = number of individuals assessing each concept
- T_i = the technical feasibility of the concept, as evaluated by the i^{th} individual
- E_i = the ease of demonstration of technical feasibility in terms of financial and manpower resources, as evaluated by the i^{th} individual
- P_i = the probability of user acceptance of the concept if it is demonstrated to be technically feasible, as evaluated by the i^{th} individual
- I_i = the impact or significance of successful implementation of the concept, as evaluated by the i^{th} individual

Quantities between 0 and 1 were individually assigned to each of the T_i, E_i, P_i, and I_i parameters to reflect quantified value judgements for each parameter.

Over 100 application concepts were identified and over one-third of these had sufficient priority to warrent Lewis Research Center in-house and/or contractual efforts involving various degrees of evaluation, development and technology transfer. The specific applications highlighted in this report represent many of these more promising applications. Some of the application concepts involve utilization of ion thruster components or thruster fabrication processes. However, most of the applications ion beam interactive processes. Experimental evaluation of many of the application concepts has required ion beam processing in the form of ion beam sputter etching, deposition or texturing through use of either 8 or 30 cm diameter ion sources in conjunction with their vacuum facilities as shown in Figs. 16 to 19.

INDUSTRIAL APPLICATIONS

Cold Welding of Ion Beam Cleaned Surfaces

Ion beam sputter etching can be used to remove surface oxides, contaminants, and adsorbed gases to produce an atomically clean metal surface. Two such metal surfaces will bond to each other at room temperature if pressed into intimate contact. Figure 20 shows such a cold welding system.[35] Copper to copper, aluminum to aluminum and copper to aluminum welds were successfully made using this system. Figure 21(a) depicts a copper to copper cold weld made by this simple spring pressure roller system. Figure 21(b) shows the result of heating the welded sample to allow some grain growth across the weld interface indicating metallic bonding at sites along the weld. This process may have application for precious metal alloy cladding of microelectronic lead frames. A larger ion beam cold welding system has been constructed to allow a broader range of materials to be clad and permit quantification of the industrial requirements for ion beam cold welding (see Fig. 22). For high rate industrial cold welding, gross cleaning would probably be done by magnetically enhanced discharge sputtering in differentially pumped chambers prior to the metal strips being maintenance cleaned by the ion beam.

Potential space applications of such a cold welding technique include fabrication and assembly of large space structures (see Figs. 23(a) and (b)). Such applications would advantageously utilize the vacuum environment of space to perform the sputter cleaning.

Corrosion Inhibition by Ion Bombardment

Energetic ion bombardment of surfaces will cause implantation of the bombarding species which may alter the corrosion characteristics of metals. For the typical ion energies (<10 keV) produced by most conventional ion sources, only very shallow implantation occurs. However, preliminary tests performed by Wilbur[36] using only a 200 eV mercury ion beam has indicated that ion bombardment doses of 5 to 15×10^{17} mercury ions/cm^2 reduces oxidation of carbon steel. The cause of the observed corrosion inhibition is, at present, not known and is somewhat surprising because it is achievable at such low energies. Comparison with other bombarding species may provide some insight as to the physical or chemical processes involved. The use of broad low energy ion beams may allow a convenient process for creating corrosion inhibiting surfaces on sheet steel.

Die Casting Die Coatings

Dies used for industrial production of cast aluminum parts are quite expensive and represent a significant portion of the cost of the cast article to the consumer. Unfortunately, die casting dies

have a limited lifetimes due to the cyclic stress of their operational environment. Typically, molten aluminum is injected into a die made of H-13 die steel causing the die skin in intimate contact with the injected aluminum to rapidly thermally expand. After the aluminum cools to a frozen state the die is separated and the cast article ejected. The hot die surfaces are then sprayed with a water-lubricant to cool the die and to provide a surface coating that aids in the release of the cast article while preventing the aluminum from soldering to the die surface. The waterlubricant spray quickly contracts the hot die skin thus putting it in tension. This process is typically repeated for tens of thousands of castings. As a result of this cyclic stressing of the die surface, thermal fatigue cracking of the die skin initiates. With continued die use the cracks grow as shown in Fig. 24 to become so large that the cast article has their impression and often requires additional finishing for aesthetic acceptability. Ultimately gross die failure occurs from these large cracks.

A potential technique to increase die lifetime may come through inhibition of crack initiation or the retardation of crack propagation. Use of different bulk die materials would be very expensive because of the machining costs associated with these tough low-thermal-expansion materials. A thin adherent sputtered deposited coating over the H-13 die steel may be a cost-effective technique to reduce thermal fatigue cracking. The Lewis Research Center in collaboration with the American Die Casting Institute and the Metallurgy Department of Case Western Reserve University is currently evaluating the use of sputter deposited coating to increase die lifetime.[37,38] A wide variety of candidate coating materials have been tested by Mirtich[39] for suitability in terms of coating adherence for various film thicknesses from 0.5 to 10 μm. The coating materials included precious and refractory metals and metal oxides, nitrides, and carbides. Various coating deposition processes have been evaluated including ion beam sputter cleaning and deposition, R.F. sputter deposition, and ion plating. Promising candidate die coating materials were then evaluated by Wallace[37] in cyclic (15 000 cycles) molten aluminum dunk tests using sputter deposited coatings over H-13 die steel specimens (see Figs. 25 and 26). Preliminary results of these tests indicate that 1 μm thick molybdenum, tungsten, and platinum ion beam sputter deposited coatings (after sputter cleaning) reduce the maximum crack length and total crack area.[39] Actual production die cavity tests will be performed to determine the merits of such coatings in a functional environment.

Coatings for Steel Belting in Radial Tires

The tire industry produced approximately 183 million tires in 1978 with a large percentage of these being radial ply tires. Warrenty adjustments associated with the typical 2 to 3% return rate to the manufacturer for radial tire defects has been conservatively estimated to represent a yearly cost of 20 to 30 million dollars.[34]

Problems associated with rubber adhesion to steel belting in radial tires has been of significant concern. Van Doij,[40] discusses the fundamental aspects of rubber adhesion to brass plated steel tire cords. Currently, the steel belting wires are electroplated with brass then drawn through dies to reduce the brass coating thickness to 0.1 to 0.3 μm. Durable rubber bonding to the brass coating requires the development of $Cu_{1.95}S$ at the brass/rubber interface. The zinc in the brass helps in controlling the Cu to S ratio. The copper to zinc ratio of the brass and the thickness of the brass coating influence, in a time dependant fashion, the specific copper sulfide present and thus significantly affect the adhesion.

Through the use of sputter cleaning and deposition one can deposit thin and uniform copper or copper and zinc coatings on the steel belting strands. The ability to control composition and thickness of the deposit may enable increased durability of the rubber adhesion to the belting. By use of ion beam sputter cleaning and deposition of 0.05 μm copper films were deposited by Mirtich (of NASA Lewis Research Center) on steel belting strands. These strands were then vulcanized to rubber and evaluated for adhesion in an Instron tensile machine. The results to date are very encouraging and warrent further experiments.[34]

Diamondlike Coatings

Diamond is in a metastable state of equilibrium at room temperature and pressure and is therefore a difficult crystal to fabricate near such conditions. Various techniques have been used, however, to deposit diamond like films both epitaxially on diamond and on other substrate materials. Because most of the processes result in deposition of both graphitic and tetrahedral bonds, periodic selective removal of the graphitic phase is required.[41] Aisenberg[42] and Spencer[41] have reported the use of ion beams to deposit diamondlike films through simultaneous carbon sputter deposition and etching. Spencer[41] reports that carbon ions along with carrier gas ions with energies of 40-50 eV were impinged upon various substrate materials in a manner so as to produce polycrystalline films of tetrahedrally-bonded cubic diamond with particle sizes of 50-100 Å and with single crystal regions up to 5 μm in diameter. Single aperature ion sources were employed in which carbon surfaces at cathode potential within a carrier gas discharge were used as the source of carbon ions. The use of broad beam multiaperture ion sources to perform the diamondlike film deposition was considered in the IBAR program to be worthy of evaluation because of the potential of using these devices to coat large areas at higher deposition rates as would be needed for any industrial production of these films. Some of the potential applications of diamondlike films include semiconductors and protective coatings for optical surfaces such as eyeglasses and high speed aircraft polycabonate windshields.

A collaborative research effort has been established with NASA, 3M Manufacturing Co. Applied Science Laboratories[43] and the Angus Research Corp.[44] to use a 30 cm diameter ion source at the NASA Lewis Research Center to sputter deposit carbon films. The deposited films are being characterized by such technologies as elemental analysis, electron microscopy, Auger electron spectroscopy, X-ray diffraction, electron diffraction, multiple total reflection infrared spectroscopy, and X-ray photoelectron spectroscopy.

Two types of carbon deposition experiments have been performed to date by Mirtich.[39] One of experiments used methane as the source of carbon by feeding that gas into the discharge chamber of a 30

cm diameter argon ion source. The methane, along with a proportion of Argon gas, was then innized and accelerated at low voltages toward a target surface. The target surface could also have a D.C. or R.F. potential applied to it as desired.

A second deposition technique was used in which a 30 cm diameter argon ion source was used to sputter etch a carbon target as the source of carbon for deposition. The substrate which received the carbon deposition was simultaneously sputter etched using an 8 cm diameter argon ion source.

Samples of deposited films are currently being characterized to determine if they are diamondlike.

Simultaneous Deposition and Sputter Polishing

Ion beam polishing, abrasive polishing, electropolishing, and machining are methods currently being used to polish metal surfaces for optical or asthetic purposes. These methods typically remove material from the surface often exposing contaminants and inclusions, while failing to fill in voids. Sputter or vapor deposition incident perpendicular upon a rotating surface simultaneous with grazing incidence ion beam sputter etching can produce a reasonably dense void-free polished surface. Such surfaces are potentially suitable for laser mirror having a high damage threshold.[45] Figure 27 depicts the above concept for ion beam sputter etching simultaneous with either vapor deposition or sputter deposition. Figure 28 is a scanning electron photomicrograph of a copper substrate that was microscopically scratched with sandpaper prior to simultaneous copper sputter deposition and sputter polishing. The lower half of the photograph shows the initial scratched copper surface which was protected from direct deposition by a colloidal carbon coating which was later removed after the test. The upper half of the photograph shows the sputter polished deposit which appears smooth and void free. Results from profilometer traces of these surfaces indicate that the root-mean-square roughness of the simultaneously sputter deposited and polished coating is smoother than the sanded substrate but rougher than a mechanically polished surface. Although a simultaneously sputter deposited and polished surface is not as smooth as a mechanically polished surface, it may have a higher laser damage threshold because there should not be as many localized sites of high optical adsorption as occurs on mechanically polished surfaces. The additional roughness of the sputter treated surface may result in an increase in the amount light that is diffusely rather than specularly reflected.

Modification of Optical and Electrical Properties of Surfaces

Ion beam natural texturing of some polymers and alloys or seed texturing of many pure metals has been shown by Hudson, Mirtich, Weigand, and Sovey to result in microscopic surface textures whose optical properties are substantially modified.[46,47] Figure 29 shows scanning electron photomicrographs from Ref. 47 of 8 μm thick polyimide (Kapton®) after exposure for various durations to a 1000 eV argon ion beam at 1.8 mA/cm^2. Figure 30 shows the effect of various durations of ion beam natural sputter texturing upon the spectral transmittance of the polyimide.[47] The ion beam sputtering etching of polyimide, as with many polymers, creates a thin surface coating of free carbon from the polymer chain scission processes occurring during ion bombardment. This coating along with the morphological changes in the surface results in altered conductivity, reflectance, adsorptance, and transmittance as shown in Fig. 31.[47] The conductivity and increased emittance of ion textured polyimide may be of application for space solar concentrators to prevent differential charging and to maintain desired temperatures.

Seed textured metals shown in Fig. 32 have grey to grey-black appearances due to their surface structures decreasing their reflectance (as also shown in Fig. 32). The reflectances of polished surfaces of these metals are much higher than for textured surfaces. Because textured surfaces have high solar adsorptances as a result of a left standing surface microstructure rather than a painted or deposited on coating, a potential exists for their application as central receiver surfaces for space or earth based solar concentrators without concern of surface degradation due to spalling or peeling. A space experiment on a shuttle launched Long Duration Exposure Facility is currently planned to evaluate optical property durability of such surfaces in space.

Traveling Wave Tube Depressed Collectors

Depressed collectors used in traveling wave tubes (TWT's) to collect the spent electron beam from the microwave amplifier portion of the TWT can have significant impact on the overall efficiency of the microwave amplifier system. Power is lost if, in the process of spent electron beam collection, secondary electrons are produced or the primary electrons are reflected. As a result of those potential power loss considerations, it is desirable to choose depressed collector materials that both satisfy the fabrication and operational constraints and, in addition, have a low secondary electron emission ratio, and a low reflected primary electron yield.

Sputter textured surfaces of some metals and pyrolytic graphite have surface microstructures that tend to trap electrons (both primary and secondary electrons) when subjected to electron bombardment. Wintucky, Curren, and Sovey[48] have shown that textured pyrolytic graphite has a lower secondary electron emission and reflected primary yield than carbon soot which has long been regarded as the ultimate surface for capturing electron beams without significant secondary or reflected primary electron release. Because pyrolytic graphite has a low sputter etch rate and can survive high temperatures, discharge chamber triode sputtering was used, as shown in Fig. 33, to produce a natural texture (see Fig. 34). It is not known at present what causes this natural texture to develop in pyrolytic graphite. This natural texture also develops in common polycrystalline graphite. The purity of the graphite does not seem to play a significant roll in the development of natural texture in pyrolytic graphite, because similar structure is developed in both graphite pyrolyzed from natural gas and high purity synthetic methane.

Figure 35 compares the secondary electron electron emission ratio and reflected primary electron yield of smooth pyrolytic graphite, discharge chamber triode-sputter-textured graphite and soot. A space traveling wave tube experiment for an advanced communication satellite is currently being planned by the NASA Lewis Research Center which utilizes

such sputter textured surfaces for it depressed collectors.

Fluoropolymer Bonding

Ion beam sputtering of fluoropolymers such as polytetrafluoroethylene (PTFE Teflon®), fluorinated ethylene propylene (FEP Teflon®), perfluoroalkoxy (PFA Teflon®), and polychlorotrifluoroethylene (CTFE Teflon®) causes the development of a natural texture as shown in Fig. 36.[49] The size and shape of the surface microstructures is dependent upon the sputtering conditions. Such textured surfaces allow strong adhesive bonding of these fluoropolymers which are typically difficult to bond in a high strength durable manner. The bonding adhesive must be applied as a fluid and have a small enough contact angle with the fluoropolymer to allow the uncured adhesive to flow in and around the surface microstructures. When the adhesive hardens the surface microstructures are then potted in the adhesive thus forming a predominantly mechanical bond to the adhesive. The tensile and shear strength epoxy bonds to ion beam natural textured fluoropolymers has been demonstrated to be superior to conventional sodium/napthalene chemically etched surface treatment as a surface preparation technique (Fig. 37 and Ref. 47). In addition, Fig. 38 shows the tensile and shear strengths of various epoxy bonded textured fluoropolymers.

There are numerous applications for fluoropolymer bonding that in general deal with anchorage of fluoropolymers to other materials for the purposes of taking advantage of the fluoropolymers electrical, thermal, chemical, and nonsticking or tribological properties. Some of the potential applications include: printed circuit board laminates, flexible flat lead laminates, formed laminates for electronics cans, food processing equipment surfaces and bridge bearing surfaces. Figure 39 shows an electret microphone whose circuit board has a PTFE Teflon® sheet laminated to it prior to being perforated with two holes. As can be seen by the light appearing areas, where delamination has occurred, the electret fabricated with the textured PTFE Teflon® survives the perforating much better than the untextured PTFE Teflon . The industrial application of utilizing ion beam textureo fluoropolymer laminates is being evaluated by the TME Corp. of Hudson, New Hampshire under NASA Contract.[50,51]

Cost effective texturing of fluoropolymers will, of course, require that the sputtering durations be reasonably short. One technique that may speedup the texturing process is to dust the fluoropolymer surface with thin dispersed layer of fine sputter resistant particles. The fine particles would act as a sputter resistant mask and produce left standing microstructures on the fluorpolymer surface that are significantly higher than the natural texture. Figure 40 is a scanning electron photomicrograph of natural textured FEP Teflon® in which two small sputter resistant particles have enabled full etch height left standing pillars to develop which, as can be seen, are much taller than the surrounding natural texture. Various techniques have been evaluated, in a preliminary manner, to distribute and attach particles across the fluoropolymer surfaces such as dusting the surface, pressing particles into the surface, and electrophoretic deposition.[52] Figure 41, for example, is a scanning electron photomicrograph of a sputter etched PTFE Teflon® surface that was covered with silica particles to produce large microstructures.

Ion beam sputter texturing of fluoropolymers on a production scale would probably require large areas to be treated while minimizing the number of times the vacuum facility must be evacuated or bled up. Feeding wide fluoropolymer sheets on a reel-to-reel system past rectangular beam ion sources appears to be a practical batch treatment approach.[42] A reel-to-reel fluoropolymer batch texturing system is currently being developed by Technics, Inc. under NASA contract.[53] The design drawings and performance characteristics of a commercial grade 5x40 cm rectangular beam ion source, suitable for reel-to-reel fluoropolymer texturing, have been developed and published by Kaufman and Robinson.[54,55] This rectangular ion source shown in Fig. 43 is designed to operate on argon gas and produce a 500-1500 eV ion beam with up to 3 mA/cm^2 current density average at distance 10 cm downstream from the ion source.

Liquid Crystal Alignment Surfaces

Oblique ion beam incidence on metal oxide surfaces will cause the development of directionally oriented left standing surface microstructures. Figures 44(a) and (b) are scanning electron photomicrographs (by Wintucky, Mahmood, and Johnson,[56]) of SiO_2 and ZrO_2 surfaces that have been bombarded by an argon ion beam at an angle of 40° from the plane of the surface. Such surfaces are capable of producing homogeneous alignment of nematic liquid crystal molecules. The use of ion beam sputter textured alignment surfaces instead of the more conventionally used obliquely vapor deposited SiO_2 surfaces, may enable the emergence of new types and applications of liquid crystal displays. Specifically, the high extinction ratios (>1000), small twist angles of (<3°) and small (<1°) tilt bias angles may enable satisfactory alignment at higher temperatures and have greater visibility.[56,57] Improved performance liquid crystal display devices would have a strong potential market place in large area displays for the automotive, marine, and avionics industry. The small tilt bias angle of ion beam sputter surfaces may allow the operation of surface mode displays in which only the liquid crystal material at the alignment surface is switched. Such surface mode devices are capable of switching at audio frequencies. Surface mode liquid crystal devices such as communication light modulators and planar replacements for cathode ray tubes may also be potential applications. The American Liquid Xtal Corp., under NASA contract,[57] will experimentally evaluate the optical, electrical, and environmental performance of ion beam sputter etched liquid crystal display test cells. They will also evaluate the cost-effectiveness and market potential of utilizing these cells for specific applications and types of displays.

Texture Bonding

The textured surfaces of metals (whether they are natural or seed textured) can be used to mechanically interlock with other metal textured surfaces. This is accomplished by placing the textured surfaces toward each other and plastically deforming the surface microstructures of one surface into the other as shown in Fig. 45. Surface textures such as those of tantalum seed textured copper (Fig. 32(a)) and aluminum (Fig. 32(c)) can be mechanically bonded by simply a hammer blow to nest and deform the microstructures. Table II lists the shear and tensile strengths of copper-copper, aluminum-aluminum, and

copper-aluminum texture bonds. Although the bond strength are not large, there may be applications of this one-timemetal-Velcro® in large space structures where bonding without adhesives may be desirable for thermal or cleanliness reasons.

Nucleate Boiling

Textured surfaces enhance nucleate boiling heat transfer rates over smooth surface materials because of the increased number of bubble nucleation sites. Figure 46(a) shows a scanning electron photomicrograph of Ta seed textured copper. The nucleate boiling heat transfer rate of this surface using freon 113 as the working fluid is compared to an untextured copper surface in Figure 46(b).[58] Such improved heat transfer characteristics if demonstrated as durable, may significantly reduce the size and cost of industrial reboilers since less heat transfer area would be needed for a given boiling task.

Capacitors

The capacitance of a parallel plate capacitor is simply

$$C = \frac{k\epsilon_0 A}{d}$$

where

K = dielectric constant
ϵ_0 = permittivity of free space
A = capacitor area
d = capacitor plate separation

Ion beam sputtering may potentially be used to increase this capacitance by: sputter depositing materials with a higher dielectric constant, K; texturing the capacitor electrode surface to increase the area, A; or to sputter deposit thinner dielectrics and reduce d.

Thin film capacitors fabricated from ion beam sputter deposited electrodes and PTFE Teflon® have been successfully fabricated with dielectrics as thin as 0.1 μm.[27,28]

Efforts to increase the effective surface area of capacitors by ion beam texturing has been investigated by Topich.[59] Tantalum seed texturing of silicon was first performed to produce 0.1 to 1.6 μm cones then the textured surface cones were oxidized in dry O_2 at 1050° C for 1 hour to create the dielectric layer. The oxidized cone surface were then metalized with aluminum. Although the capacitance per unit area was increased by up to a factor of 2.3, they exhibited a diode like characteristic similar to Schottky diodes thus greatly reducing their utility as capacitors.

Hollow Cathodes for Magretic Fusion Neutral Beam Injection Sources

Electron bombardment ion thrusters utilizing hollow cathodes have been operated on hydrogen propellant by Sovey and Mirtich.[60] The technology associated with such a device is suitable for utilization in hollow cathode deuterium ion sources for fusion neutral beam injection systems. A study assessing the applicability of ion thruster technology to neutral beam injection systems has been performed by Schwirzke.[61] Replacement of short lived filaments with hollow cathode should allow reliable and durable injection source operation with reduced maintenance requirements.

BIOMEDICAL APPLICATIONS

The ability to chemically or morphologically alter surfaces of biological materials and implants in ways previously unavailable has provided many new biomedical application concepts that may some day result in improved surgical implant devices or new medical diagnostic techniques.[62,63]

Biomaterial Modification by Ion Beam Processing

Materials used in the fabrication of surgical implant devices must satisfy a wide range of constraints if acceptable long term performance is required. The chemical, morphological and mechanical characteristics of these biomaterials play an important role with respect to resulting tissue response and implant durability. Ion beam processing (sputter etching, deposition, or texturing) can alter these biomaterial characteristics in a manner potentially useful for improvement of the performance, durability, or tissue response of surgical implants. In addition sputter etching or texturing of biological tissue may provide a new type of diagnostic capability.

Surface chemical modification of biomaterials. - Ion bombardment of biomaterial surfaces in the energy range of hundreds to thousands of electron volts will generally cause some surface chemical and morphological changes in a material if it is anything other than a pure single element material.

In the case of sputtering of metal alloys, such as used in orthopedic implants, sputter etching causes a change in the surface element population. Initially, as a surface is being sputter etched, the high sputter yield elements are preferentially removed. As the surface atom population of the alloy begins to increase in the proportion of the remaining high sputter yield material, the sputter efflux composition will approach the bulk material composition in terms of relative abundances of each of the species. However, the sputter etched alloy skin will have an abundance of low sputter yield elements (typically the higher melting temperature refractory metals). This altered compositional layer is probably just a few monolayers thick and may be quickly further altered or removed in a biological environment.

Ion bombardment of organic materials, if performed at sufficiently low arrival power densities to prevent bulk thermal decomposition, will cause molecular fragmentation. Sputter etching of polymeric materials will, however, cause chain scission and the possible exposure of free radicals.[17,62] As a result, surface chemistry can range from being identical to substantially different from the parent material depending upon the specific material chemistry. Two methods that have been used to help characterize the chemical consequence of ion beam sputtering of biopolymers are the use of Electron Spectroscopy for Chemical Analysis (ESCA) and contact angle measurements. ESCA studies of surface chemistry alterations and contact angle characterization of biopolymers has been previously reported in Refs. 64 to 66 and are summarized in Tables III

and IV. Because sputter etching typically causes both chemical and surface morphological changes it is difficult to attribute alterations in contact angle or mechanical properties specifically to one or the other cause. However, by sputter polishing one can minimize the morphological alterations while allowing chemical modifications to take place. In-vivo tests of such materials have been performed and are reported under the Soft Tissue Implant Section.

Surface morphology modification of biomaterials. - Surfaces of most biomaterials can be morphologically altered by means if ion beam sputter etching surface morphologies appropriate for tissue ingrowth can be produced by sputtering through electroformed screen mesh masks that are held in intimate contact with the target. The resulting sputter etched surface pits are shown in Fig. 47. The sputter etch rate of the screen mesh relative to the target material determines the maximum depth to which the pits can be sputter etched prior to complete sputter loss of the mesh. For high sputter yield target materials such as polytetrafluoroethylene (PTFE Teflon®) small closely-spaced pits can be etched which are much deeper than they are wide.

Some of the known biopolymers which develop a natural texture as a result of ion beam sputtering as demonstrated by Weigand[65] and are shown in Fig. 48. Polymers that do not develop any significant natural texture include polyethylene and silicone rubber (Silastic®).

A natural (Fig. 11) or seed texture (Fig. 49) can be generated in most of the orthopedic alloys. As can be seen, the surface microstructures are typically a few microns high or smaller.

Associated with both the screen mesh mask and seeding techniques to alter surface morphology there is some contamination of the target material with the mesh or seed material. This can be partially removed by further sputter etching after the mesh or seed material target is removed. Short durations of such cleanup sputter etching does not substantially alter the previously developed surface features. However, a small amount of these materials remain entrapped via sputter etch and redeposition processes. This is very apparent in nickel mesh sputter etching to produce pits in white polytetrafluoroethylene (PTFE Teflon®) whose surface is considerably darkened as a result of entrapped nickel. Cleanup sputter etching and aqua regia acid bathing appears to eliminate much of the mesh atoms but a small fraction usually remains entrapped.

In addition to surface texturing biomaterials, experiments have been performed concerning the sputter etching of biological derived materials. Sputter etching by ion beam or R.F. sputtering has been performed on teeth,[67] corn pollen[68] normal, and pathological (sickel cell and hemoglobin abnormality Hb-Köln) red blood cells,[69] snail neurons,[70] fibroblast (BHK21 clone C_{13} and similar cells having undergone malignant transformation),[71] and normal and malignant human subependymal glioma cells.[71] Many of these tests have shown that ion sputter texturing can be used as a dignostic technique for pathological discrimination. For example, ion beam texturing of such fragile biological entities as chromosones may allow unique or additional visualization of chromosone ultrastructure morphology. This could result because sputter yield differences would provide a uniquely different discriminating mechanism to that of current staining and banding techniques used for karyotypic investigations.

Transfer casting. - Frequently a morphology desirable for biomedical application is achievable by ion beam sputtering but not in the specific biomaterial required. When the biomaterial desired is an elastomer, a potential solution exists. The desired morphology can be sputter etched or textured in a fluoropolymer such as polytetrafluoroethylene then the biopolymer desired can be cast (in air or partial vacuum) in a liquid uncured state over textured surface. Upon curing the elastomeric polymer is then peeled of the sputter modified substrate to yield a transfer cast negative of its surface morphology. Figure 50 depicts such a transfer cast technique using silicone rubber (silastic®) peeled from a polytetrafluorethylene (PTFE Teflon®) surface with an array of pits produced by ion beam sputtering through an electroformed nickel screen mesh. As can be seen from Fig. 50(a) a few pits failed to release the silicone rubber pillars upon transfer casting. In many cases a thinnly applied mold release agent may assit in a satisfactory release. Other biopolymers such as segmented polyurethane (Biomer®) have been successfully transfer cast (see Fig. 51[72]).

The small surface features of a natural sputter textured polytetrafluoroethylene surface can also be transfer cast. The resulting morphologies are shown in Fig. 52.[72] Release agents used to assit in peel off from such small surface features must be applied as a very thin layer to prevent fill in of these features.

Peritoneal Implants

Peritoneal implants (implants placed within the peritoneum) have been used to evaluate cellular response to biomaterials. The peritoneal cavity of a rat is a convenient environment for the characteristics of cellular interactions with foreign surfaces. The continual bathing and exchange of fluids in the pentoneal cavity, in addition to the presence of a variety of cell types, affords an ideal in vivo tissue culturing system.

The pertioneal cavity of male Sprague Dawley rats were used by Picha[73] to evaluate the kinetics and histology of cell attachment to ion beam natural textured polytetrafluoroethylene (PTFE Teflon®). Ion beam sputter-polished polytetrafluoroethylene samples along with smooth surfaced segmented polyurethane and 2-hydroxyethylmethacrylate (a commercial opthalmic grade) samples were also implanted to allow a comparison between the response to textured and untextured implants of identical and different chemistry. All implant samples were 0.8 cm in diameter and approximately 1 mm thick. For further comparison purposes some of the polytetrafluoroethylene samples had a pitted surface formed by sputtering through a screen mesh and other samples were natural textured over only one-half of the surface with the remaining surface being smooth and untreated.

The results of documentation of cell attachment as a function of implantation duration for the various surface textures and materials are shown in Fig. 53. As can be seen, cells much more readily attach to the natural textured polytetrafluoroethylene surface than any of the other smooth surfaces

in spite of its hydrophobicity. Texturing polytetrafluoroethylene increases cell attachment by an order of magnitude over smooth (ion polished or untreated) surface polytetrafluoroethylene. Figure 54 compares the cell attachment to smooth and natural textured polytetrafluoroethylene samples after 3 days of implantation. The principal cells observed in attachment to the implants were macrophages, lymphocytes, and to a lesser degree mast cells. Surface texturing was also found to increase the formation of multinucleated giant cells.

Because of the cell attachment affinity of the natural textured surfaces, the potential exists for using this capability to evaluate diseased states that are characterized by the lack of cellular adherence to surfaces. Of specific potential application are hematological disorders with platelet disfunction or blood protein disorders.[73]

Soft Tissue Implants

A great variety of soft tissue implants are currently being used in cosmetic plastic and reconstructive surgery. Ion beam sputtering provides a capability to fabricate unique surface morphologies on many biomaterials, thus allowing experiments to be performed to understand the effect of surface texture on soft tissue response. Studies involving natural sputter textured soft tissue implants of polytetrafluoroethylene and polyoxymethylene (Delrin®) have been performed using Sprague Dawley rats.[74,75] Ion polished and untreated samples of both materials were also implanted. All implants were 1 cm diameter disks of specific thicknesses (50, 125, or 250 um) and were placed immediately adjacent to the fascia of the intercostal musculature.

The soft tissue response to both sputter polished and untreated implants of polytetrafluoroethylene and polyoxymethylene were identical as determined by histochemical and histological examination. Ion beam sputter texturing of polytetrafluoroethylene and polyoxymethylene implants induced the following modifications in the mononuclear phagocytes adjacent to the implant surface: increased cell adhesion, increased metabolism, increased acid phosphatase activity, increased vacuolization, increased filopodia formation, and increased foreign body giant cell formation. The kinetics of the fibrous capsule formation are also altered by the presence of textured surfaces as shown in Fig. 55.[75]

The ability to alter fiberous capsule formation is of significant importance to reconstructive surgery of the breast. Soft tissue response leading to fiberous capsule contracture is one of the most common difficulties associated with mammary prostheses.[33] Research directed to evaluate tissue response including fiberous capsule contracture is currently being performed in rats by Gibbons[76] using simulated mammary prosthesis. The implants consist of a fluid cylinder whose tissue contacting surfaces are transfer castings from ion beam sputter textured polytetrafluoroethylene. Pillar surfaces similar to Fig. 51 are being investigated in these experiments.

The humoral components of the exudate associated with implants is altered by the presence or absence of surface texture on the implant.[76] Experiments have been performed with exudate extracted from within hollow cylindrical subcutaneous implants having smooth or ion beam natural textured polytetrafluoroethylene surfaces. The exudate extracted from implants within rats was then evaluated for growth stimulation ability by using 3T3 cell cultures to measure cell number and tritiated thymidine incorporation. The results of these tests comparing smooth and textured surfaces indicate increased cell growth activity for exudate extracted from textured implants within approximately the first week of implantation. At later times there is no significant differences in cell growth activity between smooth and textured surfaces.

Cardiovascular Prostheses

The utilization of ion beam surface modification of biomaterials for investigations involving blood contacting surfaces has been of significant interest. Tests involving direct ion beam sputter natural texturing of biopolymers have indicated significant changes in blood response result as a consequence of both chemical and morphological surface alterations. Figure 56 shows a segmented polyurethane vascular patch implant used to evaluate the effect of ion beam sputter surface modification.[63] The implants with chamfered edges and embedded sutures were exposed to a 20 $\mu A/cm^2$, 500 eV, xenon ion beam for 30 minutes. Figure 57 shows scanning electron photomicrographs of the surface before and after ion beam sputtering. Some insight relating to the surface chemical changes may be inferred in Tables III and IV even though a different bombarding species was used. The sputtered and untreated implants were implanted against the inside walls of canine femoral and carotid arteries in a manner so as to prevent blood exposure of the sutures. The results of the experiments indicate significant differences in the blood response between the sputtered and untreated implants for implantations of 1 hour as shown in Fig. 58. After 4 days implantation very little difference if any is apparent. As a consequence of these tests, it was apparent that further testing should be performed in a manner to allow discrimination between blood response due to morphological as opposed to chemical surface alteration.

The use of transfer cast biopolymers peeled from ion beam textured surfaces allows morphological changes to be fabricated with minimal surface chemical alteration. Two areas of application currently being experimentally investigated involving such transfer casts of blood contacting surfaces are microvascular grafts and left ventrical assist devices.

Microvascular grafts. - Thrombogenic behavior of current arterial vascular grafts has limited the range of application of such devices to relatively large diameters (>5 mm) graft applications. A need exists in reconstructive surgery for occlusion free synthetic grafts of approximately 1 mm diameter. Experiments are currently being carried out by Gibbons[76] to compare the performance of transfer cast textured polymers with microporous polymers in microvascular grafts in Sprague Dawley rats. The grafts will be implanted as arterial segments in the intrarenal aorta and proximal femoral artery. Transfer castings will be fabricated by a peel off of the cured polymer from a screen mesh sputter etched polytetrafluoroethylene mandral. Figure 59 indicates the sputter etching technique to produce a pitted surface on the polytetrafluoroethylene mandrel. Once the peeled off graft is again turned inside out, it will have a pillar surface texture on

its inside (blood contacting) surface. Pillar structures 17 to 28 μm wide by the same and double in height will be evaluated. Similar size bulk porous graft coatings will be fabricated for blood response comparison purposes by using the replamineform technique[77] with the sea urchin Heterocentrotus trigonarius.

Left ventricular assist devices. - One of the most difficult technical challenges facing the biomedical engineer is the development of a satisfactory blood contacting surface for implantable blood pumps. Biomaterial mechanics, dynamics, durability, surface morphology and chemistry are among the many considerations pertinent to the choice of an appropriate blood pump bladder material. The use of transfer cast biopolymers from ion beam textured surfaces provides the opportunity to investigate variations in blood pump surface morphology using bladder materials currently of interest. A cooperative program[78] has been established between the NASA Lewis Research Center, Thermo Electron Corporation and the National Heart Lung and Blood Institute to evaluate blood response to surface morphologies transfer cast from ion beam textured surfaces. Left ventricular assist devices, sized for potential human application (see Fig. 60), will be implanted in calves. The blood pump bladders will be fabricated by transfer castings from shaped and sputter textured polytetrafluoroethylene mandrels. Figure 61 depicts the function of the axisymmetric bladder. The blood contacting surfaces of such a bladder must be designed so as to minimize neointima thickness and remain well attached to it as well as to reduce the probability of embolic complications. A variety of transfer casting techniques have been explored using approaches other than ion beam sputtering to fabricate textured mandrel surfaces. The results of blood pump bladder tests using these types of textured surfaces have shown that the neointimal lining is at least as thick as the bladder surface texture.[78] Conventional silicone rubber mandrel fabrication and electrostatic fibril flocking techniques have prevented the evaluation of surface textures (and therefore neointima) smaller than approximately 250 μm. The application of ion beam sputtering techniques as shown in Fig. 59 using bladder shaped polytetrafluoroethylene mandrels allows fabrication of bladders having surface microfeatures in the 0-300 μm range. The heights of the resulting surface pillars, similar to those shown in Fig. [illegible] are simply dependent upon the duration, current density, and ion energy used for the mandrel sputtering. The bladders will be fabricated out of segmented polyurethane (Biomer®).

Hydrocephalus Shunts

The obstruction of cerebrospinal fluid flow pathways or its inadequate absorption via the arachnoid villi into the venous blood of the brain results in hydrocephalus. The occurrence of hydrocephalus is quite common. An estimated one infant in 300 is born with the condition and an additional one in 100 acquires it as a result of childhood illnesses such as meningitis.[79] Hydrocephalus is also more prevalent in developed nations where a higher survival rate for premature infants exists. Without surgical treatment approximately one-half of the infants would die and the other half suffer from severe mental retardation.[80] Surgical correction involves pressure controlled shunting of the cerebrospinal fluid. Typically a perforated silicone rubber catheter is implanted in one of the lateral ventricles of the brain with its perforated tip located near the frontal horn (see Fig. 62). The cerebrospinal fluid then passes through a pressure regulating valve and is then typically shunted to the right atrium of the heart or the peritoneal cavity. The shunt will fail to function if the inlet ventricular catheter aperatures become blocked by cellular ingrowth of the chorid plexus or cellular debris within the cerebrospinal fluid. Shunt flow failure will also occur if the ventricle collapses due to improper valve function causing over drainage.

Ion beam sputtering can be used in conjunction with screen masks (see Fig. 59) to produce polytetrafluoroethylene tubes with many small apertures as shown in Fig. 63. The use of sputter etching to perforate the inlet ventricular cathether allows fabrication of catheters having two orders of magnitude increase in aperture density over that of conventional catheters (because approximately 1100 apertures each 20 μm in diameter can be placed along a 1 cm length of catheter). The catheter itself being comprised of one or more tubes each being only 0.44 mm in diameter. The large number of inlet apertures may reduce the tendency for the shunt to draw in and trap debris or tissue which would then cause flow obstruction.

The feasibility of using ion beam sputter ventilated polytetrafluoroethylene microtubules to shunt cerebrospinal fluid directly from the lateral ventricals upward to the subarachnoid space is being investigated by Foltz.[81] This shunting concept, shown in Fig. 64, does not use a valve and returns the cerebrospinal fluid to its site of normal adsorption. The investigation involves bench flow testing and hydrocephalic canine tests to be performed using microtubules as shown in Fig. 63 in which both the inflow and outflow ends are perforated.

Percutaneous Connectors

Penetrations of the skin for the conveyance of electricity, liquid or gaseous fluids or mechanical forces require an effective seal at the skin-percutaneous connector interface to prevent infection. The potential applications of percutaneous connectors cover a broad spectrum of devices such as muscle stimulators, hemodialysis canulas colostomy or ileostomy orifices, intraveneous catheters and skeletal extensions for amputation devices. Satisfactory long term use of many of these percutaneous devices has frequently been inhibited because of epidermal cell ingress and growth along the implant-tissue interface. The resulting marsupialization results in a loss of a body fluid seal and ultimately infection occurs. Surface texture and porosity have been shown to reduce epithelial cell down growth in animal tests involving velour fabric and porous percutaneous connectors.[82,83] However, the use of bulk porous materials permits bacterial invasion via the interconnected pores.

The use of ion beam sputter textured or transfer cast polymer surfaces provides a surface roughness without bulk porosity. Such surfaces have been evaluated by Pitha and Gibbons[84] in the dorsum of cats using polytetrafluoroethylene (Teflon®), polyoxymethylene (Delvin®), and segmented polyurethane (Biomer®). The implant configuration is shown in Fig. 65. Implantation protocol including identification of Langer line orientations, exit wound geom-

etry optimization and identification of an implantation technique involving pulling the connector through a subcutaneous pocket was developed to minimize percutaneous connector performance dependence upon the degree of tissue contact with the connector at the percutaneous exit site.

A percutaneous device application effort is currently underway to identify an optimal transfer cast pillar morphology (such as in Fig. 51) in segmented polyurethane (Biomer) and to utilize this surface structure in the design of functional percutaneous connector devices.[85]

Dental Implants

Initial concepts involving the application of ion beam technology to dental implants were based on simulation of the surface morphology of the cementum by means of ion beam natural or seed texturing to achieve a higher implant success rate. These efforts utilized endosteal blade type implants (see Fig. 66) of natural textured MP35N (35% Ni, 35% Co, 20% Cr, 10% Mo) and tantalum seed textured pure titanium in a canine evaluation.[86] Figure 67 compares the surface morphology of cementum with an untreated and tantalum seed textured pure titanium. The textured surface morphology of MP35N can be seen in Fig. 11. The lack of sufficient numbers of implants prevented any statistically significant conclusions from being drawn as to whether a closer simulation of cementum morphology resulted in improved dental implant performance.

Canine tests have also been performed to evaluate zirconia coated (by R.F. sputter deposition) cobalt-chromium-molybdenum dental implants in which the surface texture was either smooth or pitted at the osseous level by sputtering through an electroformed screen mesh.[87] The pits were square (150 μm wide on each edge by 80 μm deep) and the zirconia coating was 0.5 μm thick. The implant test periods for evaluation ranged from 6 weeks to 1 year and 21 pitted and 21 smooth implants were evaluated. The results of clinical evaluation of the performance of the implants indicated a success to failure ratios of 0.6 for the pitted surface implants and a 2.3 for the smooth surface implants. The increased failure rate of the pitted surface implants can be characterized by gross mobility, inflammation, hyperplasia, dehiscence, and significant pericervical bone loss.

Cylindrical aluminum oxide implants with sputter etch pitted surfaces have also been evaluated as canine dental implants.[88] The pits were approximately 150 μm on each edge by 35 μm deep (see Fig. 68). Results of experiments involving 10 pitted and 10 smooth implanted for 6 months indicate no statistically significant difference in the clinical performance or mechanical retention of the implants. Sputtering pits in the surface increased the flaw density and reduced the mean strength of the material. However, in vivo aging (in canine dorsum subcutaneous sites) increased the mechanical strength (higher modulus of rupture and decreased Weibull modulus) of the textured implants and reduced that of the smooth implants.

A Dental Implant Assessment Seminar[89] was held at the Case Western Reserve University School of Dentistry on May 3, 1979 to review assess the results of Babbush's ion beam textured dental implant experiment[86] and identify a suggested direction for future research. The seminar consisted of a panel of 13 members which involved peer group participation of other dental implant researchers. As a result of the findings of this seminar a greater emphasis was placed on examination of use of textured surfaces at the gingival percutaneous location rather than at the osseous level. This recommendation was based on information indicating that a significant fraction of dental implant failures occur as a result of peridontal disease resulting from an ineffective percutaneous seal rather than problems associated with anchorage in bone. Subsequent to these findings a dental implant canine evaluation effort has been established[90] which specifically focuses on the identification of the morphological requirements to produce an effective percutaneous seal at the site of gingival penetration. The surface morphologies to be examined will be both high and low modulus polymers such as epoxy (Hysol®729), segmented polyurethane (Biomer®), and silicone rubber (Silastic®). The surface microstructure textures will be produced by transfer casting from polytetrafluoroethylene which has a pitted surface produced by ion beam sputtering through an electroformed nickel mesh mask (see Figs. 50 and 51). The surfaces to be evaluated will be on the cylindrical collar around a threaded 316L stainless steel implant. To reduce the tendency for epithelial cell downgrowth, two techniques will be evaluated which allow a 1 month precursor ingrowth of the subcutaneous tissue to the textured collar prior to percutaneous gingival penetration: (1) subcutaneous implantation prior to punching a hole in the gingiva for percutaneous penetration (see Fig. 69(a)) and (2) subcutaneous implantation prior to slow pressure necrosis by a wide-headed screw to enable an eruption of the percutaneous penetration (see Fig. 69(b)).

Orthopedic Implants

Orthopedic prostheses typically require firm mechanical anchorage to the skeletal structure to insure satisfactory long term performance. Most of the current artificial joints utilize a polymethylmethacrylate bone cement for stem fixation (Fig. 68). This less than optimum fixation method can result in stem loosening and is the most important cause of failure.[91] A variety of techniques have been employed in an attempt to provide stem fixation without the use of bone cement. Most of these techniques involve changes in the shape or porosity of the stems.[91] Large surface undulations in the stem may, with time, provide satisfactory anchorage. However, other serious consequences of that approach must be considered such as how long the patient must remain immobile to allow adequate bone ingrowth, inability to easily revise the implant if latent mechanical failure or infection occurs and reduction in fatigue strength resulting from the large surface undulations. Small surface undulations in orthopedic implants have been examined to a limited degree which utilize porous surfaces. Current fabrication techniques using scintering or diffusion bonding generally result in high surface area porous coatings having pore depths that are several orders of magnitude deeper than the pore diameters. Such surface porous metal coatings inhibit the removal of implant corrosion products and thus compromise the ability to reach an adequate state of homeostasis, especially for deep pore cellular ingrowth.

Ion beam sputter etching of a pitted surface morphology (by sputtering through a screen mesh) or

a natural texture can provide surface microroughness without the presence of deep pores. Implant evaluation of such surfaces have been performed by Gibbons[92,93] using pitted and textured surface cylindricals implanted in the cortex of canine femurs (see Figs. 71 and 72). The results of sputter etched pits 150 μm square by 28 to 60 μm deep in 316 LVM stainless steel, titanium (6% Al, 4% V), cobalt-chromium-molybdenum alloy, and MP35N (35% Ni, 35% Co, 20% Cr, 10% Mo) implants indicate bone-implant interfacial shear strengths from 0.97×10^7 to 1.24×10^7 Pa (1400 to 1800 lb/in.^{2}).[62] These shear strengths are also comparable to those of bulk porous implants and potential homeostasis difficulties should be reduced because the sputter pitted surface areas are much smaller than bulk porous surfaces. The results of similar tests of natural textured (see Fig. 11) MP35N and cobalt-chromium-molybdenum alloy cylindrical implants in bone show no stastically significant difference between textured and smooth implant shear strengths (both being approximately 2.7×10^6 Pa [390 lb/in.^{2}]).[93] Apparently the submicron to a few micron size surface features do not provide a mechanism for bearing shear loads in spite of the fact that similar sized surface features produce great increases in attached cell populations for peritoneal implants.

The application of sputter etched pit surface structures to direct ingrowth stem fixation will require additional knowledge of the short and long term consequences. The lack of bone cement would require other temporary fixation techniques and/or a period of patient immobility to prevent micromovement and allow sufficient time for bone ingrowth into the pitted surface. It is conceivable that electrostimulation of the stem may accelerate the ingrowth and stabilization processes. Research performed by Cochran, Bassett, and Pawluk has shown that bioelectric potentials can be stress induced in bone and conversely that the application of weak electric currents will stimulate bone formation.[94,95] The use of directly applied electrical stimulation of implants with sputter etched pits surfaces is being investigated by Pawluk and Bassett.[96] Crescent shaped implants (see Fig. 73) of 316 stainless steel and titanium (6% Al, 4% V) with pitted surfaces (etched by sputtering through an electroformed nickel screen mask) will be implanted in the cortex of canine femurs and be subjected to 5 to 8 μA of current applied to their 25.1 mm^2 of cortical bone contacting surface. Mechanical push out tests to evaluate shear strength and histological evaluation will be performed after 30 days of implantation.

The long term performance of direct ingrowth to pitted surface orthopedic implant stems may be dominated by the invivo fatigue characteristics of the implant if satisfactory stem fixation is achieved. Tensile stress fatigue tests have been performed on smooth surfaced, natural textured, and sputter pitted MP35N specimens in a physiological saline environment.[97] The results of these tests (shown in Table V) indicate a reduction in fatigue strength of approximately 50% at 2×10^7 cycles as a result of both a natural texture or pitted surface morphology in comparison to a sanded smooth surface. Thus, depending upon the implant configuration and functional demands, fatigue strength may or may not be of concern.

The hip prosthesis represents one of the most demanding stress environments for implant materials and their fixation to bone. Other orthopedic appliances may not be as demanding and yet benefit by direct ingrowth stabilization to microroughened roughened surfaces. Grommet bone liners for silicone rubber flexible implant arthroplasty of the small joints of the hand and foot are an example of one such application. A silicone rubber (Silastic® Swanson design) finger joint implant (shown in Fig. 74) may, upon repeated functional use, tear at the hinge location if sharp bone impinges upon the hinge so as to cut it. This is particularly a problem in patients with very thin bones due to osteoporosis. Failure rates from 5 to 25 percent have been reported for flexible finger joint implants.[98] The use of a grommet that fits over the stem of the implant with a flange to protect the hinge portion from being cut by bone would be of significant benefit. Such grommets should be anchored to the bone by a structured bone contacting surface; yet allow the flexible silicone rubber implant stem to slide freely during joint flexing.

A collaborative effort has been established with the NASA Lewis Research Center, the Veterans Administration, Blodgett Hospital, Michigan State University, Clemson University, University of Florida, and Dow Corning Corporation to develop and evaluate grommets suitable for protection of flexible finger joint implants.[98,101] Various materials and surface morphologies for bone ingrowth and anchorage have been considered that utilize ion thruster technology in the form of either ion beam or ion thruster fabrication technology. These include:

1. 316L stainless steel woven screen diffusion bonded to a smooth substrate of the same material (see Fig. 75). (Ion thruster anodes are fabricated of this laminate.)

2. Natural sputter textured pyrolytic graphite (see Fig. 34).

3. Natural sputter textured cobalt-chromium-molybdenum as a lost wax cast alloy (see Fig. 76).

4. Photochemically etched pillars on titanium-6%Al-4%V (see Fig. 77). (This process is used in the fabrication of ion thruster accelerator grid systems and other thruster components.)

5. Ion beam sputter deposited bioglass. (Certain compositions of glasses containing Na_2O, CaO, P_2O_5, and SiO_2 develop a chemical bond to bone.)

The results to date from Univ. of Michigan's rabbit knee evaluation indicate that 316L stainless steel diffusion bonded grommets provide firm anchorage but suffer from delamination and breakup probably as a result of crevice corrosion. Pyrolytic graphite grommets are too brittle and also breakup. Efforts are now being focused to experimentally evaluate natural-textured cobalt chromium and photochemically etched pillar-surfaced titanium-6%Al-4%V in both the rabbit knee and domestic goose (anser anser) ulna implants. Basic feasibility experiments are being performed on putter deposited bioglass to determine if a satisfactory composition can be successfully sputter deposited and to evaluate its bone bonding characteristics.[101]

CONCLUDING REMARKS

Research and development of the electron bom-

bardment ion thruster has resulted in a significant amount of technology that may have spinoff benefits. Ion thruster technology associated with thruster fabrication processes, thruster components and utilization of the exhaust ion beam has applicability in nonpropulsive areas. Many of the attractive areas of potential spinoff applications of ion thruster technology involve ion beam interaction with materials by means of sputter etching, deposition, or texturing. The Ion Beam Applications Research Program at the NASA-Lewis Research Center was established in 1975 as a technology specific spinoff effort to identify, evaluate, develop, and transfer to the user community nonpropulsive applications of ion thruster technology. Numerous industrial and biomedical applications have been identified and are now in various stages of experimental evaluation. Ion beams may be used as a diagnostics tool or as a microfabrication process to enable the development of new or improved materials, products, and processes.

ACKNOWLEDGEMENTS

The author greatfully acknowledges the following individuals whose creativity, enthusiasm, and efforts have contributed significantly to the NASA Lewis Research Center's Ion Beam Applications Research Program:

Sandy Felder, NASA Lewis Research Center
Wayne Hudson, NASA Headquarters
Mike Mirtich, NASA Lewis Research Center
Bob Roman, NASA Lewis Research Center
Jim Sovey, NASA Lewis Research Center
Al Stein, NASA Lewis Research Center
Jack Weigand, NASA Lewis Research Center
Ed Wintucky, NASA Lewis Research Center

REFERENCES

1. "Ion Propulsion for Spacecraft," NASA-Lewis Research Center, Cleveland, OH, 1977.
2. Kaufman, H. R., "Technology of Electron-Bombardment Ion Thrusters," Advances in Electronics and Electron Physics, Vol. 36, Academic Press, New York, 1974, pp. 265-373.
3. Kerslake, W. R. and Banks, B. A, "Evolution of the 1-mlb Mercury Ion Thruster Subsystem," AIAA Paper 78-7118, Apr. 1978.
4. "30-Centimeter Ion Thrust Subsystem Design Manual," NASA TM-79191, 1979.
5. Byers, D. C. and Banks, B. A., "Survey of Electron-Bombardment Thruster Research," IEEE Transactions on Plasma Science, Vol. PS-2, No. 2, June 1973, pp. 1-9.
6. Cybulski, R. J., Shellhammer, D. M., Lovell, R. R., Domino, E. J., and Kotnik, J. T., "Results From SERT I Ion Rocket Flight Test," NASA TN D-2718, 1965.
7. Kerslake, W. R. and Ignaczak, L. R., "SERT II Extended Flight Thruster System Performance," AIAA Paper 79-2063, Oct. 1979.
8. Laznovsky, W., "Advances in Low-Energy Ion Beam Technology," Research/Development, Aug. 1975.
9. Wehner, G. K., General Mills Report No. 2309, July 1962.
10. Weijsenfield, C. H. and Hoogendoorn, A., "Cathode Sputtering By Rare Gas Ions of Low Energy," Proceedings of the Fifth International Conference on Ionization Phenomena in Gases, Munich, Vol. I, North Holland Publishing, Amsterdam, 1962, p. 124-129.
11. Keywell, F., "Measurements and Collision - Radiation Damage Theory of High-Vacuum Sputtering," Physical Review, Vol. 97, No. 6, Mar 15, 1955, pp. 1611-1619.
12. Kaminsky, M., Atomic and Ionic Impact Phenomena," Academic Press, New York, 1965.
13. Comas, J. and Cooper, C. B., "Sputtering Yields of Several Semiconducting Compounds Under Argon Ion Bombardment," Journal of Applied Physics, Vol. 37, 1966, pp. 2820-2822.
14. McKeown, D., Cabezas, A., and Mackenzie, E. T., "Annual Report on Low Energy Sputtering Studies," July 1961.
15. Carter, G. and Colligon, J. S., Ion Bombardment of Solids, American Elsevier Publishing Co., Inc., New York, 1968.
16. Commonwealth Scientific Corp., "Ion Beam Etch Rates," Bulletin No. 137-78.
17. Banks, B. A., Sovey, J. S., Miller, T. B., and Crandall, K. S., "Ion Beam Sputter Etching and Deposition of Fluoropolymers," NASA TM-78888 presented at the Eighth International Conference on Electron and Ion Beam Science and Technology, Seattle, Washington, May 21-26, 1978.
18. Sovey, J. S., "Ion Beam Sputtering of Fluoropolymers," NASA TM-79000 presented at the Twenty-fifth National Vacuum Symposium sponsored by the American Vacuum Society, San Francisco, Calif., Nov. 28-Dec. 1, 1978.
19. Priestley, J., The History and Present State of Electricity with Original Experiments, vol. 1, Third edition, Bathurst and Lounder, London, 1775.
20. Grove, W. R., "On the Electro-Chemical Polarity of Gases," Transactions of the Royal Society, London, Vol. 142, p. 87, 1852.
21. Meadows, G. A. and Free, B. A., "Ion Eteching to Expose Crystal Structure, AIAA Paper 79-2117, Oct. 1979.
22. Wehner, G. K., "Sputtering by Ion Bombardment," Advances in Electronics and Electron Physics, vol. 7, Academic Press, New York, 1955, p. 239.
23. Stewart, A. D. G., "Investigation of the Topography of Ion Bombarded Surfaces With a Scanning Electron Microscope," Proceedings of the Fifth International Congress on Electron Microscopy, Vol. 1, Paper D-12, 1962.
24. Guentheschultze, A. and Tollmien, W., "New Investigation on the Cathode Sputtering of the Glow Discharge; V - The Nature of the Surface of the Cathode," Zeitschrafo Fuer Physik, Vol. 119, Nos. 11-12, 1942, pp. 685-695.
25. Wehner, G. K. and Hajicek, D. J., "Cone Formation on Metal Targets During Sputtering," Journal of Applied Physics, Vol 42, No. 3, 1971, pp. 1145-1148.
26. Hudson, W. R., "Ion Beam Texturing," NASA TM X-73470, 1976. Also Journal of Vacuum Science and Technology, Vol. 14, Jan.-Feb. 1977, pp. 286-289.
27. Hudson, W. R., "Nonpropulsive Applications of Ion Beams," NASA TM X-73511, 1976; also AIAA Paper 76-1015, Nov. 1976.
28. Hudson, W. R., Robson, R. R., and Sovey, J. S., "Ion-Beam Technology and Applications," NASA TM X-3517, May 1977.
29. Robinson, R. S., "Physical Processes in Directed Ion Beam Sputtering," Ph.D. Thesis, Colorado State University, Fort Collins, CO, Mar. 1979. (NASA CR-159567.)

30. Wehner, G. K., "Whiskers, Cones and Pyramids Created in Sputtering by Ion Bombardment," NASA CR-159549, 1979.
31. Grodzka, P. G., "Space Processing Applications of Ion Beams," NASA CR-135261, 1977.
32. Sellen, J. M., Jr., Zufran, S., and Komatsu, G. K., "Ion Beam Technology Applications Study," TRW Defense and Space Systems Group, Redondo Beach, CA, TRW-32100-6009-RU-00, 1978. (NASA CR-159437.)
33. Gibbons, D. F., "The Report of the Steering Committee on Biomedical Applications of Ion Thruster Technology," NASA Contract NAS3-22259, Final Report, 1980.
34. Gelerinter, E. and Spielberg, N., "Applications of Ion Beam Technology," NASA Contract NAS3-21945, Final Report, 1980.
35. Sater, B. L. and Moore, T. J., "The Use of Ion Bean Cleaning to Obtain High Quality Cold Welds with Minimal Deformation," Materials Synergisms; Proceedings of the Tenth National Technical Conference, Klamesha Lake, N.Y., Oct. 17-19, 1978, Society for The Advancement of Material and Process Engineering, Azusa, CA, 1978, pp. 548-560. (NASA TM-78933.)
36. Wilbur, P. J., "Ion Implantation to Inhibit the Corrosion of Ferrous Metals," NASA Grant NAG3-25 to Colorado State Univ., Feb. 1980-Jan. 1981.
37. Wallace, J. F., "Thermal Fatigue Behavior of Dies for Aluminum Die Casting after Deposition of Various Ion Sputtered Coatings," NASA Grant NSG-3279 to Case Western Reserve Univ., June 1979-May 1980.
38. American Die Casting Institute, "Sputtered Protective Coating for Die Casting Dies," NASA Contract NAS3-22657, 1980.
39. Mirtich, M. J., "Ion Beam Deposited Protective Coatings," AIAA Paper 81-671, 1981.
40. Van Ooij, W. J., "Fundamental Aspects of Rubber Adhesion to Brass-Plated Steel Tire Cords," Rubber Chemistry and Technology, Vol. 51, No. 3, July-Aug. 1979, pp. 605-675.
41. Spencer, E. G., Schmidt, P. H., Joy, D. C., and Sansalone, F. J., "Ion-Beam-Deposited Polycrystalline Diamondlike Films," Applied Physics Letters, Vol. 29, No. 2, July 15, 1976, pp. 118-120.
42. Aisenberg, S. and Chabot, R., "Ion-Beam-Deposition of Thin Films of Diamondlike Carbon," Journal of Applied Physics, Vol. 42, No. 7, June 1971, pp. 2953-2958.
43. "Ion Beam Sputter Deposition of Diamondlike Films," NASA Contract NAS3-21950 with G&W Manufacturing Company Applied Science Laboratories, Sept. 1979-Sept. 1980.
44. Angus, John, "Characterization of Diamondlike Films," NASA Contract NAS3-22478 with Angus Research Corporation, 1980.
45. Rutledge, S and Banks, B., "Simultaneous Ion Sputter Polishing and Deposition," NASA TM-81679, Jan. 1981.
46. Hudson, W. R., Weigand, A. J., and Mirtich, M. J., "Optical Properties of Ion Beam Textured Metals," NASA TM X-73598 presented at the Sixth Annual Symposium on Applied Vacuum Science and Technology sponsored by the American Vacuum Society, Tampa, Fla., Feb. 14-16, 1977.
47. Mirtich, M. J. and Sovey, J. S., "Optical and Electrical Properties of Ion Beam Textured Kapton and Teflon," NASA TM-73778 presented at the Twenty-fourth National Vacuum Symposium sponsored by the American Vacuum Society, Boston, mass., Nov. 8-11, 1977.
48. Wintucky, E. G., Curren, A. N., and Sovey, J. S., "Electron Reflection and Secondary Emission Characteristics of Sputter-Etched Pyrolytic Graphite Surfaces," Proposed paper to be presented at the International Conference on Metallurgical Coatings to be held in San Francisco, Calif., Apr. 6-10, 1981.
49. Mirtich, M. J. and Sovey, J. S., "Adhesive Boding of Ion Beam Textured Metals and Fluoropolymers," NASA TM-79004 presented at the Twenty-fifth National Vacuum Symposium sponsored by the American Vacuum Society, San Francisco, Calif., Nov. 28-Dec. 1, 1978.
50. TME Corp., "Bonded Metal-Polymer Laminates Using Ion Beam Texturing," Final Report NASA Contract NAS3-21934, Apr. 1980.
51. TME Corp., "Bonded Metal-Polymer Laminates Using Ion Beam Texturing," NASA Contract NAS3-22479, July 1980.
52. "Applications of Fine Particles to Metal and Organic Substrates for Ion Beam Texturing Applications," NASA Grant NSG-3193, with Lehigh Univ., Aug. 1979.
53. Technics, Corp., "Industrial Batch Texturing of Fluoropolymers," NASA Contract NAS3-22271, Dec. 1979-Jan. 1981.
54. Kaufman, H. R. and Robinson, R. S., "Industrial Ion Source Technology," NASA CR-159877.
55. Kaufman, H. R., "Rectangular-Beam Ion Source," Final Report NASA Contract C-37730-D, Colorado State Univ., July 1980.
56. Wintucky, E. G., Mahmood, R., and Johnson, D. L., "Homogeneous Alignment of Nematic Liquid Crystals by Ion Beam Etched Surfaces," NASA TM-81378 presented at the One hundred fifty-sixth Meeting of the Electrochemical Society, Los Angeles, Calif., Oct. 15-19, 1979.
57. American Liquid Xtal Chemical Corp., "Performance Evalution of Liquid Crystal Displays with Ion Beam Etched Surfaces," NASA Contract NAS3-22653, Aug. 1980.
58. Park, E. L. and Yasuda, H. K., "Nucleate Boiling from Ion-Beam Textured Surfaces and from Surfaces Coated with R.F. Plasma Deposited Polymers," Final Report NASA Grant NSG-3199, Univ. of Missouri-Rolla, 1979.
59. Topich, J. A., "Adaptation of Ion Beam Technology to Microfabrication of Solid State Devices and Transducers," NASA CR-135314, Nov. 1977.
60. Sovey, J. S. and Mirtich, M. J., "A Hollow Cathode Hydrogen Ion Source," Symposium on Engineering Problems of Fusion Research, Seventh Proceedings, Vol. 1, IEEE, 1977, pp. 315-321. (NASA TM-73783.)
61. Schwirzke, F., "Ion Thruster Technology for Neutral Beam Injection Systems on Assessment Study," UCID-4015, Aug. 1977.
62. Gibbons, D. F., "The Report of the Steering Committee on Biomedical Applications of Ion Thruster Technology," Final Report of NASA Contract NAS3-22259, Case Western Reserve Univ., Jan. 1980.
63. Banks, B. A., Weigand, A. J., Babbush, C. A., and Van Kampen, C. L., "Potential Biomedical Applications of Ion Beam Technology," AIAA Paper 76-1018, Nov. 1976. (NASA TM X-73512.)
64. Dwight, D. W., "Ion Beam Surface Modification Characterization by ESCA and SEM," Final Report NASA Grant NSG-3204, Virginia Polytechnic Institute and State Univ., June 1979.

65. Weigand, A. J., "The Use of an Ion-Beam Source to Alter the Surface Morphology of Biological Implant Materials," NASA TM-78851, Paper presented at the Society for Biomaterials Conference, San Antonia, Tex., Apr. 19-May 2, 1978.
66. Weigand, A. J. and Cenkus, M. A., "Mechanical and Chemical Effects of Ion-Texturing Biomedical Polymers," NASA TM-79245, presented at the Thirty-second Annual Conference on Engineering in Medicine and Biology, Denver, Colo., Oct. 6-10, 1979.
67. Anderson, F. R. and Holland, V. F., "Ion Bombardment Etching of Synthetic Fibers," Journal of Applied Physics, Vol. 31, No. 9, Sept. 1960, pp. 1516-1518.
68. Weigand, A. J., NASA-Lewis Research Center personal communication.
69. Stuart, P. R., Osborn, J. S., and Lewis, S. M., "The Use of Radio-Frequency Sputter Ion Etching and Scanning Electron Microscopy to Study the Internal Structure of Biological Material," Scanning Electron Microscopy/1969, Proceedings of the Second Annual Scanning Electron Microscope Symposium, IIT Research Institute, Chicago, Illinois, 1969, pp. 241-248.
70. Sugaya, E. and Onozuka, M., "Ion Shower Milling: Its Application to Cell Membrane Removal," Science, Vol. 202, No. 4373, Dec. 15, 1978, pp. 1197-1198.
71. Ambrose, E. J., Batzdorf, U., Osborn, J. S., and Stuart, P. R., " Nature, Vol. 227, No. 5256, July 25, 1970.
72. Gibbons, D. F., "Dissolution Transfer Casting of Biopolymers," NASA Grant NAG3-12, with Case Western Reserve University, Nov. 1979-May 1980.
73. Picha, G. J., "Tissue Response to Peritoneal Implants," NASA CR-159817, June 1980.
74. Gibbons, D. F., "Effect of Surface Texture by Ion Beam Sputtering on Implant Biocompatibility and Soft Tissue Attachment, NASA CR-135311, Dec. 1977.
75. Gibbons, D. F., "Effect of Surface Texture by Ion Beam Sputtering on Implant Biocompatibility and Soft Tissue Attachment, NASA CR-159358, May 1980.
76. Gibbons, D. F., "Center of Excellence for Biomedical Applications of Ion Thruster Technoklogy," NASA Contract NAS3-22443, Monthly report for Nov. 1980.
77. Chiroff, R. T., White, E. W., Weber, J. N., and Roy, D. M., "Tissue Ingrowth of Replamineform Implants," Journal of Biomedical Materials Symposium, Vol. 9, No. 4, July 1975, pp. 29-45.
78. Szycher, M., Bernhard, W., Liss, R., and Kaiser, J., "Development and Testing of Flocked Materials," Thermo Electron Corp., TE41-122-77, Apr. 1978.
79. NIH Research Advances 1976," DHEW Publication No. (NIH)76-3, 1976.
80. Milhorat, T. H., Hydrocephalus and the Cerebrospinal Fluid, Williams and Wilkins, Baltimore, 1972.
81. University of California, Irvine, "Development and Evaluation of Ion Beam Sputtered Ventilated Ventricular Catheter," NASA Contract NAS3-21963, Sept. 1979-Jan. 1981.
82. Miller, J. and Brooks, C. E., Journal of Biomedical Materials Research Symposium, No. 2, p. 251, 1971.
83. Winter, G. D., "Transcutaneous Implants - Reactions of Skin-Implant Interface," Journal of Biomedical Materials Research, Vol. 8, No. 3, 1974, pp. 99-113.
84. Picha, G. J. and Gibbons, D. F., "The Effect of Surface Texture on the Percutaneous Implant/Epithelial Response," NASA CR-165255, Jan. 1981.
85. Amtech, Applied Medical Technology, Inc., "Design, Fabrication, and Evaluation of Percutaneous Connector Devices," NASA Contract NAS3-22654, Sept. 1980.
86. Babbush, C. A., "Endosteal Blade-Vent Implants Modified by Ion Beam Sputtering Techniques," NASA CR-159463, Feb. 1979.
87. Cranin, A. N., "Ion Beam Textured Zirconium Dental Implants in Dogs," NASA Grant NSG-3216, with Brookdale Hospital Medical Center, Final Report, Nov. 17, 1980.
88. Weinstein, A. M. and Klawitter, J. J., "Evaluation of Ion-Textured Aluminum Oxide Surfaces for Permanent Prosthetic Attachment," NASA Grant NSG-3209, Final Report, Nov. 30, 1980.
89. Wisotzky, J., "Report of Dental Implant Assessment Seminar," NASA Contract C-2777-D with Case Western Reserve University School of Denistry, May 3, 1979.
90. Hottel, T. L., "The Effect of Morphological and Mechanical Parameters of Ion Sputtered Materials on the Gingival Seal of an Oral Implant Model," NASA Grant NAG3-115 with Case Western Reserve University, Nov. 1980-Oct. 1981.
91. Schaldach, M. and Hohmann, D., Advances in Artificial Hip and Knee Joint Technology, Springer-Verlag, New York, 1976.
92. Gibbons, D. F., "The Evaluation of Surface Texturing by Ion Beam Sputtering on the Mechanical Fixation and Biological Compatibility of Orthopedic Alloys in Bone," NASA Grant NSG-3151 with Case Western Reserve University, 1979.
93. Gibbons, D. F., "Push Out Test of Untextured and Ion Textured MP35N and Co-Cr-Mo Bone Implants," Final Report for NASA Contract C-28306-D with Case Western Reserve University, 1980.
94. Cochran, G. V. B., Pawluk, R. J., and Bassett, C. A. L., "Electromechanical Characteristics of Bone Under Physiologic Moisture Conditions," Clinical Orthopaedics, Vol. 249, No. 58, May-June 1968, p. 68.
95. Bassett, C. A. L., Pawluk, R. J., and Becker, R. O., "Effects of Electric Currents on Bone In Vivo," Nature, Vol. 204, No. 4959, Nov. 14, 1964, pp. 652-654.
96. Pawluk, R. J., "A Preliminary In Vivo Study of the Effects of Electrical Stimulation on Bone Ingrowth to Textured Surface of Orthopedic Implants," NASA Grant NAG3-15 with Columbia University College of Physicians and Surgeons, Dec. 1979-Nov. 1980.
97. Wintucky, E. G., Christopher, M., Bahnuik, E., and Wang, S., "Ion Beam Sputtering of Orthopedic Implant Alloy MP35N and Resulting Effects on Fatigue Properties," AIAA Paper 81-0671, 1981.
98. Swanson, A. B., "A Grommet Bone Liner for Flexible Implant Arthroplasty," Bulletin of Prosthetics Research, Vol. 17, No. 1, BPR 10-33, Spring 1980.
99. Banks, B. A., "Textured Grommets for Flexible Implant Arthroplasty of Finger Joints," Bulletin of Prosthetics Research, Vol. 17, No. 1, BPR 10-33, Spring 1980.

100. Park, J. B., "Research and Development of an Artificial Finger Joint Grommet Using Ion Thruster Technology," NASA Grant NAG3-116 with Clemson University, Oct. 1980-Sept. 1981.
101. Hench, L. L., "Evaluation of Ion Beam Sputtered Bioglass Coatings of Prosthetic Devices," NASA Grant NSG-3273 with University of Florida, Gainesville, July 1979-June 1980.

TABLE I. - SPUTTER YIELD OF VARIOUS MATERIALS BOMBARDED BY 500 eV ARGON IONS[15]

Target material and orientation where known	Sputter yield
Be	0.51
C	.12
Al	1.05
Si	.50
Ti	.51
V	.65
Cr	1.18
Fe	1.10, 0.84[10]
Co	1.22
Ni	1.45, 1.33[10]
Cu	2.35, 1.2,[11], 2.0[10]
Ge	1.1[a]
Y	.68
Zr	.65
Nb	.60
Mo	.80, 0.64[11]
Rb	1.15
Rh	1.30
Pd	2.08
Ag	3.12, 2.4,[11], 2.3,[12], 3.06[13]
Sm	.80
Gd	.83
Dy	.88
Er	.77
Hf	.70
Ta	.57
W	.57
Re	.87
Os	.87
Ir	1.01
Pt	1.40
Au	2.40, 2.5[14]
Pb	2.7[11]
Th	.62
U	.85
PbTe (111)	1.4[13]
GaAs (110)	.9[13]
GaP (111)	.95[13]
CdS (1010)	1.12[13]
SiC (0001)	.41[13]
InSb (unknown orientation	.55[13]

[a]Indicates an extrapolated value
Values without reference numbers are from Wehner.[15]

TABLE II. - TEXTURE BONDED METALS. ALL BONDS MADE IN AIR ATMOSPHERE ENVIRONMENT BY IMPACT OF A HAND HELD HAMMER

Materials	Bond strength			
	Tensile		Shear	
	lb/in.^{2}	kPa	lb/in.^{2}	kPa
Cu-Cu	33	228	83	572
Al-Al	4	28	122	841
Cu-Al	34	234	44	303

TABLE III. - ESCA SURFACE CHEMISTRY CHARACTERIZATION OF CONTROL, VACUUM EXPOSED AND ION BEAM SPUTTERED BIOPOLYMERS

(a) Surface elemental composition expressed as number of atoms relative to total carbon defined as 1.00. The surface abundance of various carbon bonds is also shown.

[C_a binding energy $< C_b$ binding energy $< C_c$ binding energy $< C_d$ binding energy.]

Samples	Elements							
	C-H or C-C C_a	C-O C_b	C=O C_c	C-F C_d	O	N	Si	F
Bioelectric polyurethane:								
Control	0.54	0.43	0.03	-----	0.27	0.018	0.064	-----
Vacuum	.60	.37	.03	0.006	.27	.013	.087	0.009
Sputtered	.71	.25	.04	-----	.19	.0069	.054	<.001
Segmented polyurethane (Biomer®):								
Control	.74	.19	.07	-----	.26	.028	.077	.007
Vacuum	.72	.19	.09	-----	.29	.041	.067	-----
Sputtered	.72	.23	.05	-----	.12	.021	.014	-----
Polyoxymethylene (Delrin®):								
Control	.38	.62	----	-----	.64	------	.05	-----
Vacuum	.23	.77	----	-----	.75	------	.002	-----
Sputtered	.86	.06	.08	-----	.16	------	.002	-----
UHMW-polyethylene:								
Control	.97	.03	----	-----	.14	------	.066	-----
Vacuum	.98	.02	----	-----	.09	------	.035	-----
Sputtered	.90	.10	----	-----	.23	------	.075	-----
UHMW-polyethylene with 10% carbon fibers:								
Control	1.00	----	----	-----	.09	------	.042	----
Vacuum	1.00	----	----	-----	.11	------	.065	-----
Sputtered	1.00	----	----	-----	.14	------	.006	-----
32% Carbon impregnated polyolefin:								
Control	1.00	----	----	-----	.097	------	.53	-----
Vacuum	1.00	----	----	-----	.062	------	-----	-----
Sputtered	1.00	----	----	-----	.028	------	-----	-----
Silicone rubber (Silastic®):								
Control	1.00	----	----	-----	.47	------	.53	-----
Vacuum	1.00	----	----	-----	.49	------	.58	-----
Sputtered	1.00	----	----	-----	.50	------	.45	-----
Cross-linked polyurethane (Tecoflex®):								
Control	.59	.39	.02	-----	.26	.020	.052	.01
Vacuum	.62	.35	.04	-----	.27	.029	.051	.17
Sputtered	.72	.26	.03	-----	.16	.009	.024	-----
Polytetrafluoroethylene (Teflon®):								
Control	.06	.94	----	-----	.02	------	.014	1.95
Vacuum	.12	.88	----	-----	.04	------	.005	1.84
Sputtered	.08	.88	.08	.76	.03	------	.005	1.52

TABLE III. - Concluded.

(b) Surface elemental compositior expressed as atom percent for the detected elements

Samples	Elements														
	C	O	N	Si	Na	Mg	Fe	Zn	Sn	Ca	Ir	F	S	Cl	A
Bioelectric polyurethane:															
Control	74	20	1.4	4.7	-------	---	----	---	----	---	-------	-----	----	----	---
Vacuum	72	20	.9	6.3	-------	---	----	---	----	---	-------	0.6	----	----	---
Ion-textured	79	15	.5	4.2	-------	---	----	---	----	---	0.03(μ)	<.1	0.4	----	0.4
Segmented polyurethane (Biomer®):															
Control	72	19	2.1	5.5	-------	---	0.2	---	----	---	-------	.5	.5	0.2	---
Vacuum	71	20	2.9	4.7	0.04(?)	---	.2	---	----	---	-------	-----	.3	.6	---
Ion-textured	85	11	1.8	1.2	.15	---	<.03	---	----	---	-------	-----	.09	----	.4
Polyoxymethylene (Delrin®):															
Control	57	37	1.5	3.2	-------	---	----	---	----	0.3	-------	-----	.2	.3	---
Vacuum	57	43	---	.1	-------	---	----	---	----	---	-------	-----	.03	----	---
Ion-textured	85	14	---	.2	-------	---	----	---	----	.5	-------	-----	----	----	.1
UHMW-polyethylene:															
Control	81	12	.2	5.4	.7	0.7	----	---	----	---	-------	-----	----	.7	---
Vacuum	88	8.2	---	3.1	-------	.3	----	---	----	---	-------	-----	.5	----	---
Ion-textured	73	17	.7	5.5	.1	1.5	----	1.0	----	---	-------	-----	.6	.3	.2
UHMW-polyethylene with 10% carbon fibers:															
Control	87	7.6	.4	3.7	-------	.4	----	---	----	---	-------	.3	.2	----	---
Vacuum	83	9.2	.7	5.1	-------	1.2	----	---	----	---	-------	-----	.3	----	---
Ion-textured	86	12	.4	.5	-------	.8	----	---	----	---	-------	-----	.3	.1	.2
32% Carbon impregnated polyolefin:															
Control	85	8.2	.4	4.5	-------	---	----	.2	----	---	-------	1.6	.8	.2	---
Vacuum	83	8.2	.7	3.6	-------		----	.4	----	---	- -----	3.1	.6	.07	---
Ion-textured	95	2.8	---	----	-------	- -	----	.4	----	---	-------	.1	1.3	----	---
Silicone rubber (Silastic®):															
Control	50	23	---	----	-------	---	----	---	----	---	-------	-----	----	----	---
Vacuum	48	24	---	28	-------	---	----	---	----	---	-------	-----	----	----	---
Ion-textured	51	25	---	23	-------	---	----	---	----	---	-------	-----	.7	----	.3
Cross-linked polyurethane (Tecoflex®):															
Control	75	19	1.5	3.8	-------	---	----	---	0.04	---	-------	1.0	----	----	---
Vacuum	66	18	1.9	3.4	-------	---	----	---	.68	---	-------	11	----	----	---
Ion-textured	84	13	.7	2.0	-------	---	----	---	.06	---	-------	<.06	----	----	-.3
Polytetrafluoroethylene (Teflon®):															
Control	34	.7	---	.5	-------	---	----	---	----	---	-------	65	----	----	---
Vacuum	35	1.2	---	.2	-------	---	----	---	----	---	-------	64	----	----	---
Ion-textured	39	1.0	---	.2	-------	---	----	---	----	---	-------	60	----	----	---

Note: Values followed by ? indicate a weak signal from the element was possibly present but it was close to the detection limits; < indicates no signal was observed but an upper limit was calculated from the data; -- indicates no observation of a signal.

TABLE IV. - WATER CONTACT ANGLE MODIFICATION OF ION BEAM SPUTTERED BIOPOLYMERS

Material	Untreated surface		Argon ion textured surface		Nitrogen ion textured surface
	Ref. 64	Ref. 65	Ref. 64	Ref. 65	Ref. 65
Bioelectric polyurethane	70	---	70	---	---
Segmented polyurethane (Biomer®)	81	86	79	81	85
Cross linked polyurethane (Tecoflex®)	80	---	96	---	---
Polyoxymethylene (Delvin®)	62	83	0	116	82
Polyethylene	69	35	65	93	62
Polyethylene with 10% carbon fibers	83	---	54	---	---
32% Carbon impregnated polyolefin (Hexyn®)	95	86	90	97	117
Silicone rubber (Silastic®)	98	113	0	109	98
Silicone/urethane copolymer (Avecothane®)	--	114	---	126	96
Polytetrafluoroethylene (Teflon®)	99	114	129	140	15[illegible]

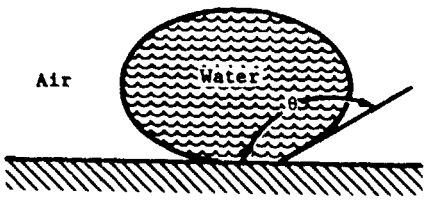

TABLE V. - FATIGUE STRENGTH OF MP35N
(35% Ni, 35% Co, 20% Cr, 10% Mo)
WITH VARIOUS SURFACE MORPHOLOGIES

Surface morphology	Estimated fatigue strength at 2×10^7 cycles*	
	N/m^2	$lb/in.^2$
Smooth surface (#600 emory cloth polished)	4.01×10^8	5.82×10^4
Natural sputter textured surface	1.94×10^8	2.81×10^4
Pitted surface formed by sputtering through an electroformed nickel mesh mask	1.59×10^8	2.30×10^4

*Average of 20 specimens of each surface morphology.

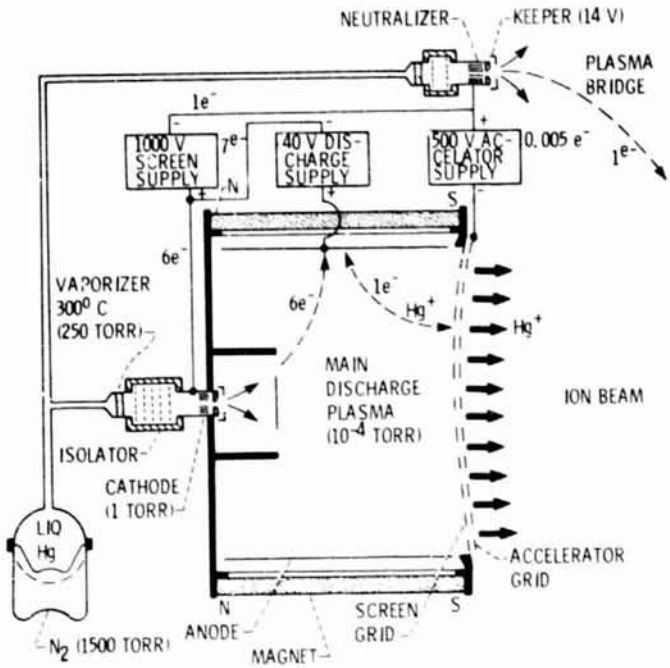

Figure 1. - Electron bombardment ion thruster system schematic.

Figure 2. - 30 cm diameter ion thruster.

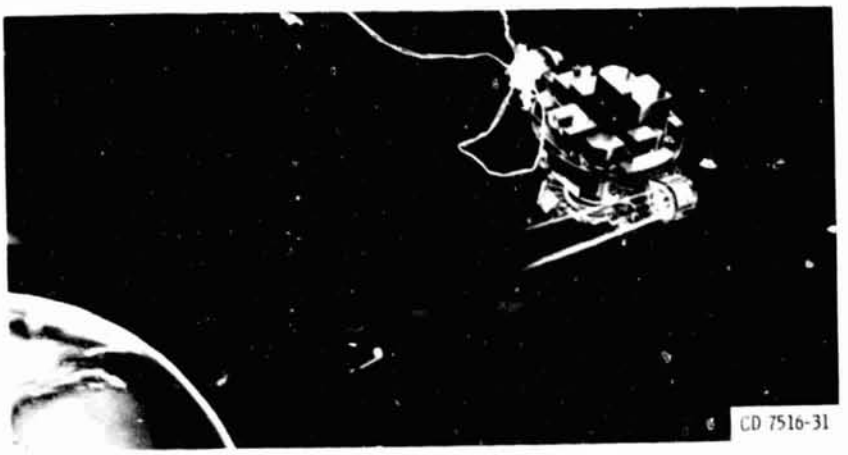

Figure 3. - SERT I spacecraft.

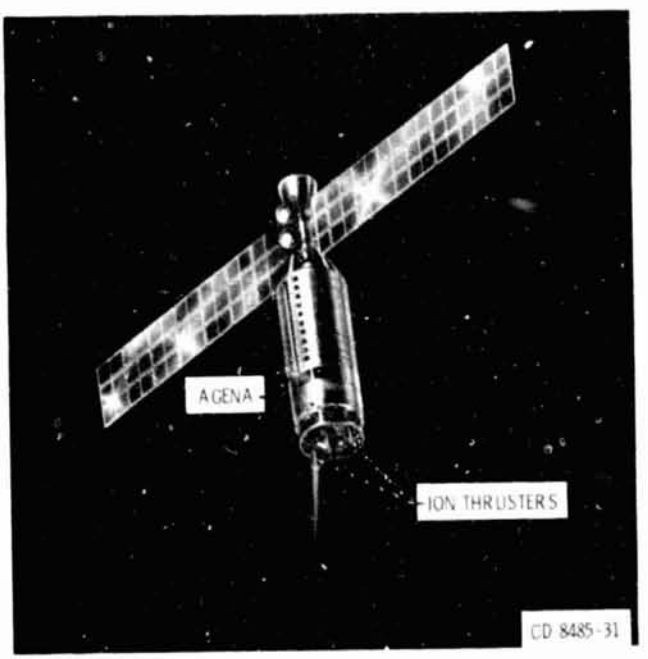

Figure 4. - SERT II spacecraft.

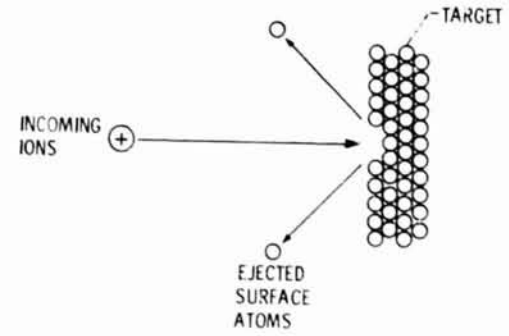

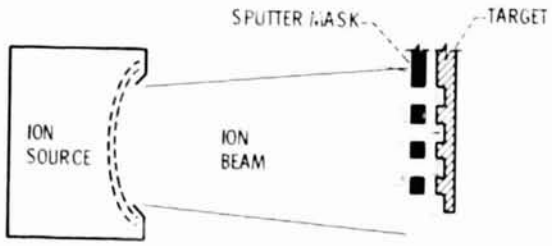

Figure 5. - Ion beam sputter etching a target partially protected by a sputter mask.

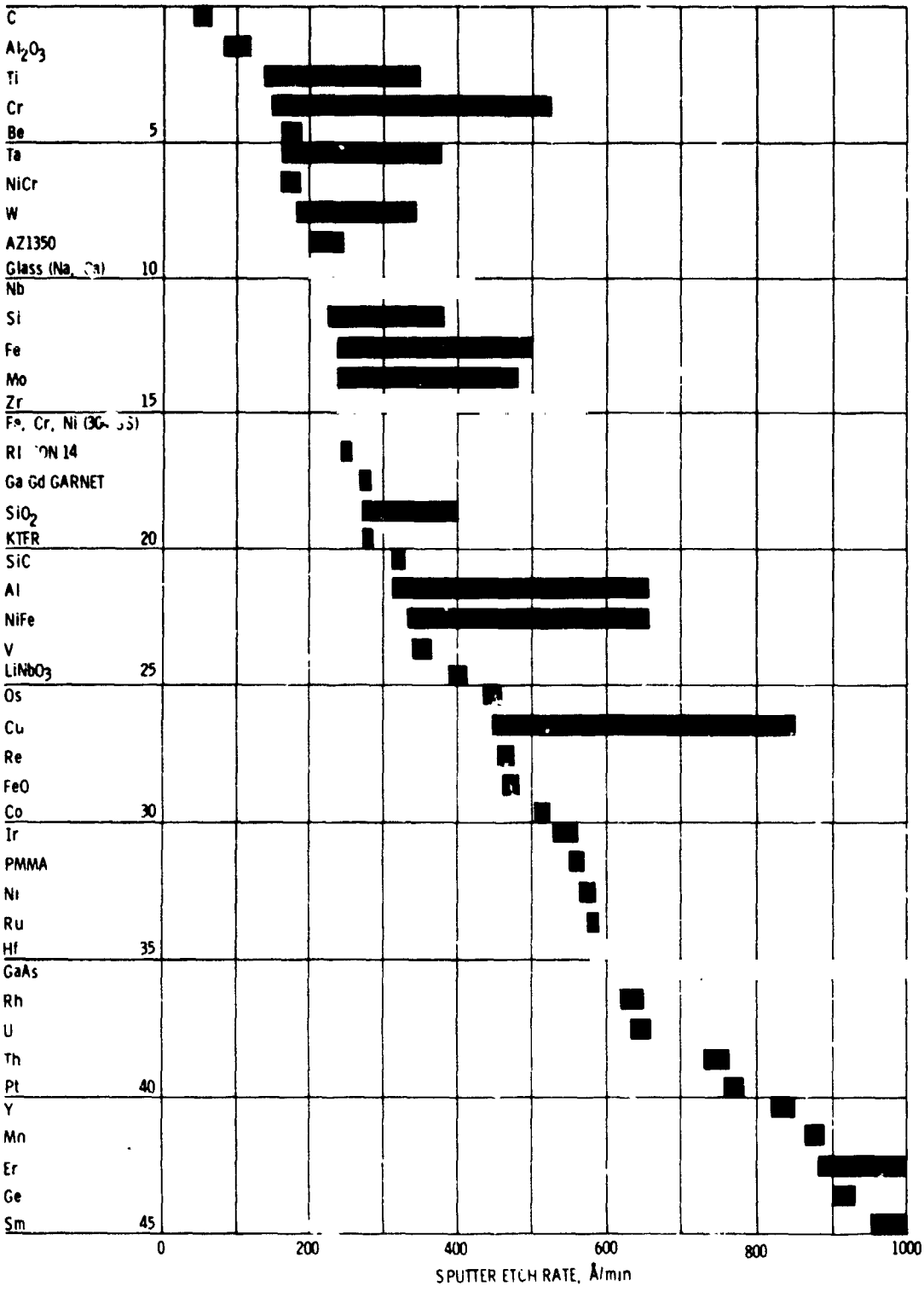

Figure 6. - Range of sputter etch rates observed for various materials bombarded by a normally incident 500 eV argon ion beam at a current density of 1 mA/cm^2 (ref. 16).

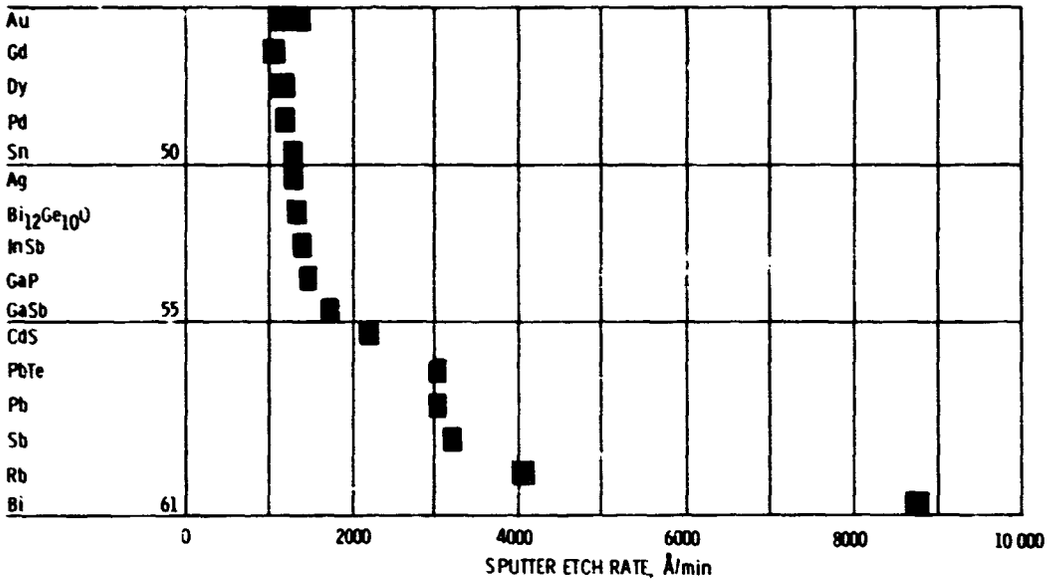

Figure 6. - Concluded.

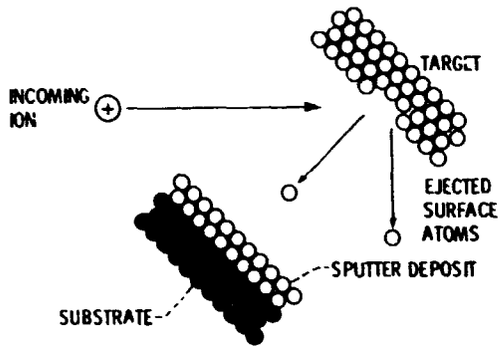

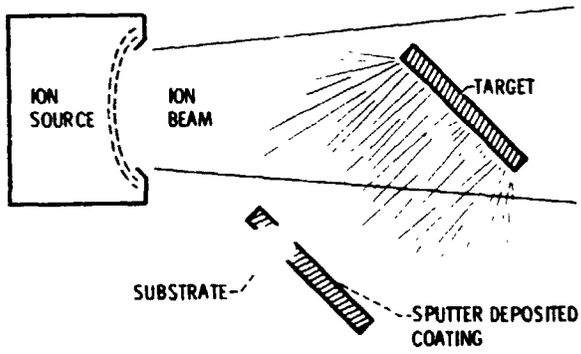

Figure 7. - Ion beam sputter deposition.

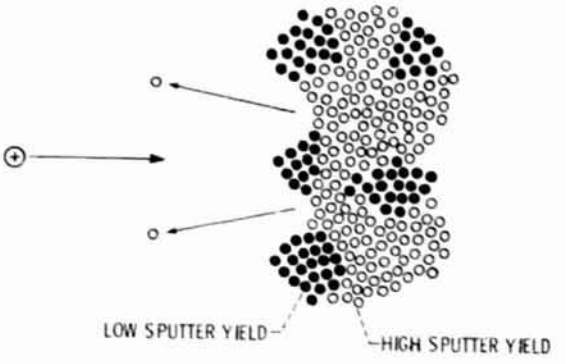

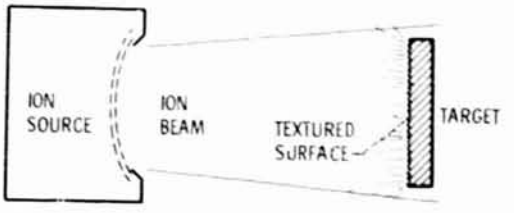

Figure 8. - Natural texturing by ion beam sputtering.

Figure 9. - Natural textured polytetrafluoroethylene (PTFE Teflon) surface after exposure to a 750 eV argon ion beam with a current density of 0.6 mA/cm^2.

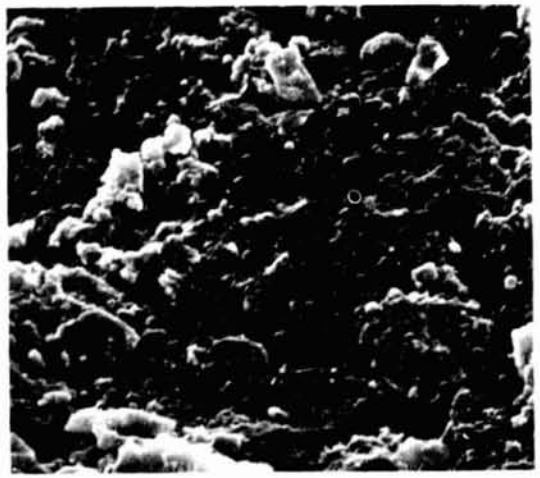

(a) UNSPUTTERED.

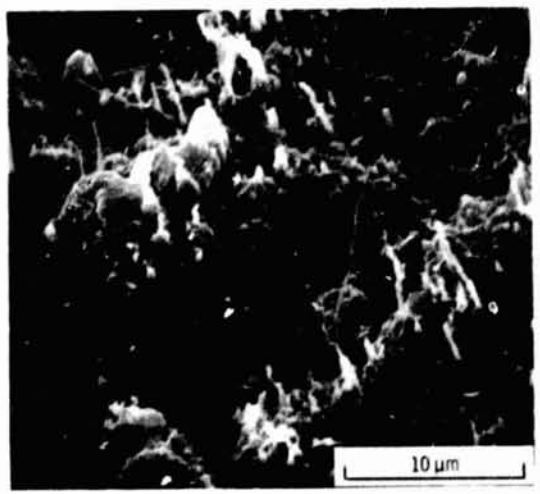

(b) NATURAL TEXTURED.

Figure 10. - Scanning electron photomicrographs of coal.

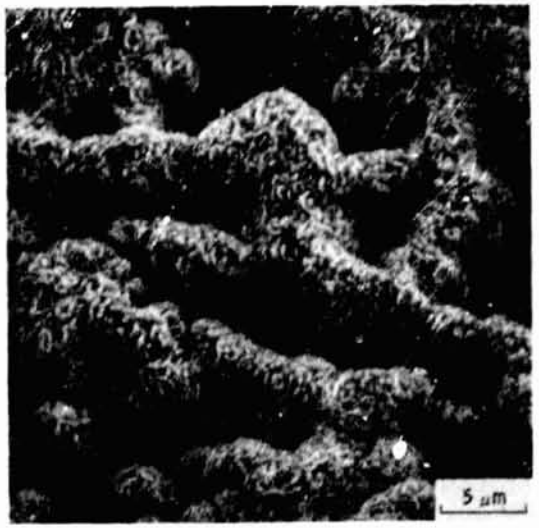

Figure 11. - Scanning electron photomicrograph of natural textured MP35N after 30 minutes of exposure to a 2000 eV xenon ion beam with a current density of 2 mA/cm^2.

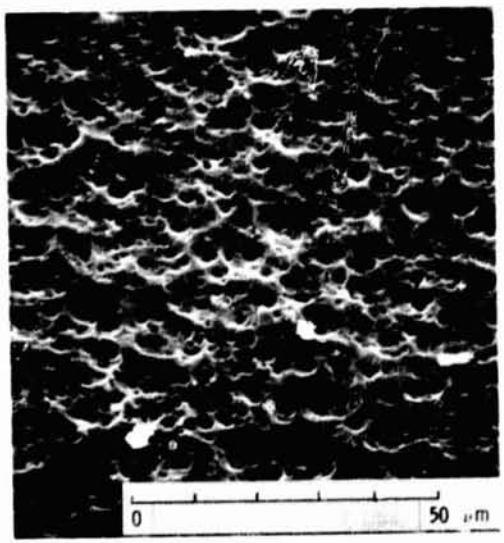

Figure 12. - Natural textured Al_2O_3 which contained voids.

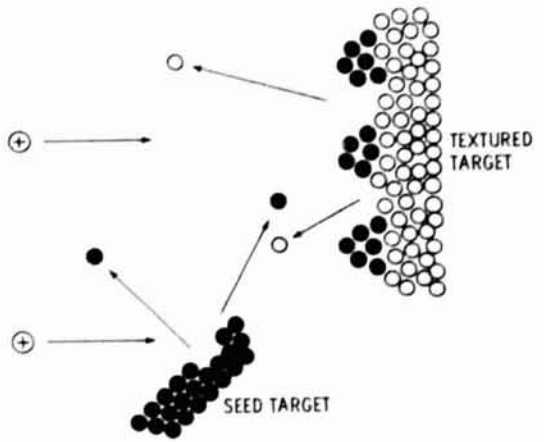

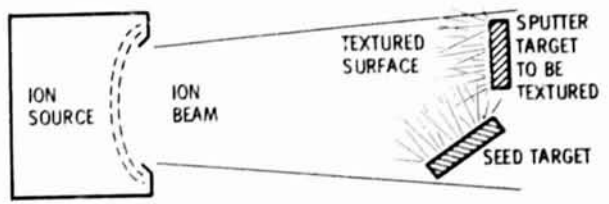

Figure 13. - Seed texturing by ion beam sputtering.

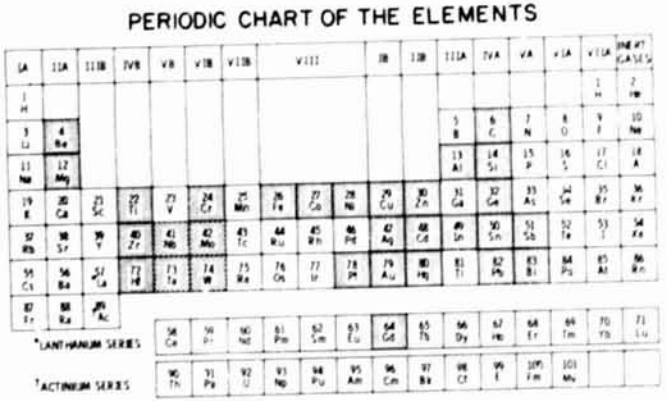

Figure 14. - The periodic chart of the elements. The shaded elements were successfully textured using tantalum as the seed material. The texturing process was unsuccessful for the cross-hatched materials. Untested elements are unshaded. Ref. 26.

(a) COPPER.

(b) SILICON.

Figure 15. - Scanning electron photomicrographs of seed textured materials using a tantalum seed.

(c) NICKEL.

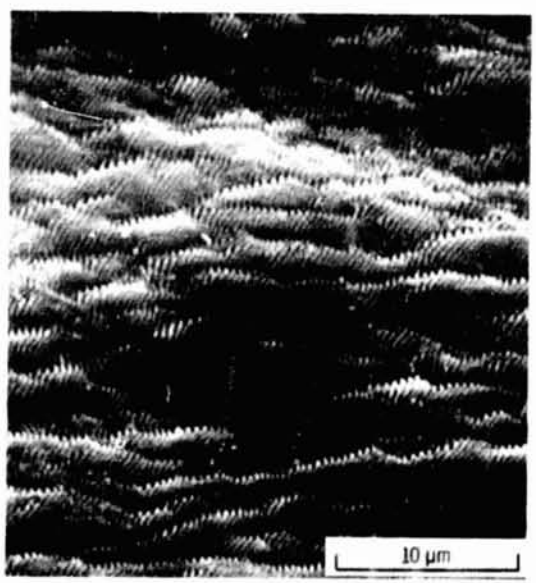

(d) PLATINUM.

Figure 15. - Concluded.

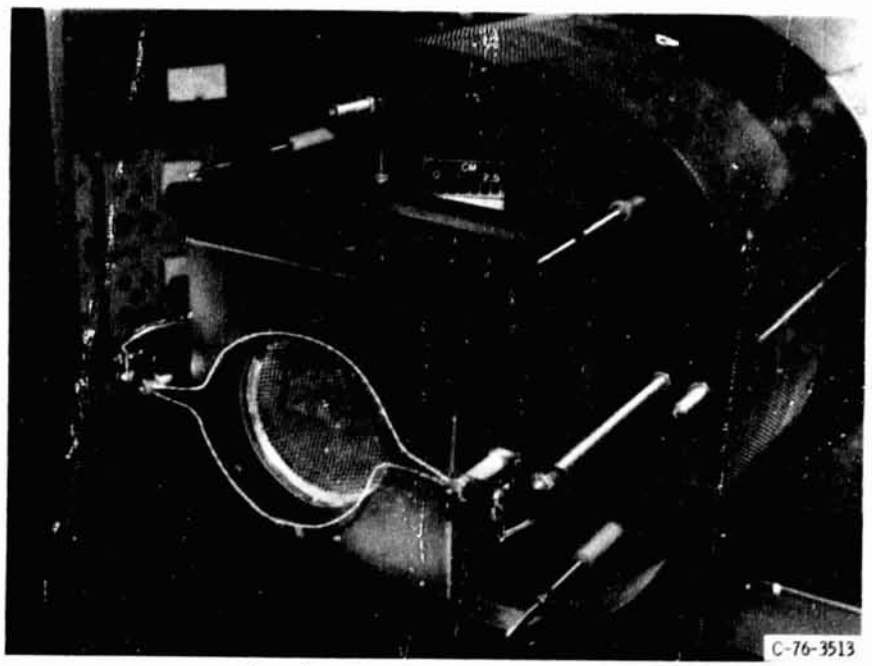

Figure 16. - 8 cm diameter argon ion source.

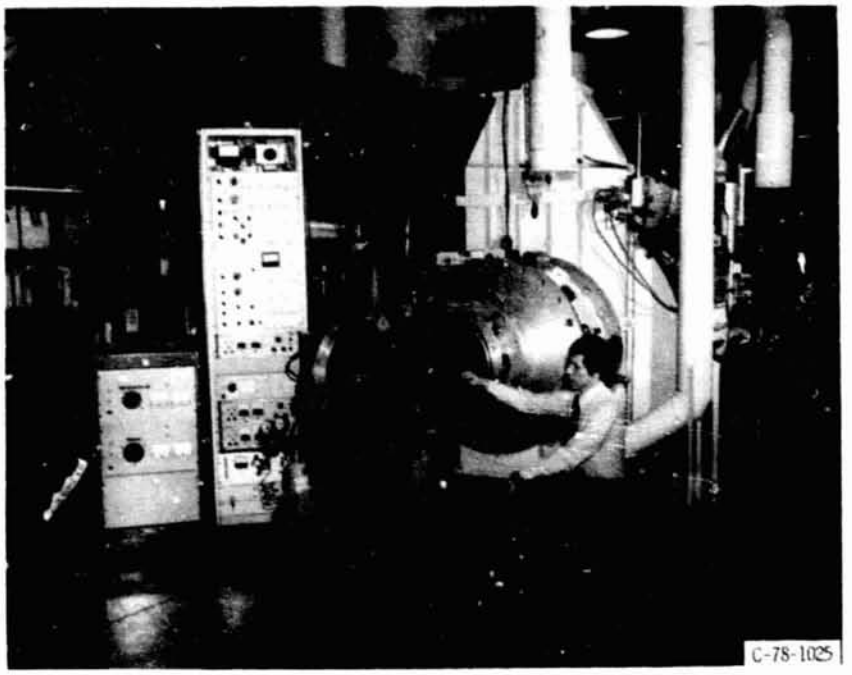

Figure 17. - 8 cm diameter ion source with vacuum facility and power supplies.

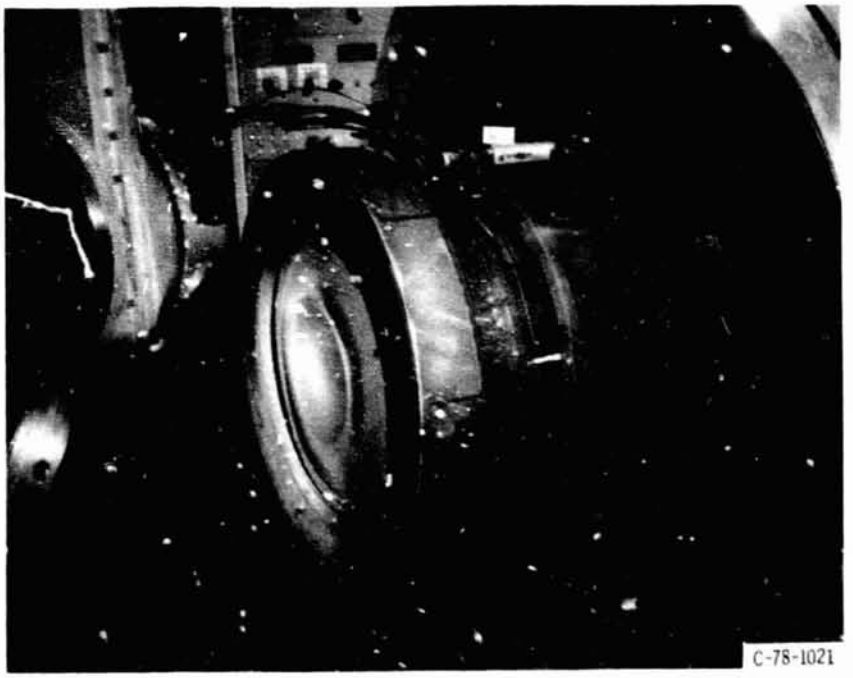

Figure 18. - 30 cm diameter argon ion source.

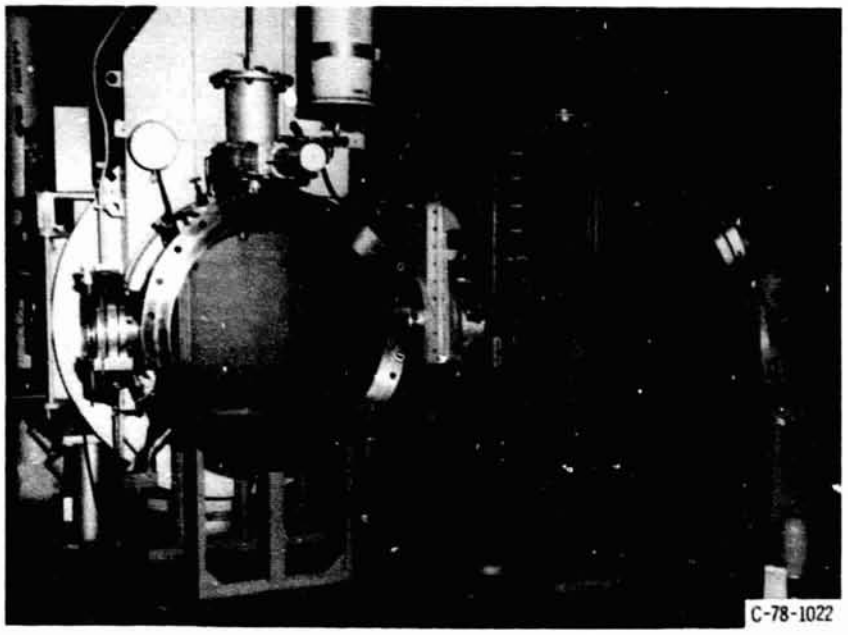

Figure 19. - 30 cm argon ion source with it's vacuum facility and power control console.

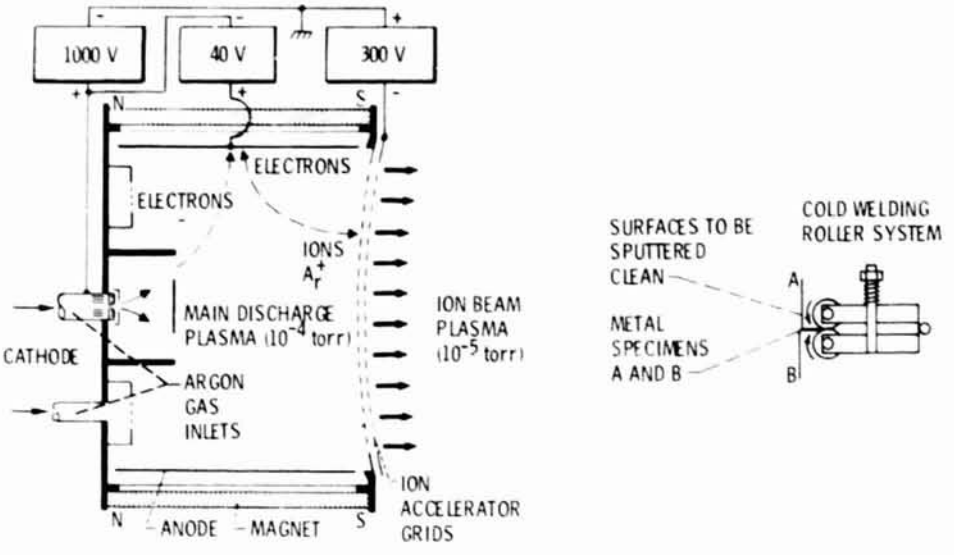

(a) BASIC SCHEMATIC FOR ELECTRON BOMBARDMENT ION SOURCE AND ROLLER SYSTEM.

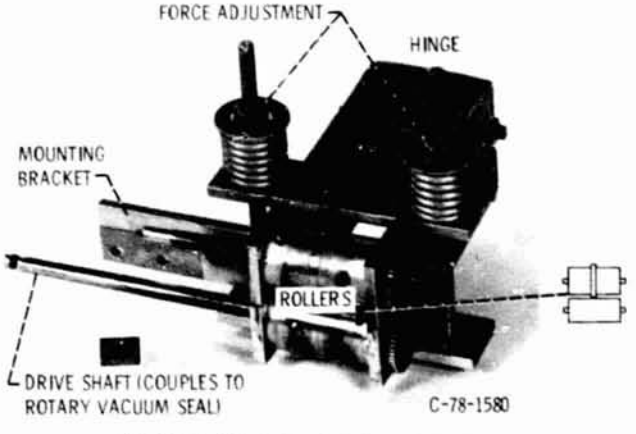

(b) COLD WELDING ROLLER SYSTEM FIXTURE.

Figure 20. - Cold welding using ion beam sputter cleaning.

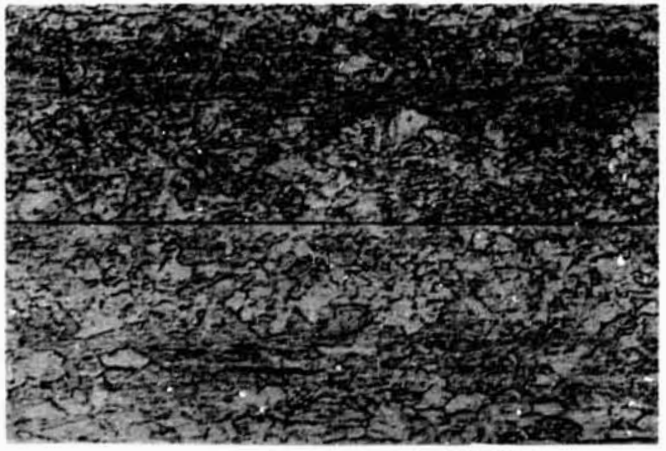

(a) AS WELDED.

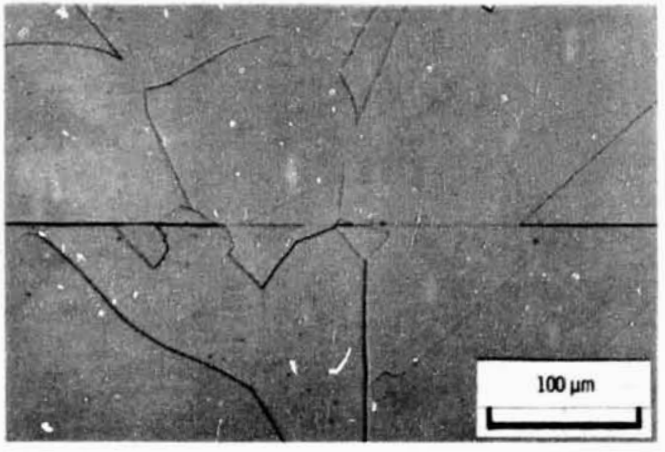

(b) HEAT TREATED AT 800° C FOR 2 hours IN VACUUM.

Figure 21. - Copper-to-copper cold weld.

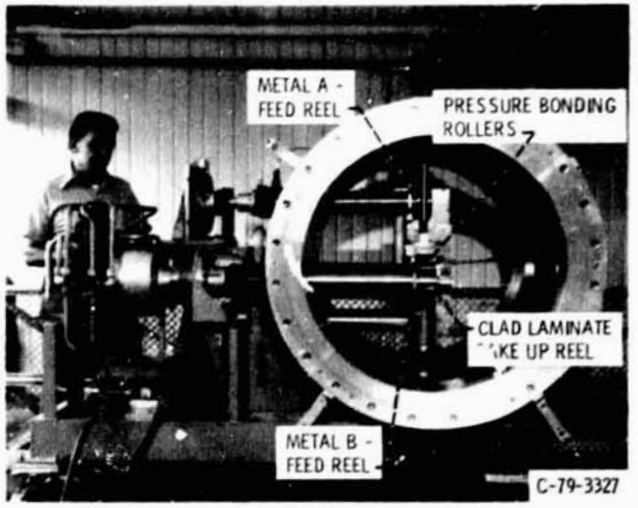

Figure 22. - Ion beam cold welding spool piece looking upstream showing metal ribbon take up and feed reels along with pressure rollers (ion source is not shown).

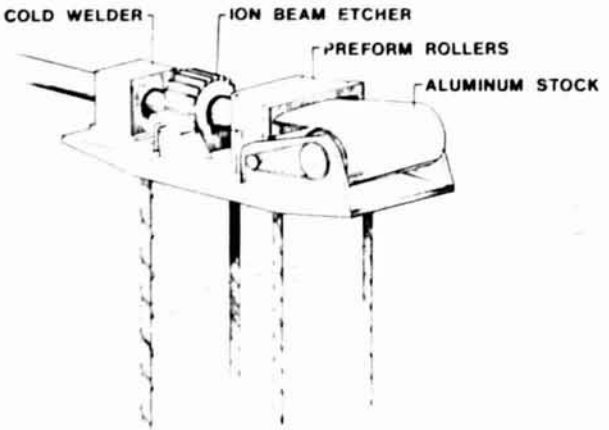

(a) FABRICATION OF A LARGE SPACE STRUCTURAL MEMBER WITH A COLD WELDED SEAM.

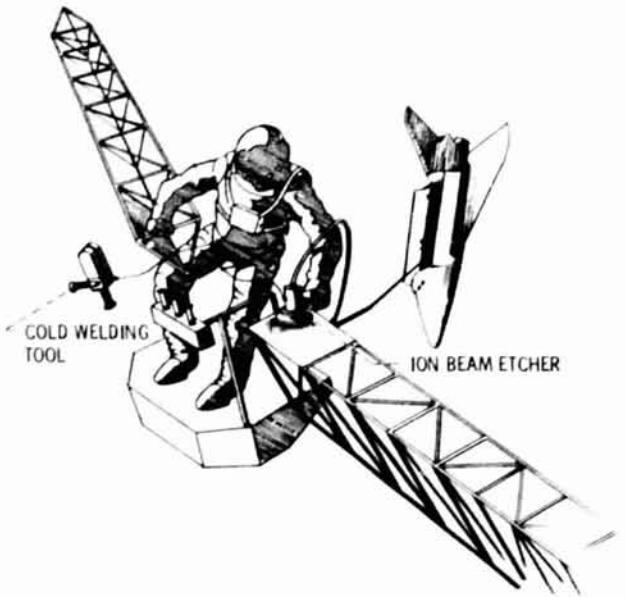

(b) ASSEMBLY OF TWO LARGE STRUCTURE MEMBERS USING ION BEAM COLD WELDING.

Figure 23. - Ion beam cold welding for large space structures.

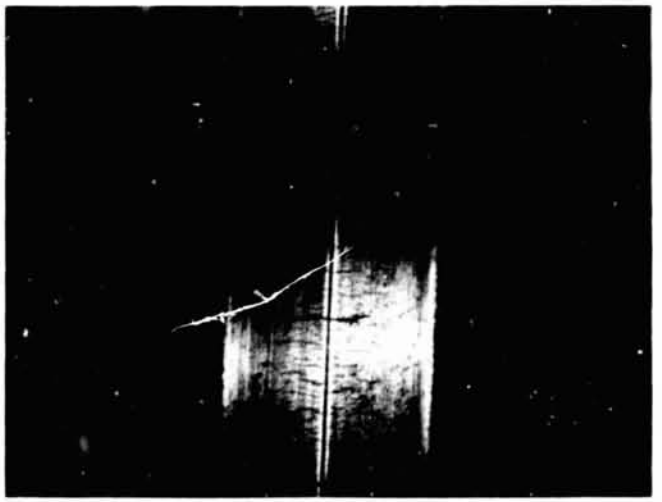

Figure 24. - H-13 die steel surface with thermal fatigue cracks.

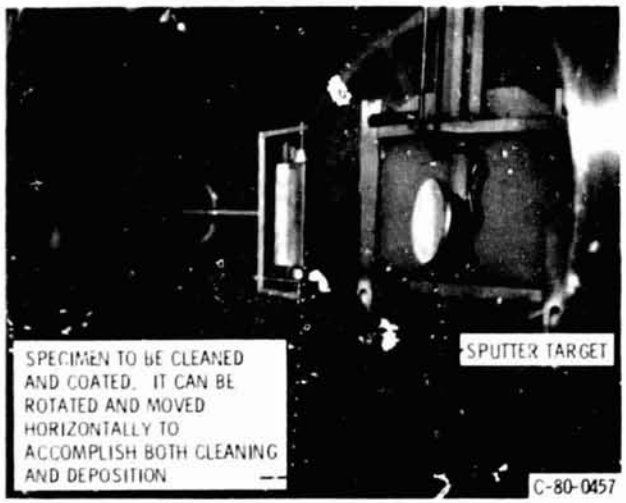

Figure 25. - Thermal fatigue dunk test specimen in vacuum facility for ion beam sputter cleaning and deposition.

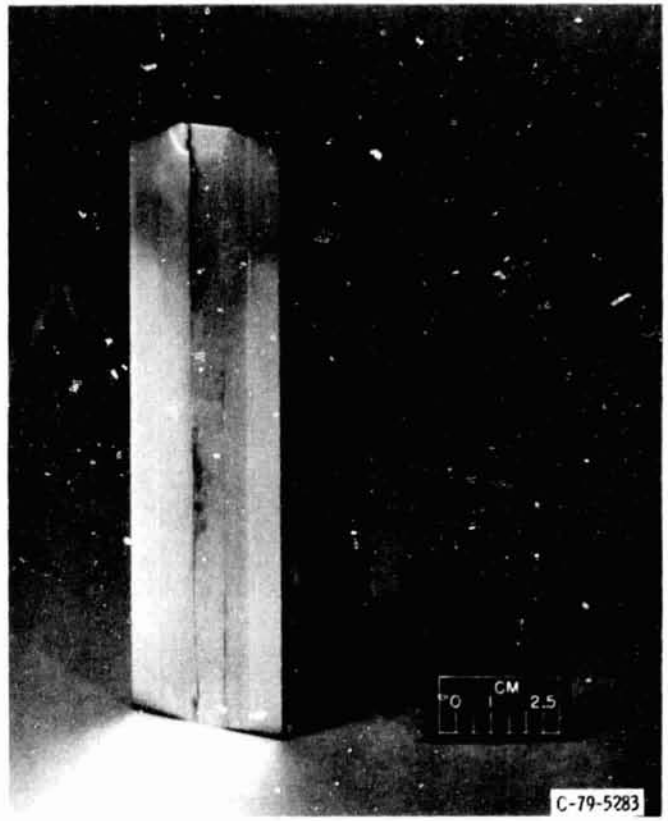

Figure 26. - Thermal fatigue dunk test specimen with sputter deposited coating on its corner edges.

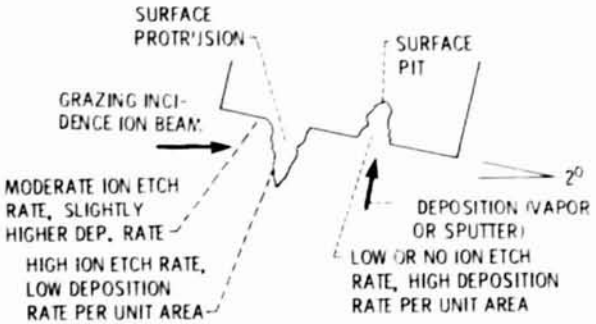

(a) CONCEPT.

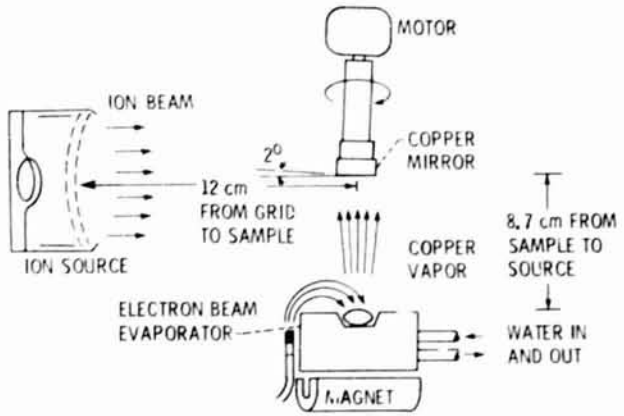

(b) SIMULTANEOUS SPUTTER POLISHING AND VAPOR DEPOSITION.

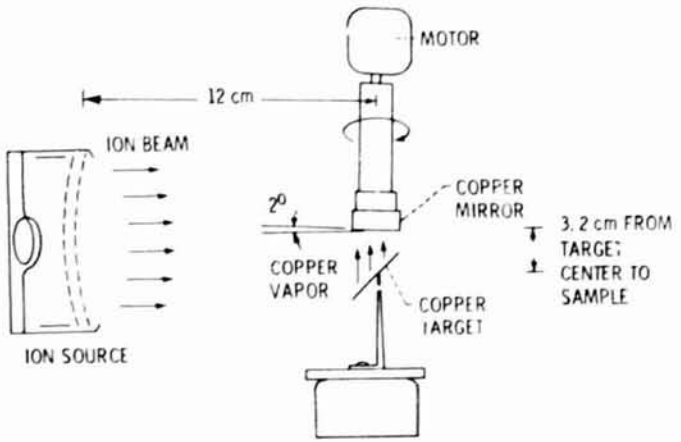

(c) SIMULTANEOUS SPUTTER POLISHING AND SPUTTER DEPOSITION.

Figure 27. - Deposition simultaneous with sputter polishing.

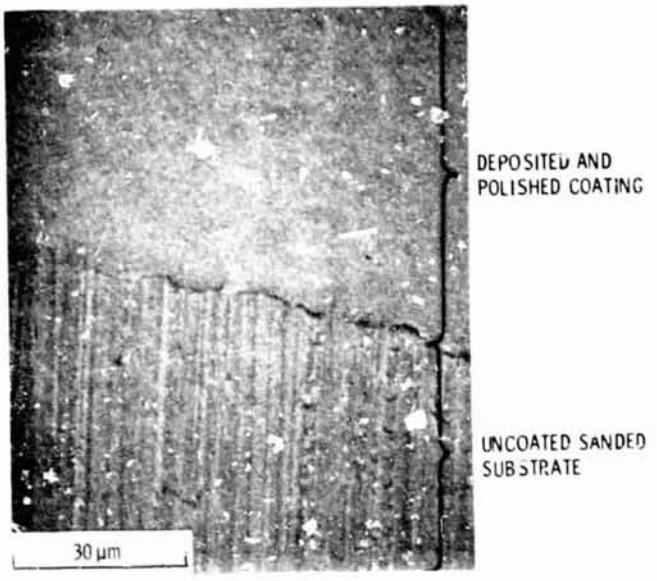

Figure 28. - Simultaneously sputter deposited and sputter polished copper coating over a sanded copper substrate. 2^{0} ion incidence angle for 1000 eV argon ions, 0.53 μm thick deposit.

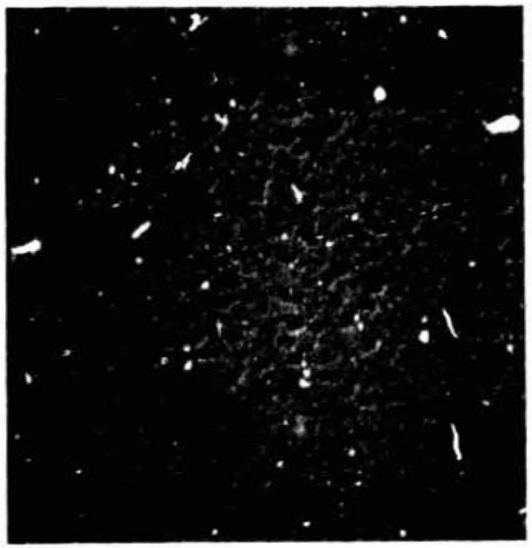

(a) 10 minute EXPOSURE.

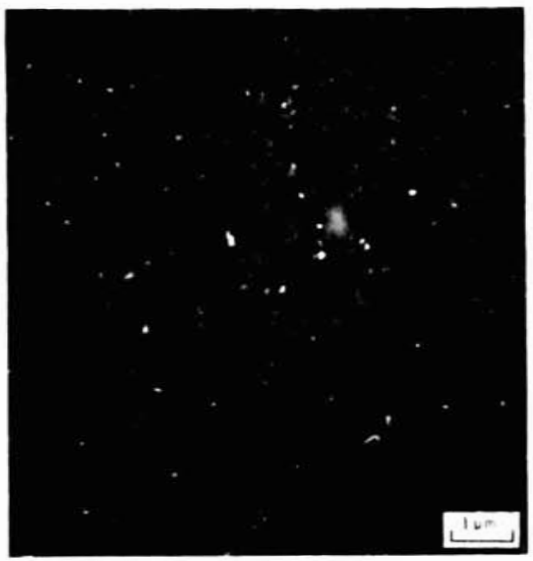

(b) 30 minute EXPOSURE.

Figure 29. - Scanning electron photomicrographs of 8 μm thick polyimide (Kapton®) after various durations of exposure to a 1000 eV argon ion beam at 1.8 mA/cm^2.

(c) 115 minute EXPOSURE.

Figure 29. - Concluded.

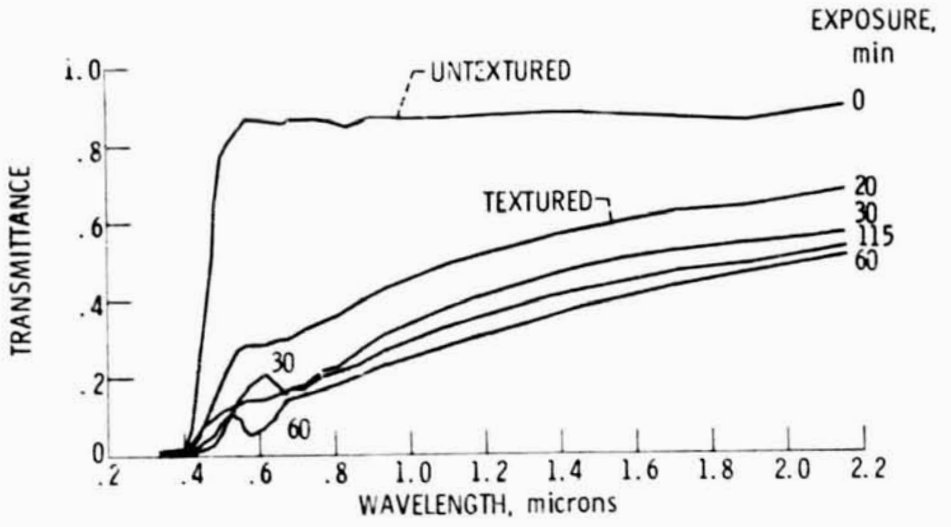

Figure 30. - Spectral transmittance of 8μm thick polyimide (Kapton®) before and after exposure to 1 keV Ar ions at 1.8 mA/cm^2.

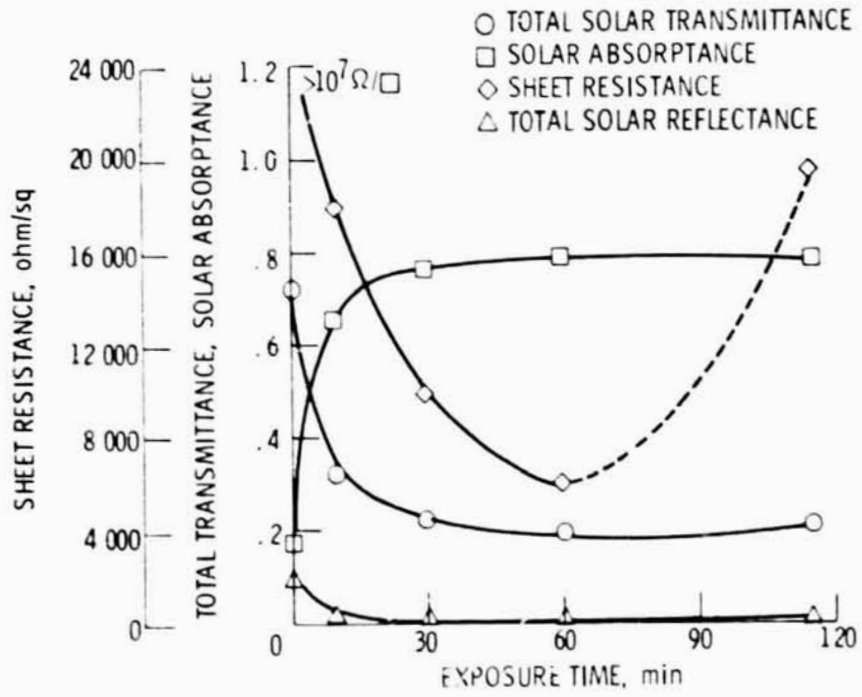

Figure 31. - Total transmittance solar absorptance, and sheet resistance versus exposure time for 8μm polyimide (Kapton®) exposed to 1 keV, 1.8 mA/cm^2 Ar ions.

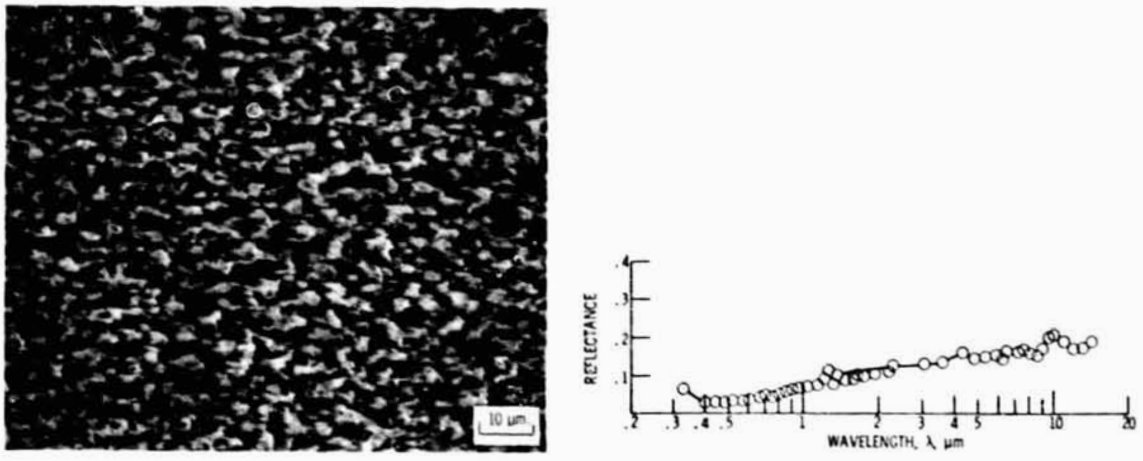

(a) COPPER AFTER 90 min OF TEXTURING.

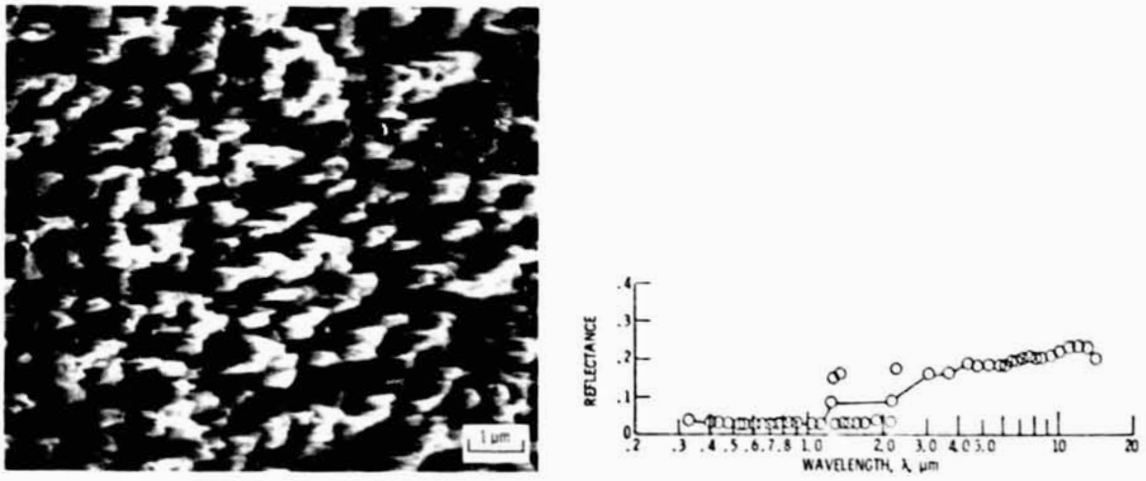

(b) SILICON AFTER 240 min OF TEXTURING.

Figure 32. - Scanning electron photomicrographs and spectral reflectance of tantalum seed textured metals (by a 1000 eV xenon ion beam at 2 mA/cm^2).

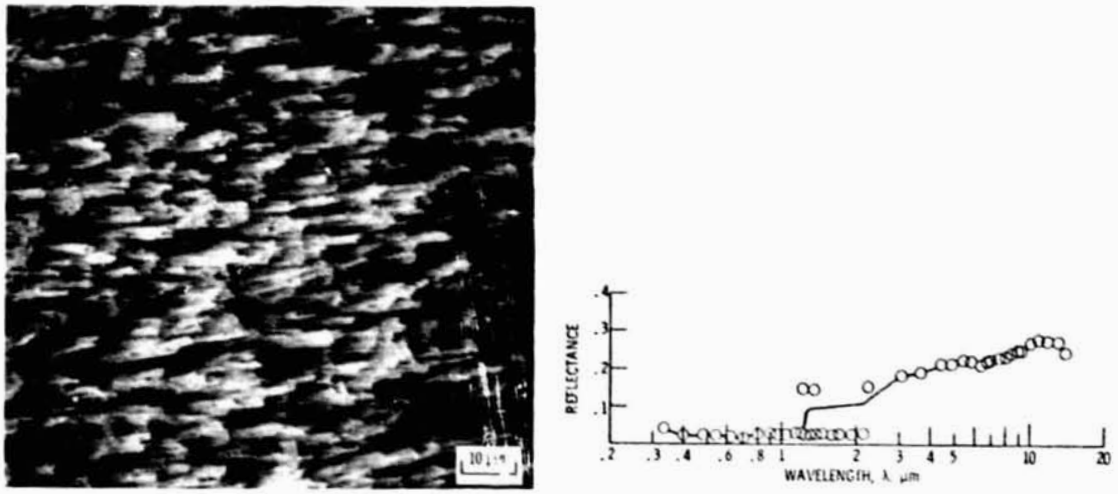

(c) ALUMINUM AFTER 270 min OF TEXTURING.

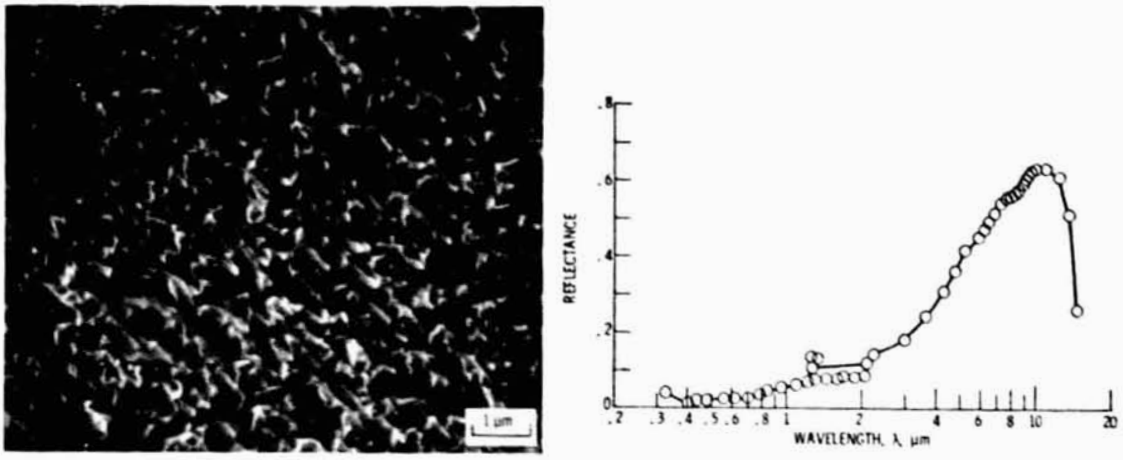

(d) TITANIUM AFTER 447 min OF TEXTURING.

Figure 32. - Continued.

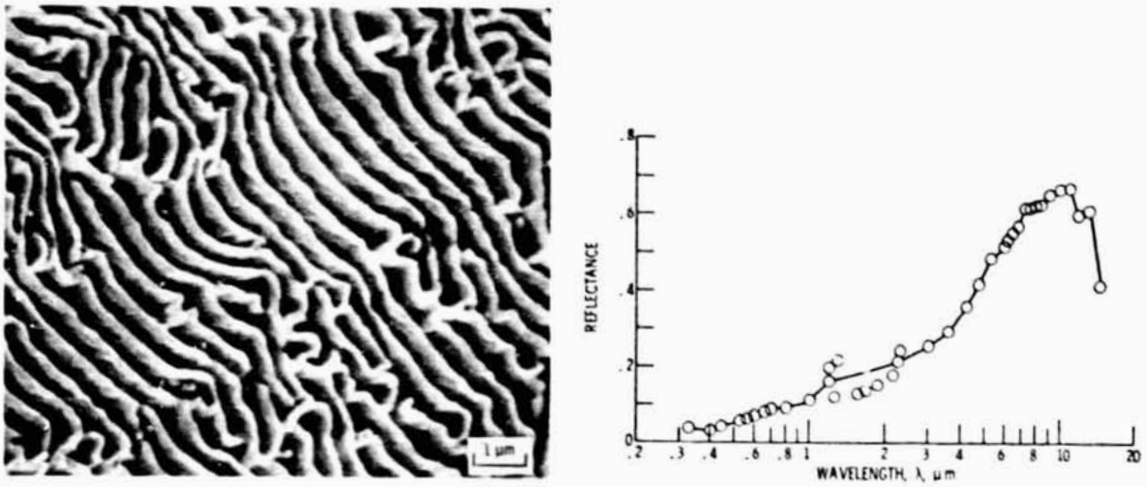

(e) 316 STAINLESS STEEL AFTER 540 min OF TEXTURING.

Figure 32. - Concluded.

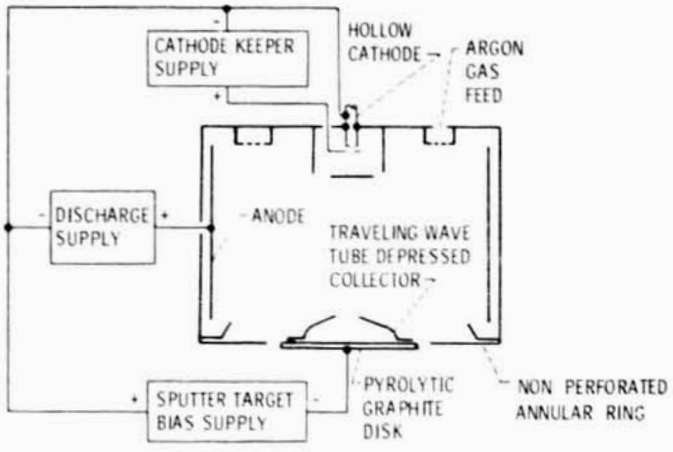

Figure 33. - Triode discharge sputtering using a 30 cm diameter argon ion source.

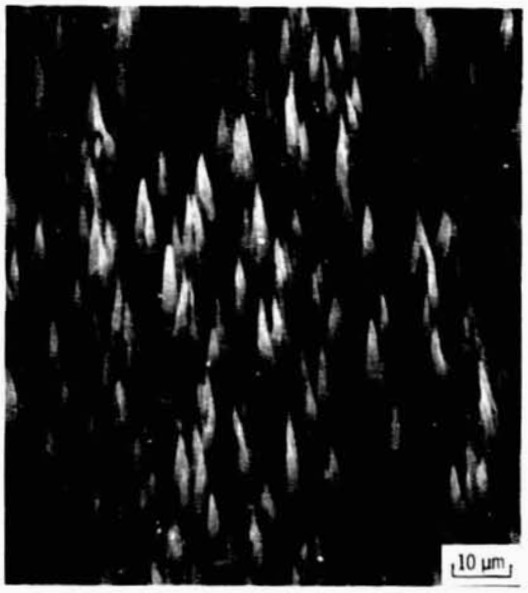

Figure 34. - Natural textured pyrolytic graphite.

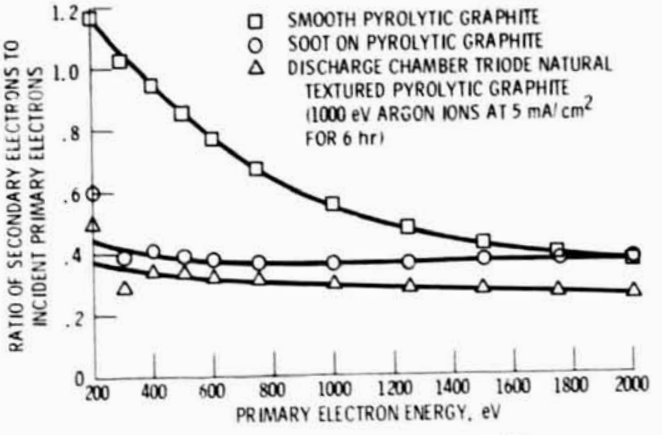

(a) SECONDARY ELECTRON EMISSION RATIO.

Figure 35. - Characteristics of normally incident electron bombardment of various carbon surfaces.

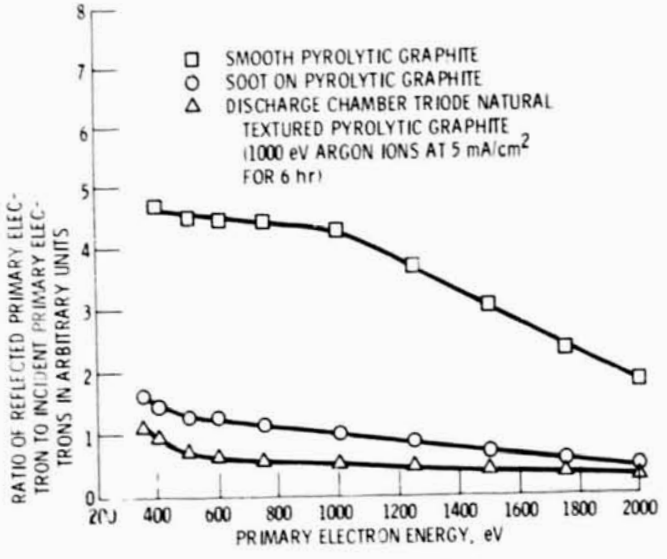

(b) REFLECTED PRIMARY ELECTRON YIELD.

Figure 35. - Concluded.

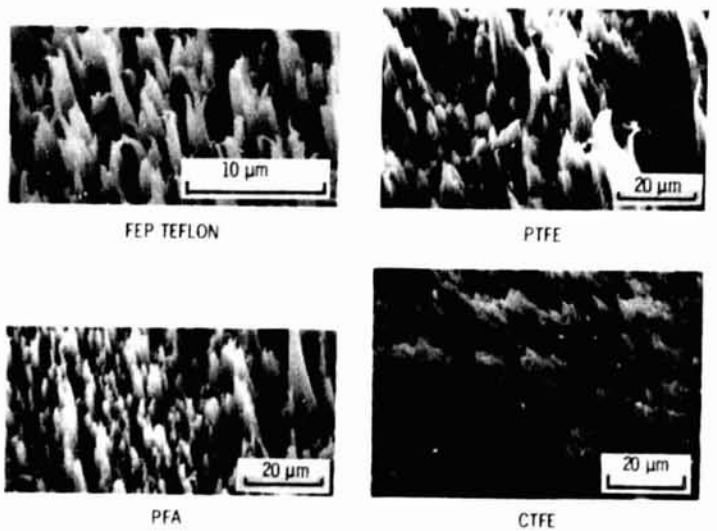

Figure 36.- Scanning electron photomicrographs of ion beam textured fluoropolymers exposed to 0.75 KeV argon ions at 0.5 ma/cm^2 for 30 minutes.

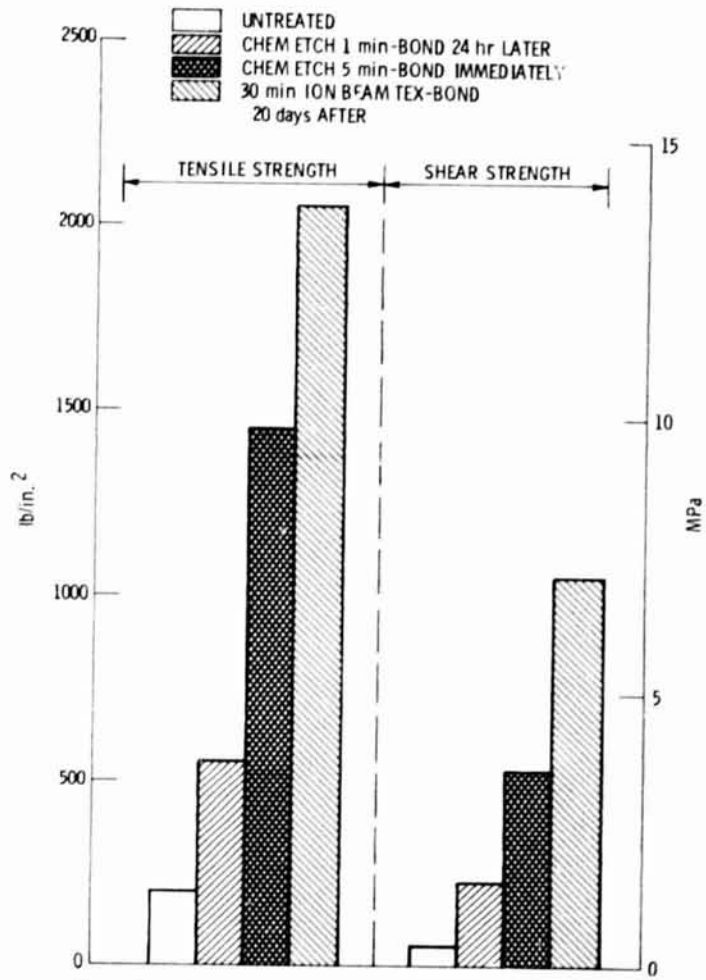

Figure 37. - Tensile and shear strengths of epoxy bonded PTFE. (Bulk tensile strength of PTFE = (3000 to 4500) psi.)

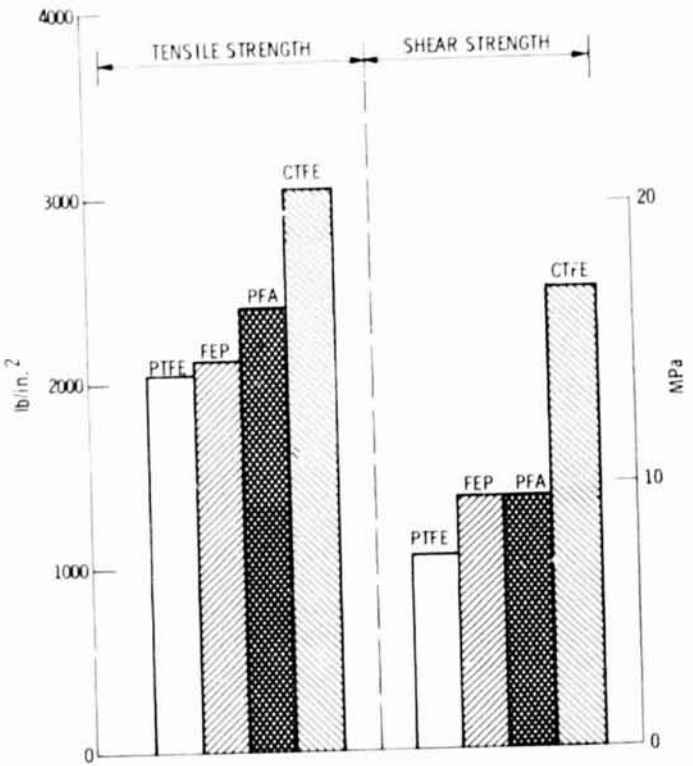

Figure 38. - Tensile and shear strengths of epoxy bonded ion beam textured fluoropolymers exposed to a 750 eV argon ion beam at 0.5 mA/cm^2 for 30 min.

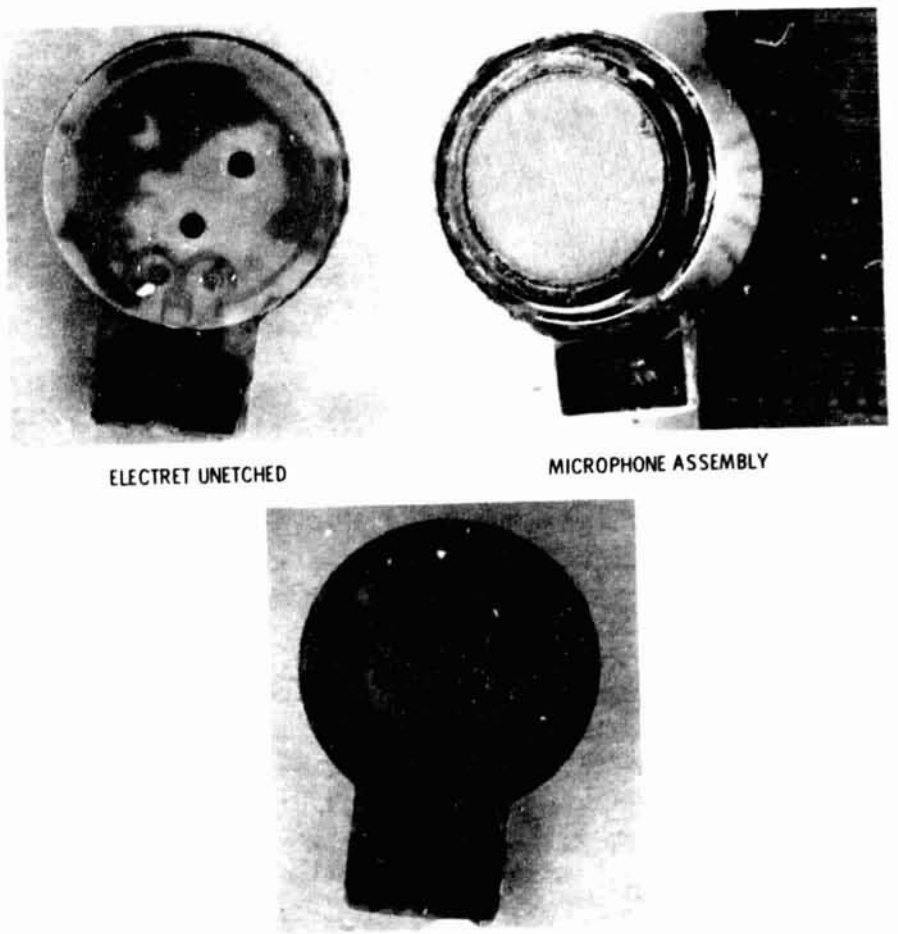

Figure 39. - Electret microphone fabricated from a PTFE Teflon® circuit board laminate.

Figure 40. - Scanning electron photomicrograph of sputtered etched FEP Teflon® surface with two dust particles on the initial surface.

Figure 41. - Scanning electron photomicrograph of a sputter etched PTFE Teflon® surface that was covered with silica particles.

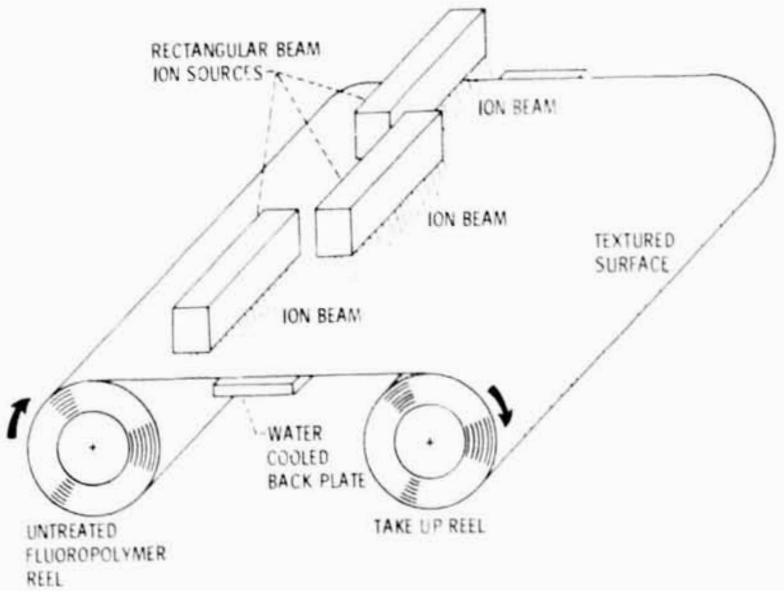

Figure 42. - Reel to reel batch texturing of fluoropolymer sheet.

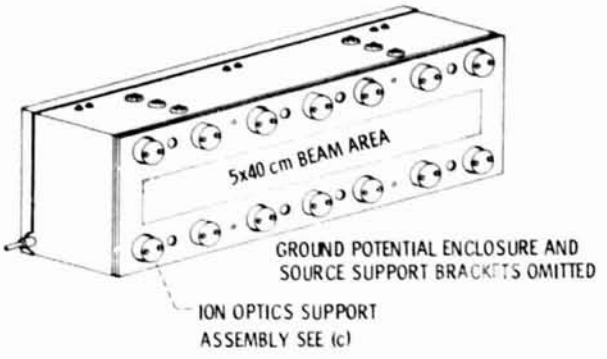

(a) OVERALL ASSEMBLY (NOT DRAWN TO SCALE).

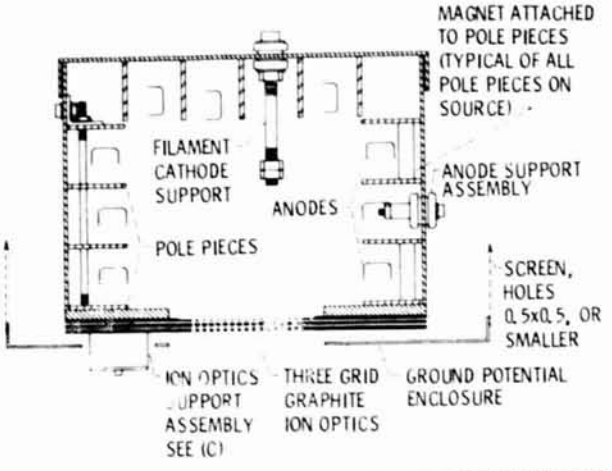

(b) CROSS SECTION OF SOURCE. THIS DRAWING DOES NOT REPRESENT ANY PARTICULAR CROSS SECTION, BUT SIMPLY INCORPORATES MOST MAJOR CONSTRUCTION FEATURES.

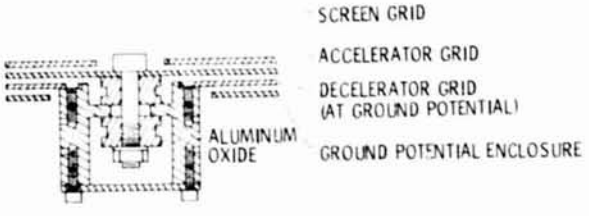

(c) ION OPTICS SUPPORT ASSEMBLY AS SHOWN TO ATTACH THE ACCELERATOR TO THE DECELERATOR GRID. THE ASSEMBLY IS ALSO USED TO ATTACH THE SCREEN TO THE ACCELERATOR GRID.

Figure 43. - Rectangular-beam ion source (ref. 55).

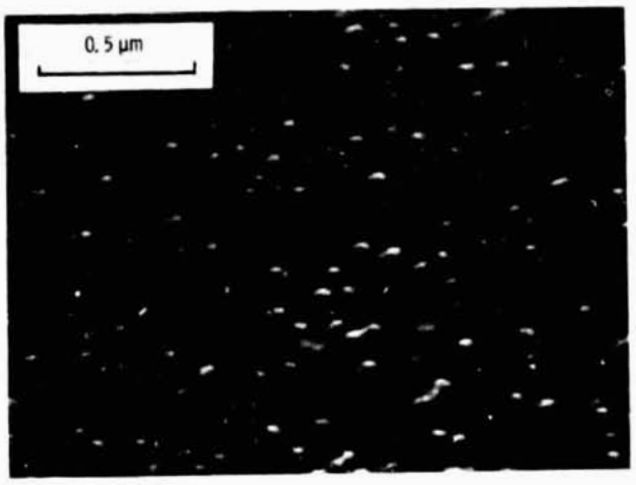

(a) SiO_2 SPUTTER ETCHED FOR FIVE MINUTES.

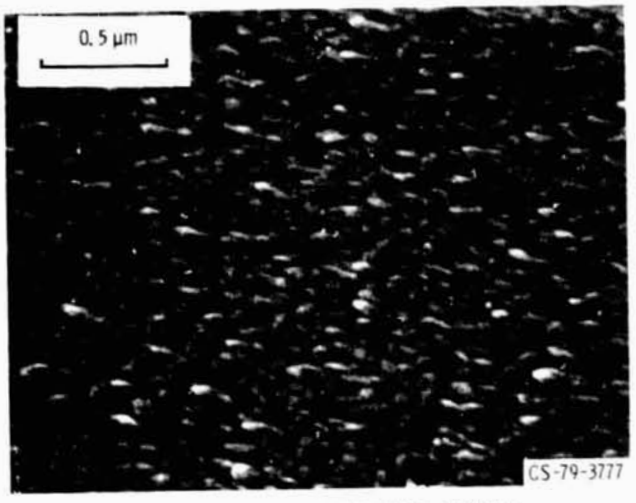

(b) ZrO_2 SPUTTER ETCHED FOR THREE MINUTES.

Figure 44. - Scanning electron photomicrographs of metal oxide sur-

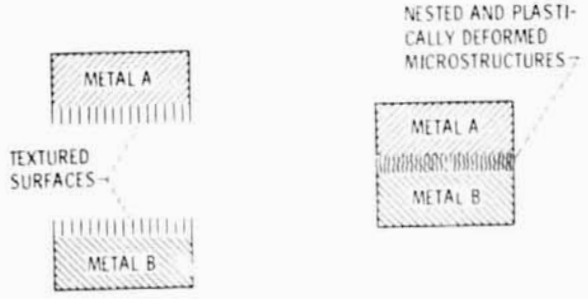

Figure 45. - Texture bonding.

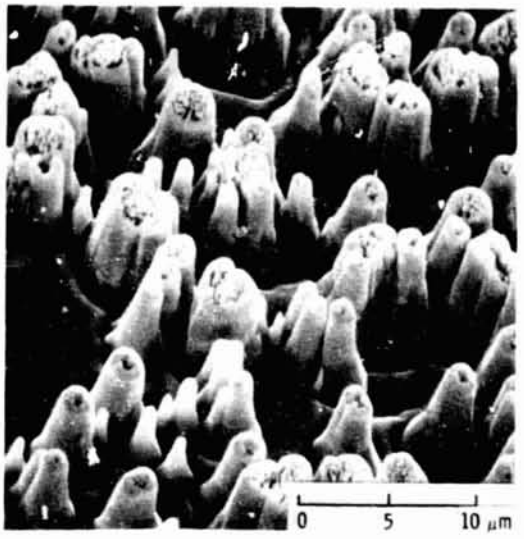

(a) SCANNING ELECTRON PHOTOMICROGRAPH OF Ta SEED TEXTURED COPPER SURFACE.

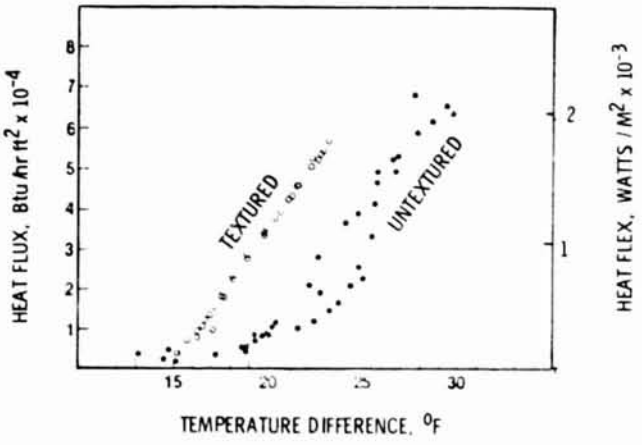

(b) HEAT TRANSFER VIA NUCLEATE BOILING FROM TEXTURED AND UNTEXTURED COPPER SURFACES.

Figure 46. - Nucleate boiling heat transfer from freon 113 boiling on textured surfaces (ref. 58).

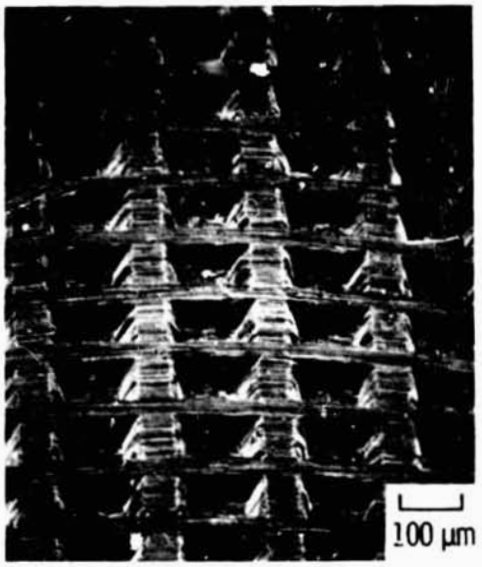

(a) COBALT, 20% CHROMIUM, 15% TUNGSTEN (REF. 65).

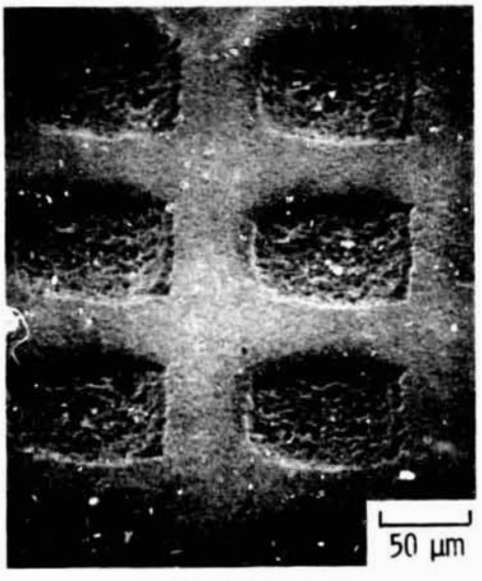

(b) ALUMINA, (REF. 65).

Figure 47. - Surface modification of biomaterials by ion beam sputter etching through electroformed nickel mesh masks.

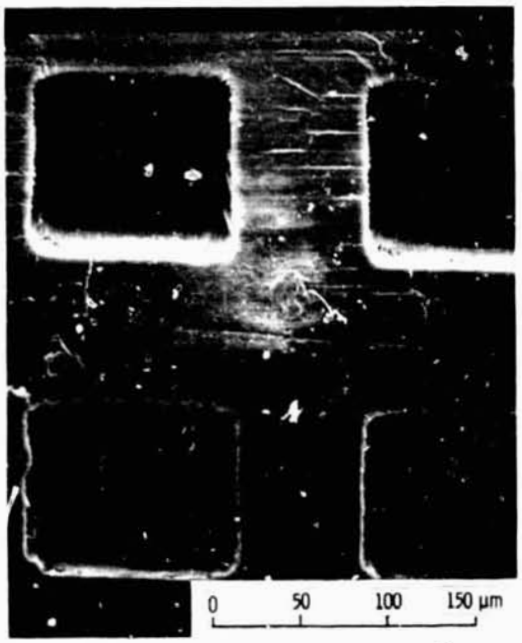

(c) POLYTETRAFLUOROETHYLENE, (TEFLON®).

Figure 47. - Concluded.

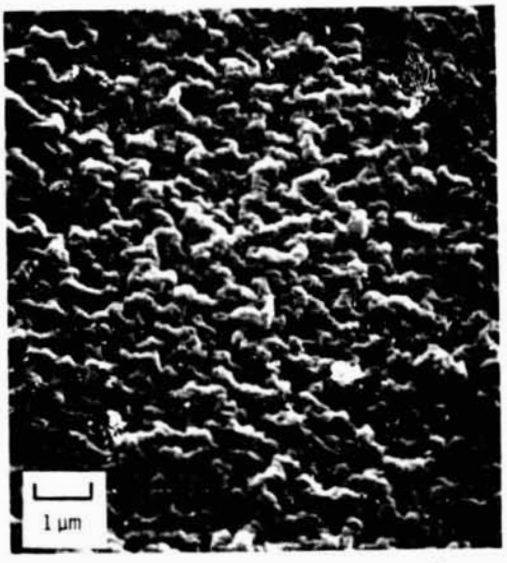

(a) SEGMENTED POLYURETHANE, (BIOMER®).

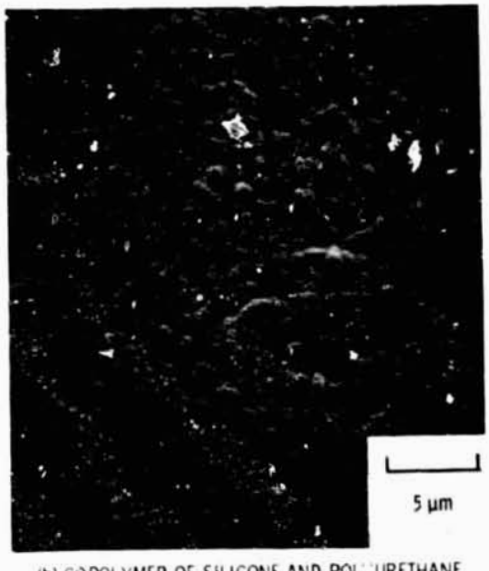

(b) COPOLYMER OF SILICONE AND POLYURETHANE, (AVECOTHANE®).

Figure 48. - Argon ion beam natural textured biopolymers (ref. 65).

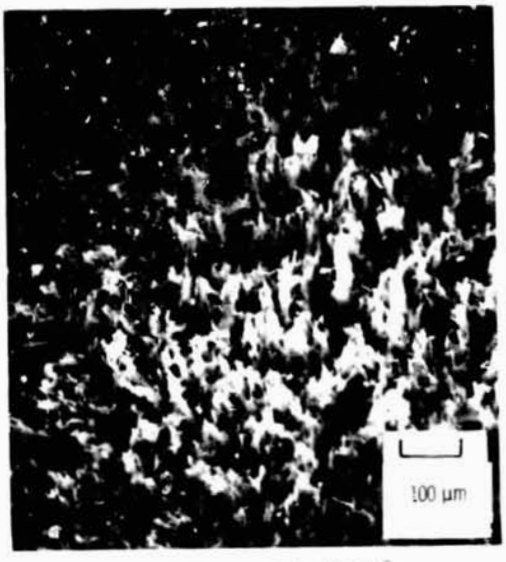

(c) POLYOXYMETHYLENE, (DELRIN®).

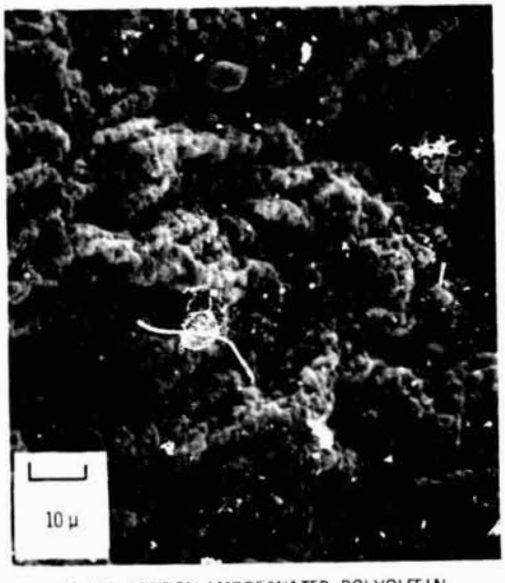

(d) 32% CARBON-IMPREGNATED POLYOLEFIN, (HEXYN).

Figure 48. - Continued.

(e) POLYTETRAFLUOROLTHYLENE, (PTFE TEFLON®).

Figure 48. - Concluded.

(a) 316 STAINLESS STEEL.

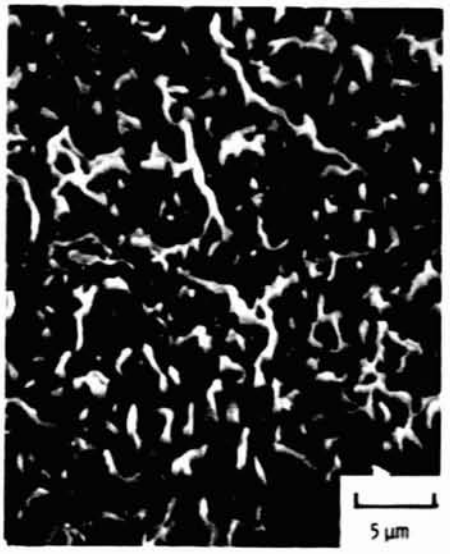

(b) TITANIUM 6% ALUMINUM, 4% VANADIUM.

Figure 49. - Tantalum seed textured orthodedic alloys using an argon ion beam (ref. 65).

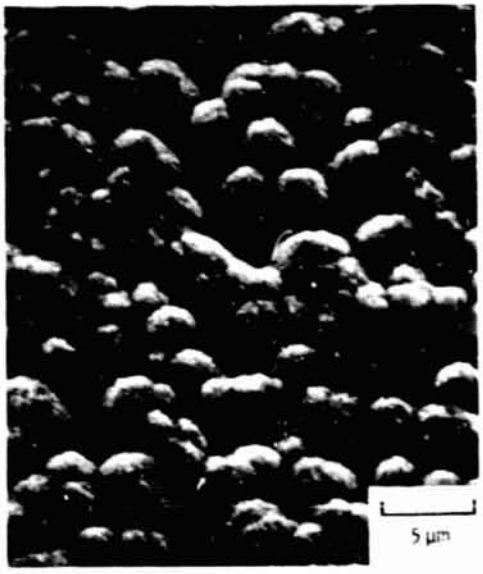

(c) COBALT - 20% CHROMIUM, 15% TUNGSTEN (HAYNES 25®).

Figure 49. - Concluded.

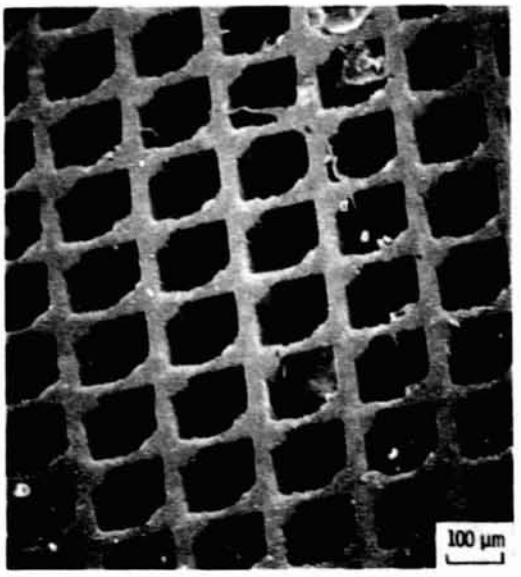

(a) POLYTETRAFLUOROETHYLENE (PTFE TEFLON®) SUBSTRATE AFTER TRANSFER CASTING SHOWING PITS PRODUCED BY ION BEAM SPUTTERING THROUGH AN ELECTROFORMED NICKEL MESH MASK.

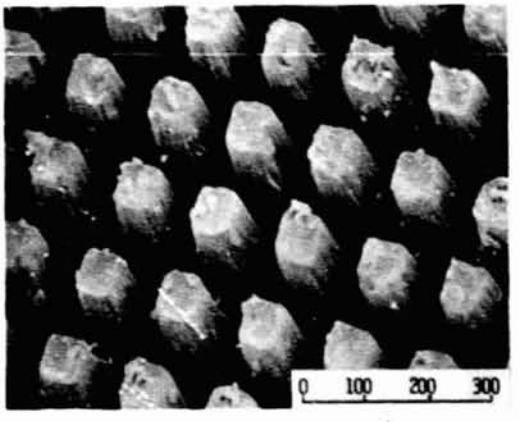

(b) SILICONE RUBBER (SILASTIC®) TRANSFER CAST PILLAR MORPHOLOGY RESULTING FROM THE NEGATIVE OF A PIT MORPHOLOGY.

Figure 50. - Transfer casting scanning electron photomicrograph.

(a) SHORT PILLARS RESULTING FROM SHALLOW PITS.

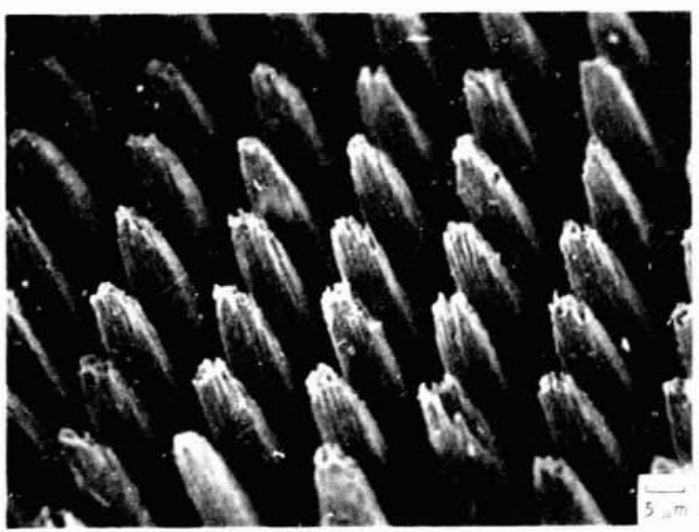

(b) TALL PILLARS RESULTING FROM DEEP PITTS.

Figure 51. - Scanning electron photomicrographs of segmented polyurethane (Biomer®) pillar surface transfer cast from polytetrafluoroethylene (PTFE Teflon®) having sputter etched pitts (ref. 72).

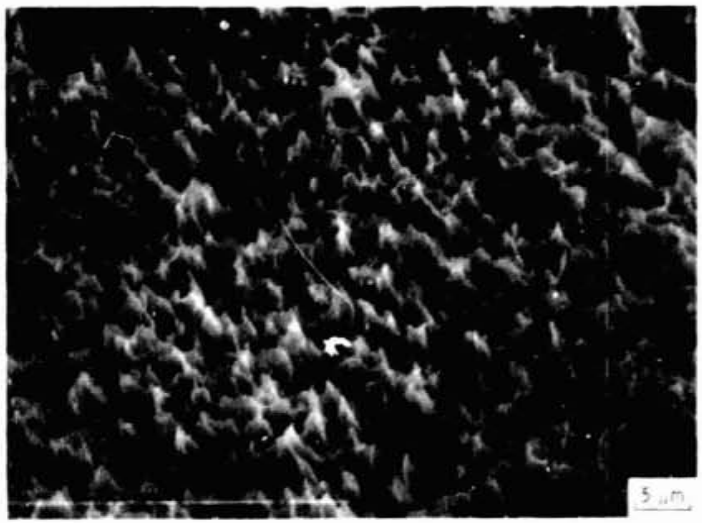

(a) RANDOM COPOLYMER OF 45% METHYLMETHACRYLATE, 55% 2-HYDROXYETHYLMETHACRYLATE (REF. 72).

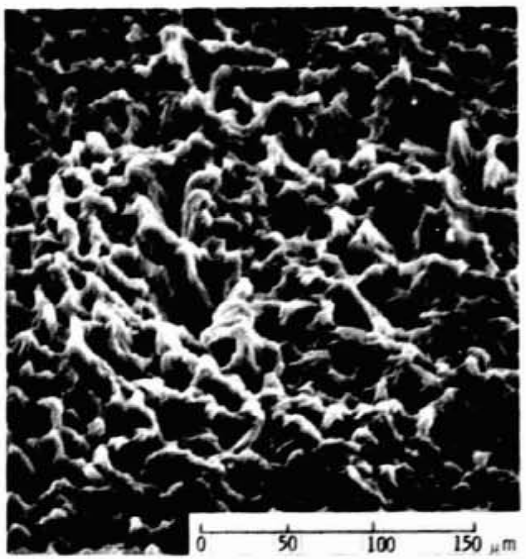

(b) SILICONE RUBBER.

Figure 52. - Scanning electron photomicrographs of transfer casts from natural textured polytetrafluoroethylene (PTFE Teflon®).

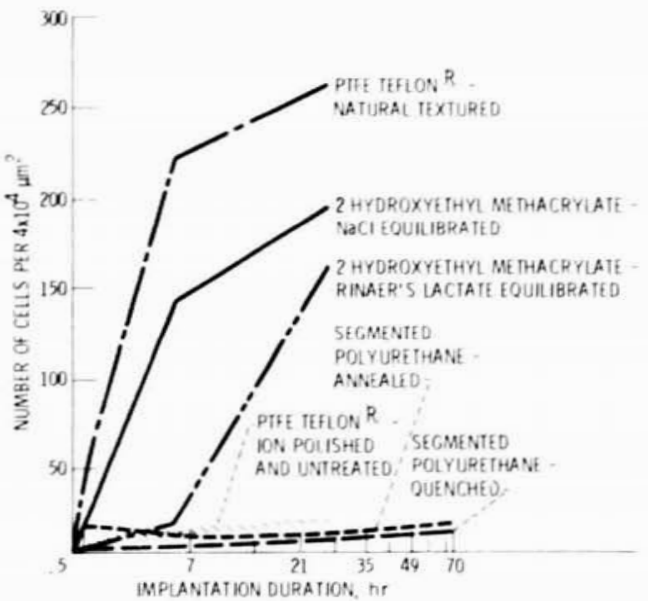

Figure 53. - Cell adhesion on peritoneal implants of various surface morphology and chemistry (ref. 73).
and chemistry (ref. 73).

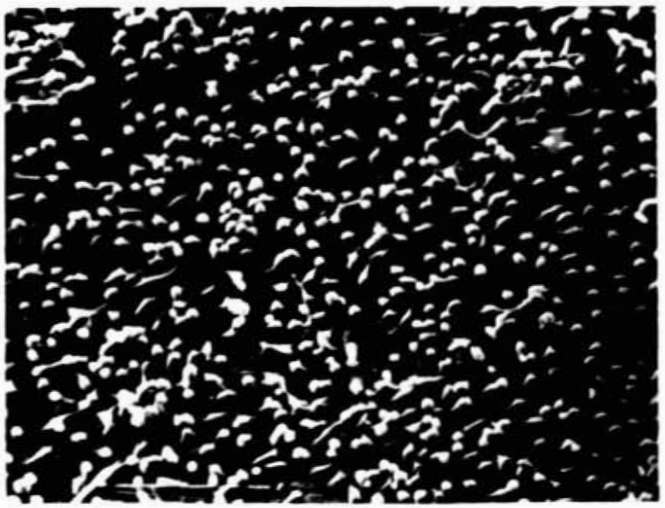

(a) CELLS ON SMOOTH SURFACE SAMPLE.

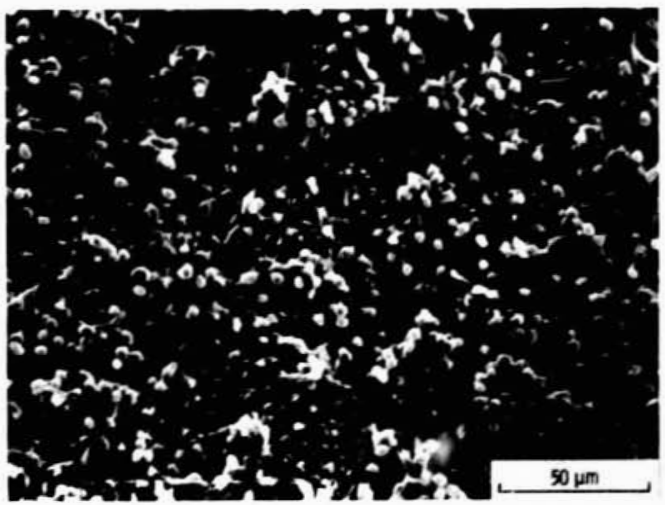

(b) CELLS ON NATURAL TEXTURED SURFACE.

Figure 54. - Scanning electron photomicrographs of polytetrafluoroethylene (PTFE Teflon®) implants after 3 days of peritoneal implantation (ref. 73).

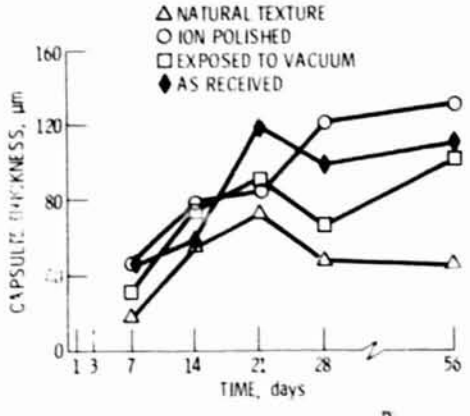

(a) POLYOXYMETHYLENE (DELVIN ®).

Figure 55. - Fiberous capsule thickness as a function of time for various surface treatments of 250 μm thick, 1 cm diameter implants in vats rats (ref. 75).

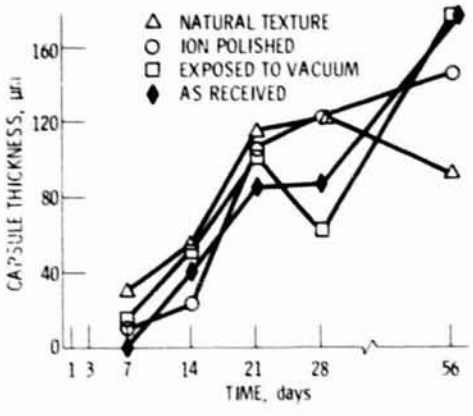

(b) POLYTETRAFLUOROETHYLENE.

Figure 55. - Concluded.

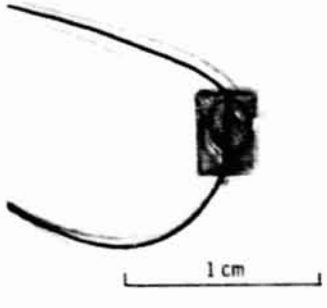

Figure 56. - Segmented polyurethane vascular implant with chamfered edges and embedded sutures.

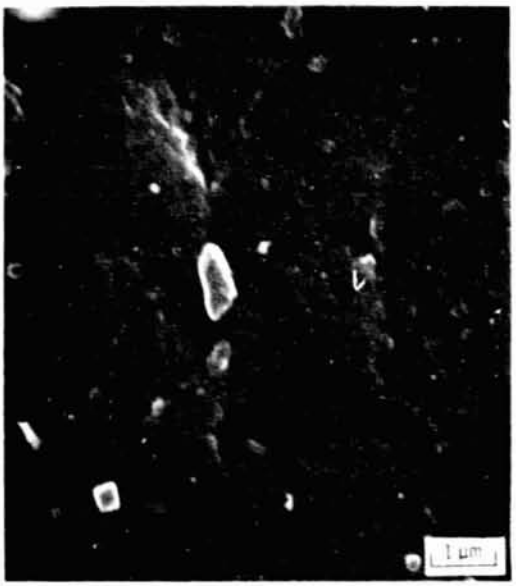

(a) BEFORE ION BEAM SPUTTERING.

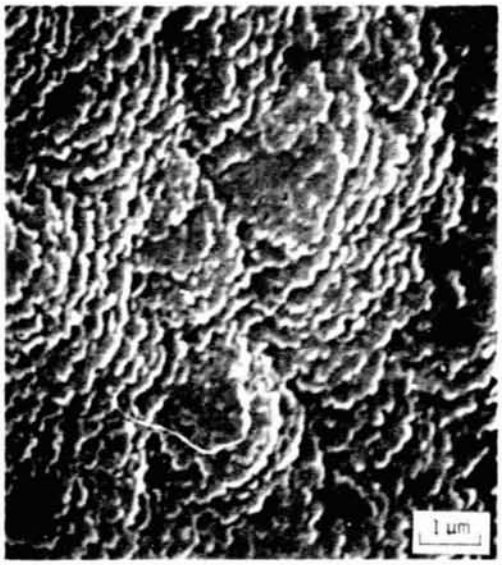

(b) AFTER ION BEAM SPUTTERING SHOWING NATURAL TEXTURE.

Figure 57. - Scanning electron photomicrographs of segmented polyurethane.

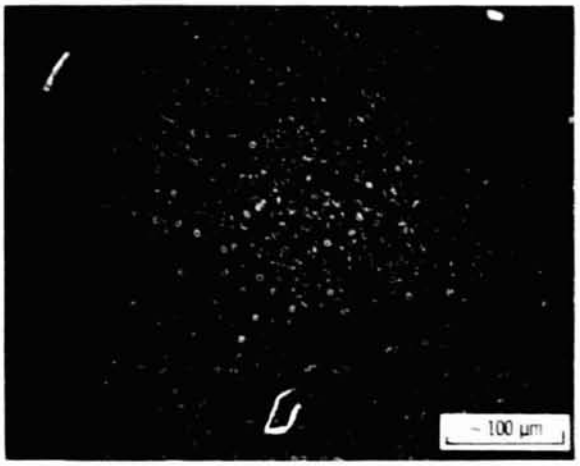

(a) UNSPUTTERED IMPLANT SHOWING A MONOLAYER COVERAGE OF PLATELETS AND LEUKOCYTES.

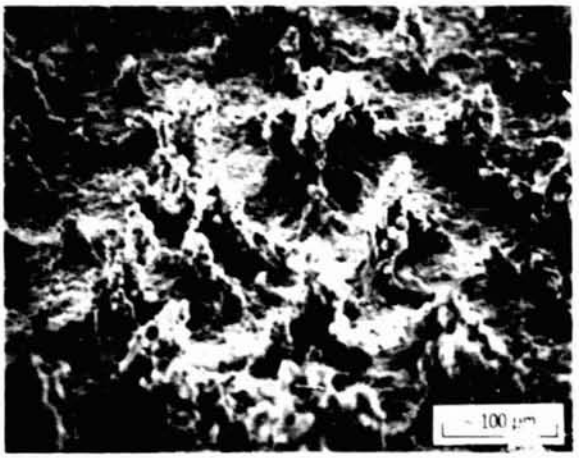

(b) SPUTTERED IMPLANT SHOWING PILLARS OF PLATELETS AND LEUKOCYTES.

Figure 58. - Scanning electron photomicrographs of segmented polyurethane implants after one hour of invivo blood exposure.

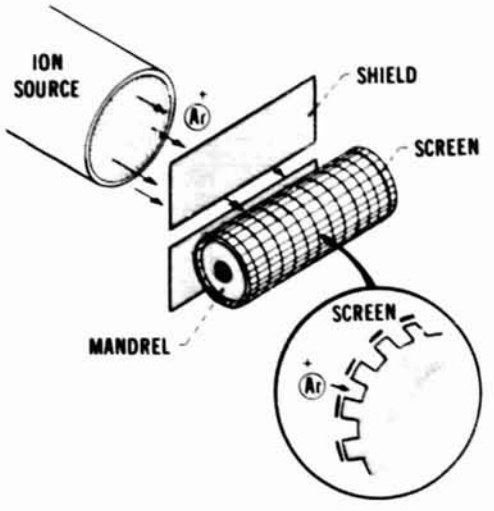

Figure 59. - Sputter etching technique to produce pits on a polytetrafluoroethylene mandrel by sputtering through an electroformed mesh screen.

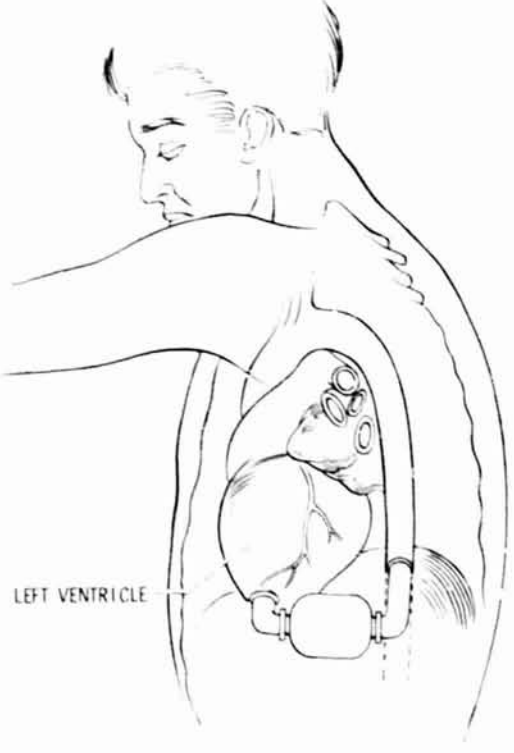

Figure 60. Left ventricular assist device.

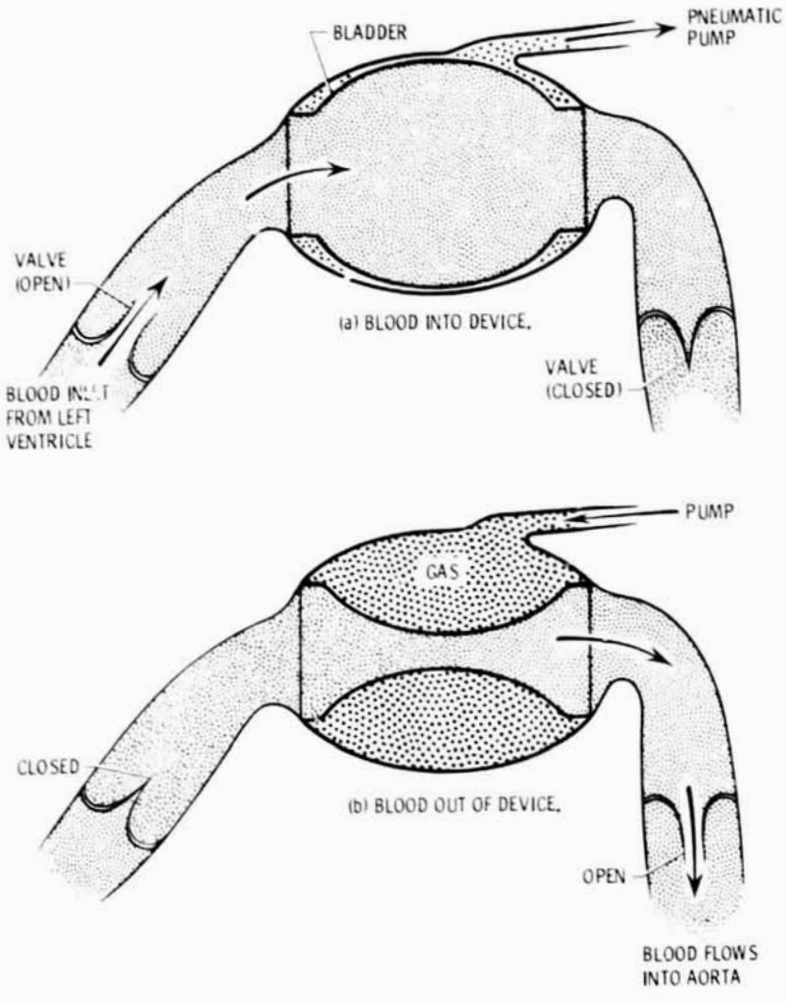

Figure 61. - Pictoral section view of left ventricular assist device operation.

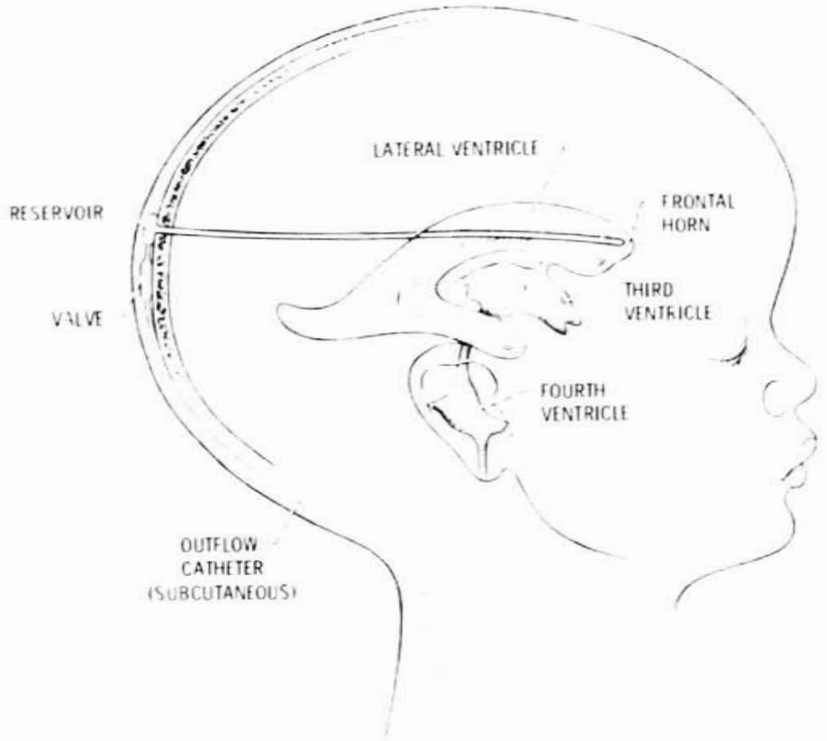

Figure 62. - Typical ventricular shunt used for treatment of hydrocephalus.

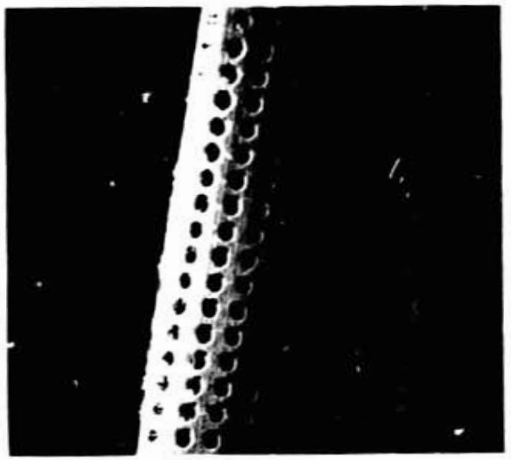

(a) SPUTTER ETCH TUBING OUTSIDE SURFACE.

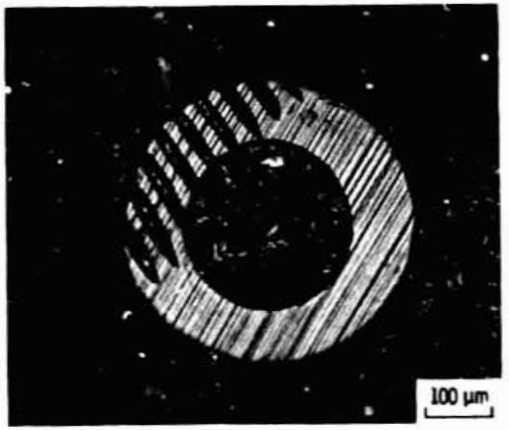

(b) SECTION VIEW.

Figure 63. - Scanning electron photomicrographs of ion beam sputter etched apertures in polytetrafluoroethylene tubing.

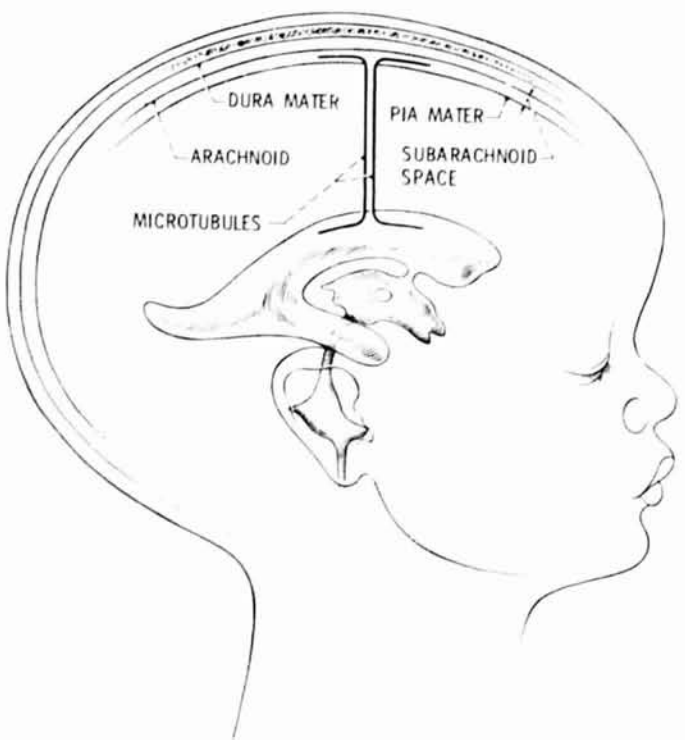

Figure 64. - Direct shunting of cerebrospinal fluid from the lateral ventricals to the subarachnoid space using sputter perforated microtubules.

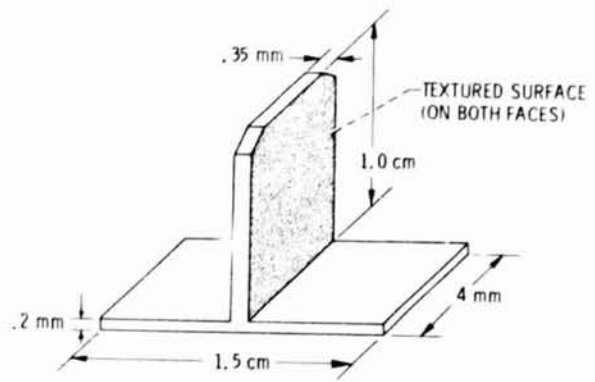

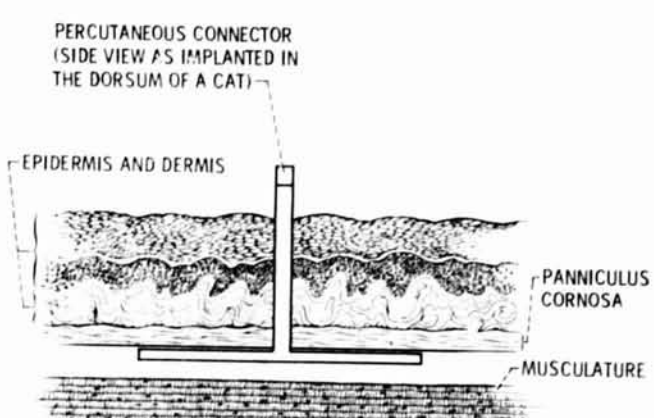

Figure 65. - Percutaneous connector configuration for evaluation of textured surface performance.

(a) - TITANIUM.

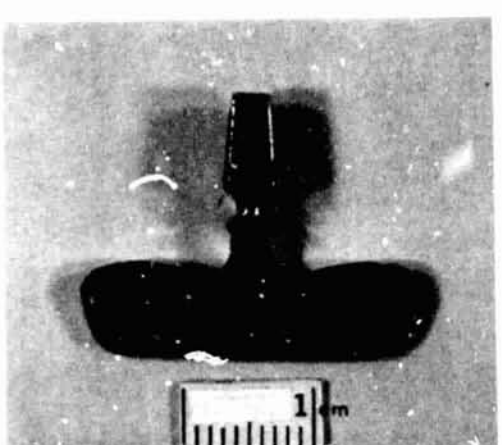

(b) MP35N.

Figure 66. - Endosteal blade implants.

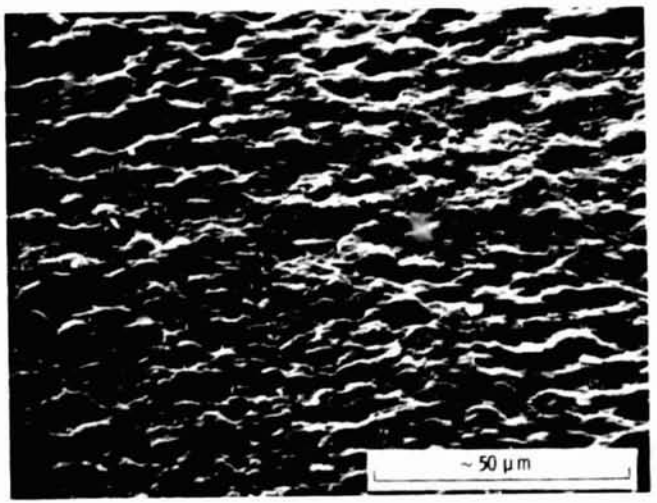

(a) NATURAL TOOTH CEMENTUM.

(b) UNTREATED PURE TITANIUM.

Figure 67. - Scanning electron photomicrograph comparison of surface morphologies of natural tooth cementum, untreated and tantalum seed textured pure titanium.

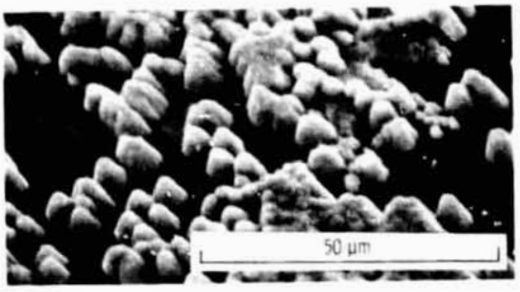

(c) TANTALUM SEED TEXTURED PURE TITANIUM.

Figure 67. - Concluded.

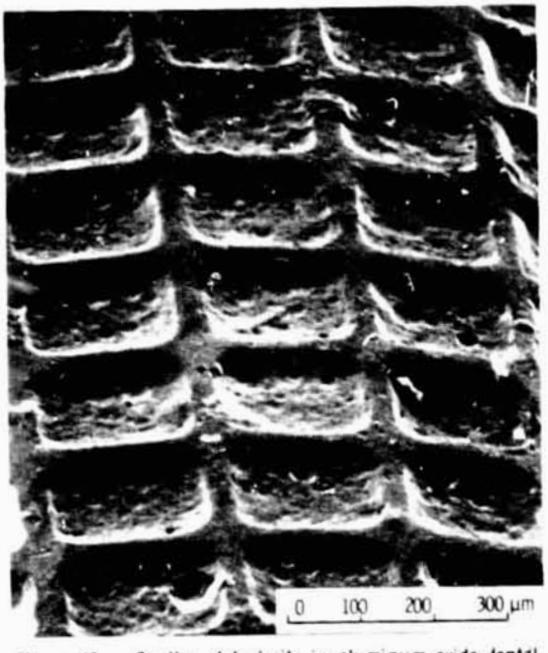

Figure 68. - Sputter etched pits in aluminum oxide dental implants formed by sputter etching through an electroformed nickel mesh mask (ref. 88).

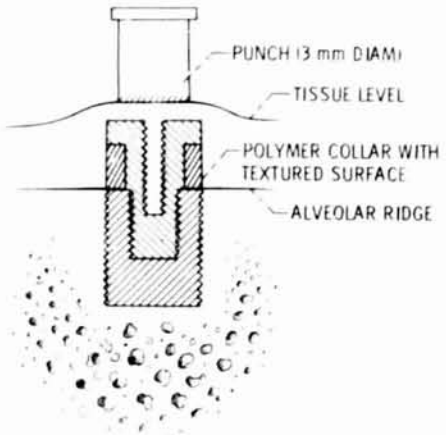

(a) GINGIVAL PUNCH ERUPTION.

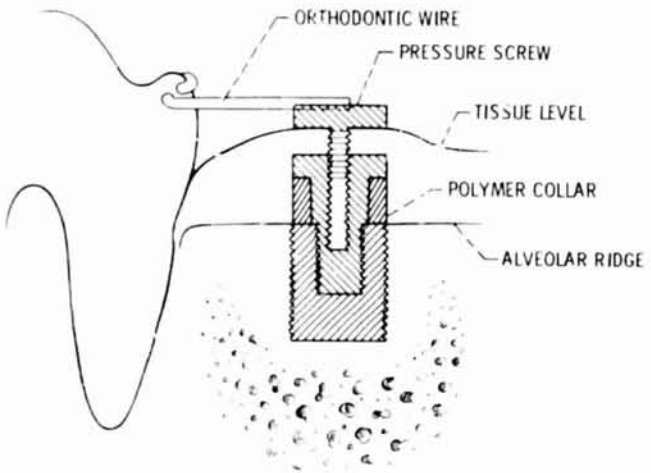

(b) PRESSURE NECROSIS ERUPTION.

Figure 69. - Dental implants for evaluation of morpological requirements for the gingival seal (ref. 90).

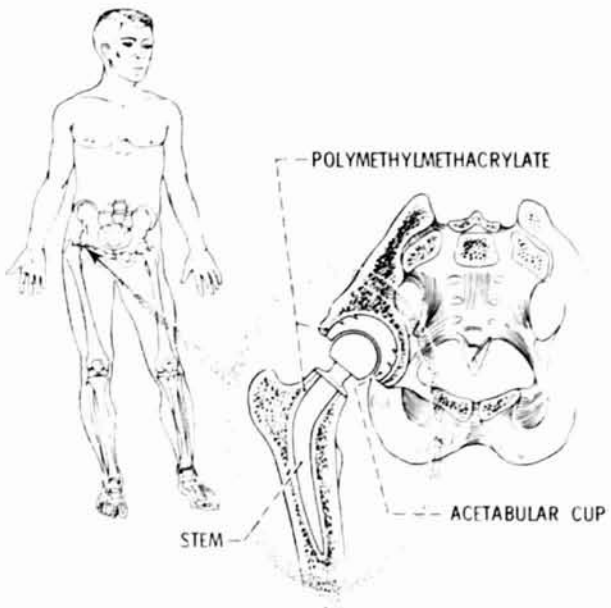

Figure 70. - Total hip prosthesis.

(a) SCANNING ELECTRON [illegible] TOMICROGRAPH OF SPUTTER ETCHED PITS I[illegible] IMPLANT CYLINDRICAL SURFACE.

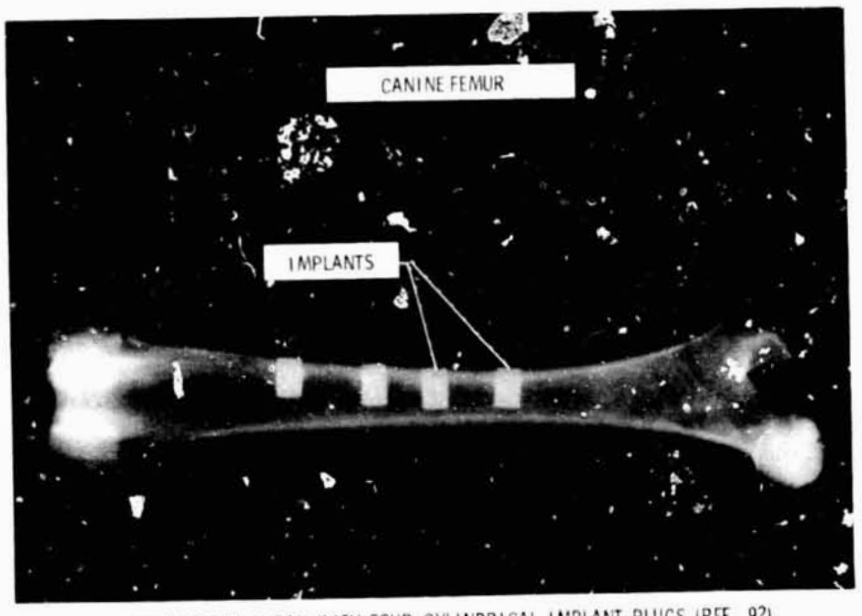

(b) CANINE FEMUR X-RAY WITH FOUR CYLINDRICAL IMPLANT PLUGS (REF. 92).

Figure 71. - Cylindrical plug implants (ref. 92).

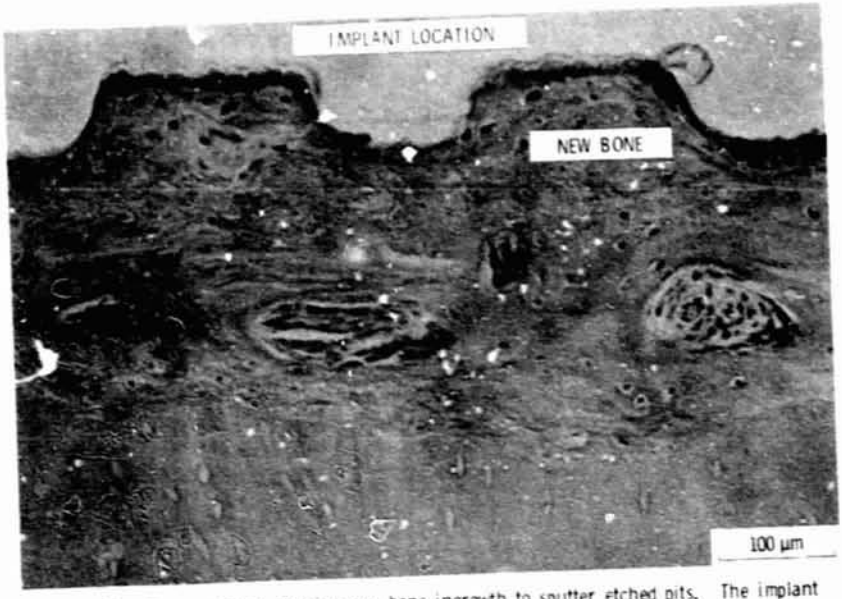

Figure 72. - Tissue section showing new bone ingrowth to sputter etched pits. The implant was removed prior to tissue sectioning (ref. 92).

Figure 73. - Typical implant for electrical stimulation tests shown after sputter etching pits with some mesh mask remaining to be cleaned off (ref. 96).

Figure 74. - Silicone rubber flexible finger joint implant (Swanson design).

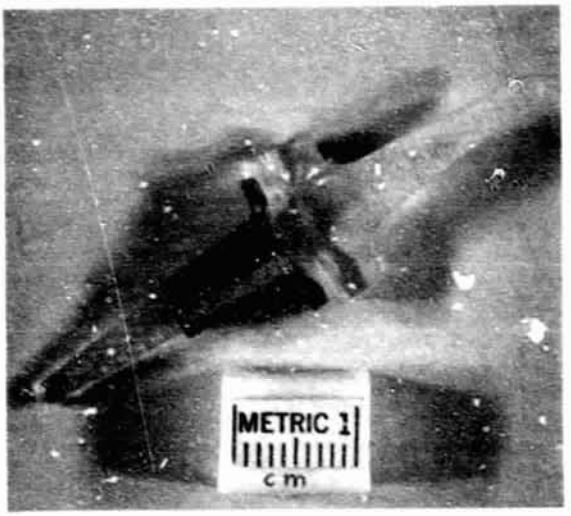

(a) SILICONE RUBBER FINGER JOINT WITH A GROMMET OVER THE PROXIMAL STEM.

(b) SCANNING ELECTRON PHOTOMICROGRAPH OF GROMMET SURFACE AND EDGE.

Figure 75. - 316 L Stainless steel grommet made of woven screen diffusion bonded to a smooth 150 um thick substrate.

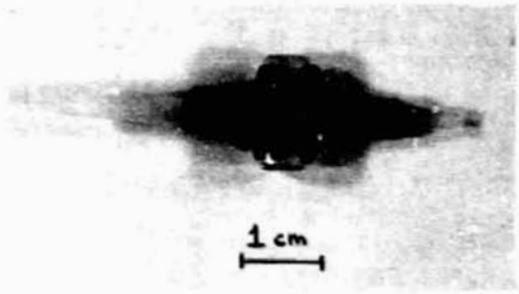

(a) SILICONE RUBBER FINGER JOINT WITH NATURAL TEXTURED GROMMETS.

(b) SCANNING ELECTRON PHOTOMICROGRAPH OF NATURAL SPUTTER TEXTURED COBALT-CHROMIUM-MOLYBDENUM CAST ALLOY.

Figure 76. - Natural sputter textured cobalt-cromium-molybdenum lost wax cast grommets.

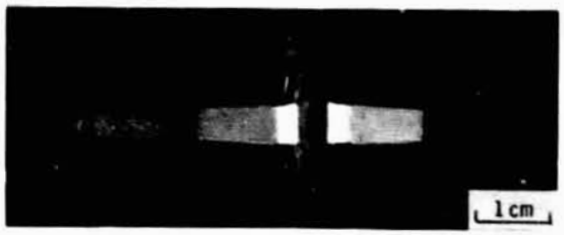

(a) SILICONE RUBBER FINGER JOINT WITH PHOTOCHEMICALLY ETCHED GROMMETS.

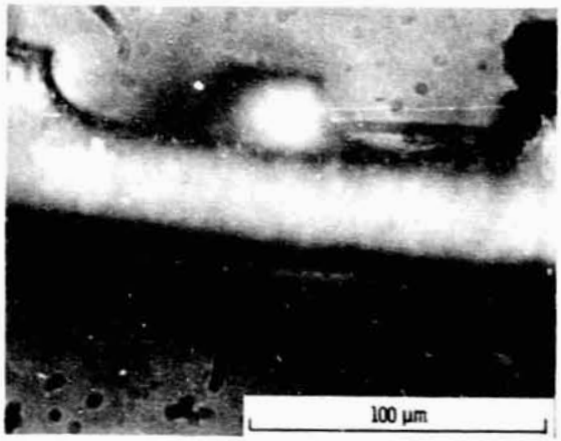

(b) OPTICAL MICROSCOPE PHOTOMICROGRAPH OF EDGE VIEW OF GROMMET SURFACE WITH PILLARS.

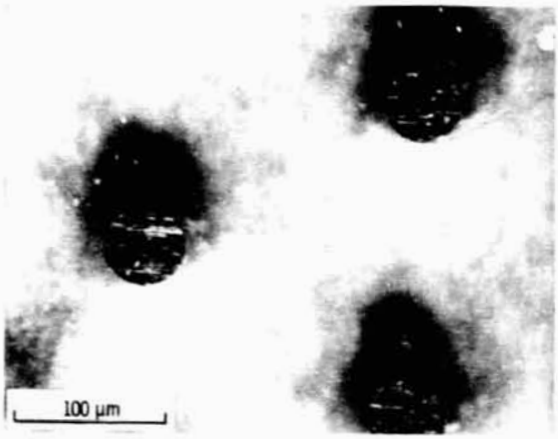

(c) TOP VIEW OF PILLAR SURFACE.

Figure 77. - Photochemically etched pillar surfaced titanium 6% Al - 4% V grommets.